# Predicting Riverbank Erosion and Accretion Using Multi-level LSTM-Based Deep Models and Satellite-Derived Land Cover Indices

by

Tasnim Rahman
21201114
Ulfat Fatema Elma
21201548
Juaria Tashin
23241054
Tamanna Afrin
21201054

A thesis submitted to the Department of Computer Science and Engineering
in partial fulfillment of the requirements for the degree of
B.Sc. in Computer Science and Engineering

Department of Computer Science and Engineering
Brac University
January 2026.

# Declaration

It is hereby declared that

1. The thesis submitted is my/our own original work while completing degree at Brac University.
2. The thesis does not contain material previously published or written by a third party, except where this is appropriately cited through full and accurate referencing.
3. The thesis does not contain material which has been accepted, or submitted, for any other degree or diploma at a university or other institution.
4. We have acknowledged all main sources of help.

**Student's Full Name and Signature:**


**Tasnim Rahman**
21201114

**Ulfat Fatema Elma**
21201548

**Juaria Tashin**
23241054

**Tamanna Afrin**
21201054

# Approval

The thesis titled "Predicting Riverbank Erosion and Accretion Using Multi-level LSTM-Based Deep Models and Satellite-Derived Land Cover Indices" submitted by

1. Tasnim Rahman (21201114)
2. Juaria Tashin (23241054)
3. Ulfat Fatema Elma (21201548)
4. Tamanna Afrin (21201054)

of Fall, 2025 has been accepted as satisfactory in partial fulfillment of the requirement for the degree of B.Sc. in Computer Science in March, 2026.

**Examining Committee:**

**Supervisor:**
(Member)

**Dr. Swakkhar Shatabda**
Professor
Department of Computer Science and Engineering
Brac University

**Co-Supervisor:**
(Member)

**Mr. Rafeed Rahman**
Senior Lecturer
Department of Computer Science and Engineering
Brac University

**Thesis Coordinator:**
(Member)

**Dr. Md. Golam Rabiul Alam**
Professor
Department of Computer Science and Engineering
Brac University

**Head of Department:**
(Chair)

**Dr. Sadia Hamid Kazi**
Chairperson and Associate Professor
Department of Computer Science and Engineering
Brac University

# Abstract

This research presents a multi-level LSTM-based deep learning framework, centered on a Bidirectional LSTM–GRU hybrid with attention, which predicts riverbank erosion and accretion by a long-term satellite-based dataset spanning from 1988 to 2025. Data covering seven rivers and multiple zones were acquired from Landsat 5, Landsat 7, and Sentinel-2 satellites. The research applied advanced geospatial processing to generate annual water masks, riverbank polygons, and extract crucial land cover indices such as NDWI, NDVI, NDBI, SAVI, MSI, NBR, and BAI, which are complemented by elevation, slope, and soil texture data to characterize riverbank environments using Google Earth Engine. Furthermore, the 1988 imagery served as a baseline for quantifying erosion and accretion changes annually on left and right banks. Data processing included cloud masking, vectorization of water bodies, best line detection for riverbank delineation, and spatial classification of banks. For each river zone and bank side, the erosion and accretion areas were spatially and temporally quantified. Moreover, a hierarchical sequence architecture is used to model temporal dependencies on a global, river, zone, and bank level using Bidirectional LSTM-GRU with attention layers. To ensure robust temporal continuity for model training, data were preprocessed through category quantization based on global tertiles and sequence interpolation to fill the missing years.The model predicts the erosion and accretion dynamics, and the effectiveness of the model is evaluated against baseline models (standard LSTM, Random Forest, XGBoost, LightGBM) and tested with the help of detailed trend analysis over time, heatmaps of the correlation, and confusion matrices. Additionally, multi-scale spatial and temporal variability and associations among rivers and bank zones were revealed by visualizations. The framework integrates remote sensing, geospatial analytics, and advanced deep learning to enable scalable and interpretable riverbank change prediction which provides valuable insights for river management, conservation, and risk mitigation strategies.

**Keywords:** Riverbank erosion; Accretion prediction; Multi-level LSTM; Bidirectional LSTM–GRU; Remote sensing; Satellite imagery; Google Earth Engine; Hierarchical modeling; Deep learning; Random Forest; XGBoost; LightGBM; Landsat 5; Landsat 7; Sentinel-2; NDWI; NDVI; NDBI; SAVI; MSI; NBR; BAI; Land cover indices; Spatio-temporal analysis; Environmental monitoring; Geospatial analysis; Time-series data; Soil and terrain influence; Class imbalance handling; Risk assessment.

# Acknowledgement

First and foremost, all praises and gratitudes are due the almighty Allah, the most merciful and graceful for his countless blessings, direction and grace. The strength, patience and perseverance required for the completion of this thesis work were granted by his will and graceness. His guidance illuminated the path and in moments of uncertainty his grace provided hope. The successful completion of this work would not have been possible without his immense support.

# Table of Contents


**Declaration** **i**

**Approval** **ii**

**Ethics Statement** **iv**

**Abstract** **iv**

**Dedication** **v**

**Acknowledgment** **v**

**Table of Contents** **vi**

**List of Figures** **viii**

**List of Tables** **xi**

**Nomenclature** **1**

**1 Introduction** **1**
- 1.1 Background . . . . . 1
- 1.2 Rational of the Study . . . . . 2
- 1.3 Problem Statement . . . . . 3
- 1.4 Objective . . . . . 3
- 1.5 Methodology in Brief . . . . . 4
- 1.6 Scopes and Challenges . . . . . 5

**2 Literature Review** **7**
- 2.1 Preliminaries . . . . . 7
- 2.2 Review of Existing Research . . . . . 8
  - 2.2.1 International Research On River Erosion . . . . . 8
  - 2.2.2 Riverbank Erosion Research in Bangladesh . . . . . 10
  - 2.2.3 Traditional and Numerical Modeling of River Erosion . . . . . 12
  - 2.2.4 Hybrid Physical-AI Models for River Erosion Prediction . . . . . 14
  - 2.2.5 The Dynamics of Riverbank Accretion and Relevant Factors . . . . . 15
  - 2.2.6 Utilization of LSTM . . . . . 16
- 2.3 Summary of Key Findings . . . . . 17

**3 Requirements, Impacts and Constraints** **19**
3.1 Final Specifications and Requirements . . . 19
3.2 Societal Impact . . . 20
3.3 Environmental Impact . . . 20
3.4 Ethical Issues . . . 21
3.5 Project Management Plan . . . 22
3.6 Risk Management . . . 22

**4 Proposed Methodology** **24**
4.1 Methodology: . . . 24
4.1.1 Spatial Zonation and Area of Interest Definition . . . 25
4.1.2 Data Visualization . . . 27
4.2 Data Collection . . . 36
4.2.1 Data Cleaning . . . 37
4.2.2 Data Transformation . . . 37
4.2.3 Feature Engineering and Temporal Dynamics . . . 38
4.2.4 Predictive Target Creation and Final Dataset Structure . . . 39
4.2.5 Data Integration . . . 40
4.2.6 Data Reduction . . . 41
4.2.7 Exploratory Data Analysis (EDA) . . . 41
4.2.8 Summary of Preprocessed Data . . . 46
4.3 Data Correction Analysis . . . 48
4.4 Preliminary Designs: . . . 52
4.5 Implementation of selected Design . . . 59

**5 Result Analysis** **65**
5.1 Result of All Model . . . 66
5.1.1 Model Result for Erosion . . . 66
5.1.2 Model Result for Accretion . . . 67
5.2 Result Analysis of Bidirectional LSTM-GRU Hybrid with Attention Mechanics . . . 67
5.2.1 Model Result for Erosion . . . 67
5.2.2 Model Result for Accretion . . . 74
5.3 Ensemble Majority Voting Results . . . 82
5.3.1 Ensemble Results for Erosion . . . 82
5.3.2 Ensemble Results for Accretion . . . 85
5.4 Summary of All Results . . . 88
5.4.1 Result Discussion of Erosion Prediction . . . 90
5.4.2 Result Discussion of Accretion Prediction . . . 93
5.5 Reasons for moderate predictive accuracy . . . 96

**6 Limitations and Recommendations for Future Work** **99**
6.1 Limitations . . . 99
6.2 Future work . . . 100
6.3 Summary of Findings . . . 101

**Bibliography** **106**

# List of Figures


1.1 Workflow . . . . . . . . . . . . . . . . . . . . . . . . . . . . . . . 5

3.1 Project plan for one year. . . . . . . . . . . . . . . . . . . . . . . . . . 22

4.1 AOIs of the Southeastern Hilly Region River (Karnaphuli) . . . . . . 25
4.2 AOIs of Coastal Rivers (Baleshwar, Bishkali, Payra . . . . . . . . . . 26
4.3 AOIs of Sundarban Estuarine Rivers (Shibsa and Pasur) . . . . . . . 26
4.4 AOIs of Northeasten River's (Surma) . . . . . . . . . . . . . . . . . . 27
4.5 Best_Line_Detection_Analysis . . . . . . . . . . . . . . . . . . . . . 29
4.6 AOI adjustments . . . . . . . . . . . . . . . . . . . . . . . . . . . . 29
4.7 Char was detected as left bank part . . . . . . . . . . . . . . . . . . 30
4.8 The right bank was not detected fully . . . . . . . . . . . . . . . . . 30
4.9 When the middle line goes vertically it only detects as left bank and no right bank . . . . . . . . . . . . . . . . . . . . . . . . . . . . . 31
4.10 Payra zone 10 left/right bank detected perfectly as the river AOI is diagonal . . . . . . . . . . . . . . . . . . . . . . . . . . . . . . . . 31
4.11 Could detect left/right bank accurately when there is no char . . . . 31
4.12 Still detects char as part of the river bank . . . . . . . . . . . . . . . 31
4.13 Flow line which indicates the left/right bank properly without any area loss . . . . . . . . . . . . . . . . . . . . . . . . . . . . . . . . 32
4.14 Could detect left bank without including Char in it . . . . . . . . . . 33
4.15 Could detect right bank without including Char in it . . . . . . . . . 33
4.16 Left bank of base year 1988 . . . . . . . . . . . . . . . . . . . . . . . 33
4.17 Right bank of base year 1988 . . . . . . . . . . . . . . . . . . . . . . 33
4.18 Water body of base year 1988 . . . . . . . . . . . . . . . . . . . . . . 33
4.19 Water body of current year . . . . . . . . . . . . . . . . . . . . . . . 33
4.20 Char of base year 1988 . . . . . . . . . . . . . . . . . . . . . . . . . 34
4.21 The intersection between the water bodies of the current year and the base year is used to derive erosion and accretion. . . . . . . . . . . . . 34
4.22 Char Erosion with Respect to the Base-Year (1988) Water Body . . . 34
4.23 Char Accretion with Respect to the Base-Year (1988) Water Body . . 34
4.24 Left Bank Erosion with Respect to the Base-Year (1988) Water Body 34
4.25 Right Bank Erosion with Respect to the Base-Year (1988) Water Body 34
4.26 Left bank Accretion with Respect to the Base-Year (1988) Water Body 35
4.27 Right bank Accretion with Respect to the Base-Year (1988) Water Body 35
4.28 Current with previous year comparison shows Left Bank Erosion . . . 35
4.29 Current and previous year comparison shows Left Bank Accretion . . 35
4.30 Current and previous year comparison shows Right Bank Erosion . . 35

4.31 Current and previous year comparison shows Right Bank Accretion however, no visible accretion has occurred and therefore nothing is shown here. . . . . 35
4.32 Current and previous year comparison shows Char Erosion . . . . . 36
4.33 Current and previous year comparison shows Char Accretion . . . . . 36
4.34 This is the AOI with all the labels on . . . . . 36
4.35 The final code works perfectly on these added conditions as well.So This method works in any orientation(diagonal, vertical, horizontal) of the river body in the aoi without any mistake. . . . . . 36
4.36 Net Riverbank Change Over Time . . . . . 41
4.37 Erosion Patterns Over Time by River . . . . . 42
4.38 Accretion Patterns Over Time by River . . . . . 42
4.39 Temporal Trends Comparison . . . . . 43
4.40 Correlational Matrix of top 25 features from Erosion Dataset . . . . . 44
4.41 Correlational Matrix of top 25 features from Accretion Dataset . . . . . 45
4.42 Before_Treatment_Boxplot . . . . . 47
4.43 Before_Treatment_Boxplot FOR EROSION EXPLICITLY . . . . . 47
4.44 Before_Treatment_Boxplot FOR ACCRETION EXPLICITLY . . . . . 48
4.45 After_Treatment_Boxplot . . . . . 48
4.46 After_Treatment_Boxplot . . . . . 49
4.47 After_Treatment_Boxplot FOR EROSION EXPLICITLY . . . . . 49
4.48 After_Treatment_Boxplot FOR ACCRETION EXPLICITLY . . . . . 49
4.49 Target Erosion Distribution . . . . . 50
4.50 Target Accretion Distribution . . . . . 51
4.51 CNN-LSTM Attention Architecture . . . . . 56
4.52 Bidirectional LSTM-GRU Hybrid with Attention Mechanism architecture . . . . . 59

5.1 Confusion matrix for the Global layer . . . . . 69
5.2 Loss, F1 Score and Accuracy Graph . . . . . 69
5.3 Confusion matrix for the Baleshwar River . . . . . 71
5.4 Loss and F1-score for the Baleshwar River . . . . . 71
5.5 ROC curves and AUC for the Baleshwar River . . . . . 72
5.6 Confusion matrix for the Global layer . . . . . 75
5.7 Loss, F1 Score and Accuracy Graph . . . . . 76
5.8 Confusion matrix for Karnaphuli River . . . . . 77
5.9 Loss and F1 Validaation of Karnaphuli River . . . . . 78
5.10 ROC and AUC of Karnaphuli River . . . . . 79
5.11 Confusion matrix of BiLSTM-GRU for the Ensemble Majority Voting for Erosion Prediction . . . . . 83
5.12 Confusion matrix of CNN-BiLSTM for the Ensemble Majority Voting for Erosion Prediction . . . . . 84
5.13 Confusion Matrix of BiLSTM-GRU for Ensemble Majority Voting for Accretion Prediction . . . . . 86
5.14 Confusion Matrix of CNN-BiLSTM for Ensemble Majority Voting for Accretion Prediction . . . . . 87
5.15 Most Erosion Prone River Zones . . . . . 91
5.16 Most Erosion-Prone Rivers . . . . . 92

5.17 Erosion Risk Heatmap . . . . . . . . . . . . . . . . . . . . . . . . . . . 93
5.18 Most Accretion Prone River Zones . . . . . . . . . . . . . . . . . . . . . 94
5.19 Most Accretion Prone Rivers . . . . . . . . . . . . . . . . . . . . . . . . 95
5.20 Accretion Risk Heatmap . . . . . . . . . . . . . . . . . . . . . . . . . . 96

# List of Tables


5.1 Global Model Results for Erosion Prediction: . . . . . . . . . . . . . . . 66
5.2 Global model results for Accretion prediction: . . . . . . . . . . . . . . 67
5.3 River wise Result: . . . . . . . . . . . . . . . . . . . . . . . . . . . . . 70
5.4 Zone-wise result of some rivers: . . . . . . . . . . . . . . . . . . . . . . 73
5.5 The results of selected banks . . . . . . . . . . . . . . . . . . . . . . . 74
5.6 River wise Accretion: . . . . . . . . . . . . . . . . . . . . . . . . . . . 76
5.7 Zone-wise Accretion Results . . . . . . . . . . . . . . . . . . . . . . . 80
5.8 The results of selected banks for Accretion: . . . . . . . . . . . . . . . 81
5.9 Ensemble Majority Voting Results for Erosion Prediction (All Models) 84
5.10 Ensemble Majority Voting Results for Accretion Prediction (All Models) 88

# Chapter 1

# Introduction

Erosion and accretion of riverbanks are dynamic processes which are influenced by natural forces and human activities. These changes need to be monitored and predicted to make river management and environmental risk mitigation effective. Satellite imagery and remote sensing offer high-resolution time series, while hierarchical LSTM models enable accurate forecasting of erosion and accretion patterns. This research provides a powerful framework for predicting riverbank change and strategic management by integrating land-cover indices derived from satellites and multi-level geospatial information.

## 1.1 Background

River erosion is a significant environmental challenge that poses serious hazards to communities, ecosystems and infrastructure, especially in the coastal regions of Bangladesh, where rivers are a significant point for socio-economic activities. These natural phenomena lead to long-term difficulties in sustainable development, resulting in the loss of agricultural land, the disturbance of livelihoods and the uprooting of communities that are vulnerable. For example, the study found that between 1993 and 2024, about 5,142.60 hectares of land along the banks of the Arial Khan River suffered erosion, exceeding the overall amount of land loss [1]. Moreover, a study on the Padma River has shown that over the past 42 years, its width has changed significantly due to erosion and sedimentation, with some areas losing an alarming rate of up to 2-4 square kilometres per year [2]. Additionally, a study on estuarine regions such as the Bishkhali River has shown that between 1991 and 2015, shoreline migration changed significantly, with maximum land right and left bank erosion reaching up to reaching 732 meters and 612 meters respectively[3]. Furthermore, research on the erosion of the Jamuna River has discovered that the amount of sedimentation in dredged areas can reach 60-80 Percent, significantly altering the shape and flow of the river. Rapid accretion processes have also contributed to dynamic changes in river channel morphology and bank stability. Spatial patterns of accretion and erosion highlight the dynamic nature of riverbanks by revealing significant sediment deposition that modifies the local landscape and influences human activity[4]. In addition, rapid changes in channels have been observed, with few areas facing more than 30 meters of vertical erosion in a single monsoon season. Satellite images also reveal major changes in the coastline between 2000 and 2010, which became worser by hydrological changes and human activities in the following years [5]. To monitor and forecast riverbank erosion precisely can be challenging due to its dynamic and complex character, which can easily be affected by factors like river flow, soil structure, rainfall, and human activity. Conventional methods for erosion measurement that are often used mostly rely on field surveys and simple hydrological models. As a result, in most cases, these methods fail to capture the complexity of the phenomenon. These methods are also time consuming. In order to resolve these issues and offer quick, precise predictions of regions that are susceptible to erosion, there is an increasing demand for sophisticated, data-driven approaches. Another reason for the growing popularity of GIS and Remote sensing methods is their ease of use and cost-effectiveness [6]. Integrating remote sensing with machine learning models can provide a robust and more accurate way to analyse erosion patterns through processing large-scale geospatial data. Implementation of these technologies can lead Through sustainable land management techniques, mitigation initiatives, and monitoring, the areas that are susceptible to erosion can be comprehensively addressed.

## 1.2 Rational of the Study

The continuous development of deep learning and remote sensing has opened up new opportunities to accurately predict riverbank erosion and accretion, which have been a significant environmental and socio-economic concern in Bangladesh. Field-based monitoring, as a method of traditional monitoring, is not only expensive but time and space-consuming. In comparison, the combination of satellite imagery and hierarchical LSTM-based deep learning can provide a scalable and data-driven approach to the more precise representation of spatial and temporal erosive dynamics.accuracy.

Remote sensing plays an important role in erosion and sediment research by mapping erosion intensity, identifying bank erosion, and assessing the vulnerability of areas prone to erosion [7]. These technologies can be assembled effectively to provide a robust framework to evaluate weak points and develop initiatives for mitigation. Remote sensing and geographic information system (GIS) methods have become gradually widespread to monitor and assess river dynamics across different spatial and temporal scales [8]. The combined application of remote sensing and GIS ensures a well-developed and stable framework to consider the weak points, identify the channel migration at the long-term, and provide the mitigation approaches that correspond to the practice of sustainable river management.

Machine learning and, specifically, LSTM-based deep learning (with Bidirectional LSTM-GRU hybrids that have attention) can be considered powerful to study patterns of erosion-accretion, geomorphological variability, and spectral indices, and the relationships that cannot be clearly detected in multi-year, multi-sensor satellite data. It has been shown in studies that geospatial techniques and machine-learning methodologies, including tree-based models and deep sequence networks, can provide highly precise analyses of erosion and accretion patterns, improving the accuracy of predictive models and contributing to sustainable river management strategies [9]. Both data and models are arranged in the hierarchical structure (Global - River - Zone - Bank) thus the sequence architecture can learn not only local spatial relationships but also long-term temporal patterns, which is a significant improvement over the traditional single-level models. Remote sensing indices such as NDVI, NDWI, NDBI, SAVI, MSI, NBR and BAI reinforce this framework by measuring vegetation health, soil water and surface water availability, which are key indicators affecting riverbank stability.

The study hence presents a hybrid approach that extends the capabilities of deep temporal learning offered by LSTM based networks alongside with Earth observation data of high resolution to deliver an automated monitoring and forecasting system. It allows predicting future erosion and accretion areas, which can be used as a decision support tool to manage rivers in a sustainable way, plan their land use, and minimize disaster risks. In addition to prediction, the research also helps in climate adaptation, as erosion patterns are closely linked to hydrological changes and water level rise.

Finally, the work is relevant to the discipline of geospatial intelligence in the field of environmental resilience and the proposed research introduces a scaling and adaptive modeling framework. It shows how combining remote sensing analysis with multi-level LSTM modeling can transform conventional erosion monitoring methods into a smart forecasting framework - eliminating the use of manual surveys and allowing for proactive action planning to protect river communities and infrastructure.

## 1.3 Problem Statement

Traditional riverbank erosion assessment methods in Bangladesh are often manual, inaccurate and unable to adequately capture both erosion and accretion dynamics over large spatiotemporal scales. This limits effective prediction and timely management of riverbank changes which is essential for protecting ecosystems and communities. Leveraging satellite imagery from multiple decades together with geospatial indices and hierarchical deep learning models this project aims to develop an automated and data-driven prediction system that accurately monitors and forecasts both erosion and accretion patterns at multiple spatial scales. This approach addresses complex hydrological and geospatial variability, providing critical insights and actionable information for sustainable riverbank management and disaster risk mitigation.

## 1.4 Objective

This research aims to develop a data-driven riverbank erosion and accretion prediction system in Bangladesh using remote sensing imagery and advanced machine learning algorithms. The goal of this is to identify high-risk areas through multi-level temporal and spatial analysis, assess the performance of predictive models and provide actionable insights for sustainable riverbank management and risk mitigation.

1. To analyze multi-temporal satellite images and geospatial indicators to predict riverbank erosion and accretion using hierarchical machine learning models.

2. To quantify and map spatial- temporal variations in land loss and land gain due to erosion and deposition over multiple decades using geospatial data analysis.

3. To integrate spectral indices and environmental variables such as NDWI, NDVI,NDBI, SAVI, MSI, NBR, BAI, elevation, slope, soil texture, and char-related metrics with hierarchical LSTM- based deep learning models to identify erosion and accretion- prone regions and understand their spatial dynamics.

4. To produce interpretable risk maps and statistics that support informed decision-making for targeted riverbank protection and conservation strategies.

In conclusion, this research suggests a flexible and scalable framework for riverbank erosion and accretion prediction and sustainable management in Bangladesh.

## 1.5 Methodology in Brief

This study focuses on understanding and predicting changes along riverbanks using satellite-based analysis. Multispectral data from **Sentinel-2**, **Landsat-5**, and **Landsat-7** were collected to create a consistent time series of river corridor imagery. After enhancing the images and clipping the areas of interest (AOIs), several spectral indices were derived, including **NDVI**, **NDBI**, **MSI**, **NBR**, **SAVI**, and **BAI**, to capture variations in vegetation cover, surface exposure, and moisture levels. Zonal statistics were then extracted for each river section to prepare the dataset for modeling.
The processed data was structured into a structure of four levels (Global, River, Zone, and Bank). The most important predictor variables were vegetation indices (NDVI, SAVI, BAI), built-up and moisture (NDBI, MSI, NBR), water-related (NDWI, MNDWI), [10][11],and geomorphic (elevation, slope, soil texture, and char-related) variables.[12] These variables are directly connected both to erosion of riverbanks and to such mitigation measures like afforestation and land use planning [10], Modified Normalized Difference Water Index (MNDWI) [11], Salinity[12], Soil-adjusted vegetation index (SAVI) [13] and Vegetation Cover.Their study goals of forecasting riverbank erosion, afforestation and soil fertility as Mitigating techniques are closely related to these variables. This study uses geospatial modeling of river basins and machine-learning baselines such as Random Forest, XGBoost, LightGBM, and LSTM-based deep sequence models,[14] including a hierarchical bidirectional LSTM-GRU architecture with attention and a 2-layer bidirectional LSTM-CNN with attention, for descriptive and predictive temporal analysis of multi-year satellite data. The combination of these models helps to improve the robustness and temporal realism of erosion and growth accretion prediction. In the sampling process, the river corridor is divided into multiple river, region, and left/right bank segments, and multi-year Sentinel-2 and Landsat image sequences are extracted for each segment to create bank-based time-series samples for modeling. The tools are remote sensing and GIS applications like Google Earth Engine, QGIS and ArcGIS to process images and perform spatial analysis and Python libraries to develop machine learning and deep learning models.[15], Quantum Geographic Information System (QGIS) [16] and Aeronautical Reconnaissance Coverage Geographic Information System (ArcGIS) [17] are the Geographic Information System (GIS) [18] that we will need python libraries for Machine Learning. After preprocessing, including band compositing and geometric correction, the model will be trained and validated using confusion

matrices. Techniques like regression, clustering, and time-series forecasting help ensure accurate model validation.

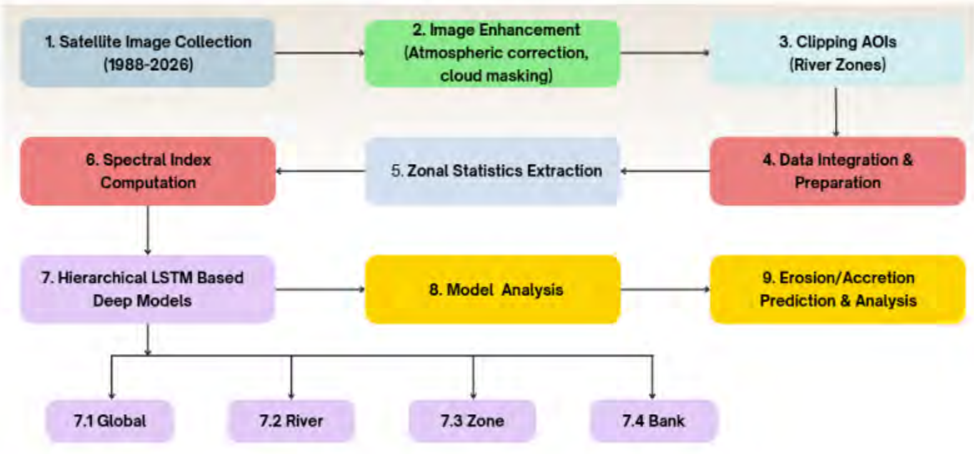


Figure 1.1: Workflow

This flowchart in Fig. 1.1, provides a brief of how to use satellite imagery to analyze river areas. First, the riverbank areas are clipped and the collected images are enhanced. After that, using hierarchical sequence models and other machine-learning methods, the river is analyzed for erosion and accretion, and the results are verified against mapped areas of erosion and growth. With the help of hybrid models, the results are validated. At the end, after the accuracy of the results are evaluated, plans for mitigation, such as afforestation zones and maps of erosion risk are carried out.

## 1.6 Scopes and Challenges

The integration of multi-temporal satellite remote sensing and hierarchical LSTM-based deep learning models provides an innovative framework for predicting riverbank erosion and accretion in Bangladesh. This project offers detailed spatio-temporal insights into river dynamics and bank morphology, improving upon traditional manual methods through automated, data-driven analysis. By leveraging spectral indices, environmental features, and multi-level time-series models (including hierarchical BiLSTM–GRU architectures and tree-based baselines), the study identifies erosion and accretion prone areas with actionable risk visualizations to support sustainable riverbank management and disaster preparedness. This framework can be adapted to similar vulnerable regions facing riverbank instability worldwide.

Despite its strengths, the study encounters several challenges. Data inconsistency, cloud and shadow masking and limited high-resolution imagery can restrict the temporal continuity and accuracy of satellite-derived measurements. The LSTM-based models might not fully capture sudden or localized geomorphological changes driven by natural calamities or human interference, which limits prediction precision. In addition, label noise from automated bankline extraction, class imbalance between low and high erosion years, high computational demand, and the need for extensive training data can create further challenges for model training and deployment.

Successful translation of predictive insights into practical riverbank stabilization and policy actions requires ongoing local engagement, governmental support and sustainable maintenance strategies.

# Chapter 2

# Literature Review

This chapter provides a comprehensive review of existing research on riverbank erosion, accration and land use land cover, with a particular focus on the application of remote sensing, GIS, LSTM and other machine learning techniques.

## 2.1 Preliminaries

River bank erosion, which is a geomorphic process driven by hydraulic forces and weathering, significantly threatens communities and infrastructure, especially in dynamic fluvial systems like coastal Bangladesh. In order to comprehend this complex process the requirements are considering interacting factors within fluvial geomorphology, including erosion, accretion, and lateral migration, governed by hydraulic forces (river flow velocity, discharge) and soil mechanics (soil type, shear strength, cohesion), further impacted by hydrological processes (rainfall) and anthropogenic influences (land use change, dredging, climate change). Remote sensing offers large-scale observation by utilizing satellite imagery like Landsat, Sentinel. These platforms provide multispectral data which enables the derivation of spectral indices. The Normalized Difference Water Index (NDWI) and Modified Normalized Difference Water Index (MNDWI) delineate water bodies and assess changes in water extent. This is crucial for monitoring channel migration and identifying erosion or accretion areas. The Soil Adjusted Vegetation Index (SAVI) assesses vegetation health and cover which is vital for bank stability. These indices, combined with elevation data (LiDAR) gives insights about land cover, topography, and moisture. After that machine learning (ML) algorithms analyze these datasets. Supervised learning (SVMs, RFs) classifies land cover and predicts erosion risk based on input features like spectral indices, soil properties, slope. SVMs construct optimal hyperplanes for class separation while RFs generate predictions from multiple decision trees for improved accuracy. Unsupervised learning (k-means clustering) identifies patterns in unlabeled data, revealing relationships between erosion and environmental factors. Deep learning (LSTM networks) captures temporal dependencies in time-series data, improving erosion and accration prediction over time, particularly useful for analyzing dynamic riverbank changes. Integrating RS data, soil information, and ML allows comprehensive erosion assessment, enabling targeted mitigation strategies: advising against development in high-risk zones of erosion and the likelihood of accretion of new land.

## 2.2 Review of Existing Research

The literature review is structured around several key themes. We first examine international research on river erosion, followed by studies specific to Bangladesh. We then discuss approaches to river erosion analysis that do not employ machine learning or satellite imagery. A study combining physical modeling and artificial intelligence for erosion prediction is also reviewed. Finally, we consider related research on accration of new land and vastly use of LSTM models.

### 2.2.1 International Research On River Erosion

The following international studies analyze riverbank erosion, accretion, and lateral migration utilizing remote sensing (RS) and geographic information systems (GIS). Satellite imagery, geospatial mapping, index calculations (NDWI, MNDWI), and machine learning (ML) methods such as Support Vector Machines (SVM) and automated image classification were the employed techniques to monitor river dynamics. These methodologies help predict land usage changes, analyze spatio-temporal patterns, and improve the accuracy of riverbank analysis. These offer insights into the global implications of riverbank changes on land use and agriculture.

This study, [19] analyses spatio-temporal analysis of the riverbank dynamics using landsat imagery of over a 49-year period (1973–2022) along the Godavari River, especially between the Polavaram Project and Dowleshwaram Barrage. To identify erosion, accretion, and unaffected zones it takes advantage of Remote Sensing (RS), Geographic Information System (GIS) and methodologies like the Support Vector Machine (SVM). Moreover, it also examines land use and land cover changes (LULCC) and how the river structure is influenced by this. The impacts of both natural and human activities on the river morphology is highlighted by providing insights into erosion and accretion cycles which is crucial for flood risk management. The key findings reveal significant shoreline shifts, increased sediment deposition, and dynamic channel alterations, impacting settlements. For safer living and agricultural procedures, stable zones were determined. Even though the study provides critical insights about flood risks and river morphology, it can be further improved with field validation, high-resolution photography, climate change analysis, and hydrodynamic modeling. A very similar article is published in 2024 where it uses MNDWI and sinuosity index to examine lateral migration and erosion-accretion trends.

This paper, [8] provides a spatiotemporal analysis of the Sankosh River's dynamic processes, including lateral movement, growth, and riverbank erosion, from 1987 to 2021 utilizing remote sensing and GIS techniques. It shows large eastward centerline migration, dynamic erosion-accretion patterns, especially in Reach C, and substantial land loss (46.5 $km^2$) and gain (48.27 $km^2$) by using sing Modified Normalized Difference Water Index (MNDWI), Sinuosity Indices, QGIS Tools, and Landsat data. According to the findings, agricultural lands and villages close to the river are vulnerable due to ongoing erosion. By using Landsat imagery of over a 49-year period (1973–2022) this study examines spatio-temporal analysis of riverbank dynamics along the Godavari River, particularly between the Polavaram Project and Dowleshwaram Barrage For identifying erosion, accretion, and unaffected zones it utilizes Remote Sensing (RS), Geographic Information System (GIS), and methodologies like the

Support Vector Machine (SVM) and the Normalized Difference Water Index (NDWI). This study also examines how land use and land cover changes (LULCC) affects river structure. The impact of both natural and human activities on river morphology has been highlighted by this study as well as it provides critical insights into erosion and accretion cycles, crucial for managing flood risks and ensuring sustainable design. The key findings reveal significant shoreline shifts, increased sediment deposition, and dynamic channel alterations, impacting settlements. For safer living and agricultural procedures, stable zones were determined. Although the study provides important information about dealing with flood risks and river morphology, it could be enhanced with field validation, high-resolution photography, climate change analysis, and hydrodynamic modeling. To improve accuracy and direct sustainable riverbank management strategies it is recommended to utilize field validation, higher-resolution data, hydrological modeling, and community involvement. Another similar paper [6] which uses the same applications to document the river study . It uses GIS and remote sensing to figure out the erosion and accretion of riverbanks along the Sudan-Nile River downstream of the Khartoum confluence over a three-decade period (1993–2023). It reveals notable accretion in Dongola (49.91 ha/year) and erosion in Berber (60.12 ha/year) along with net land gain and loss by using geospatial mapping tools and Landsat imagery. The study proposes bioengineering methodologies and community-driven solutions, connecting these dynamics to anthropogenic activities, climate change, and sediment transport in order to provide sustainable management for riverbanks. By including field validation, hydrological modeling, higher-resolution data, and participatory approaches the accuracy can be improved.

This study [20] analyzed a time series of 26 Landsat satellite images acquired by the Thematic Mapper (TM), Enhanced Thematic Mapper Plus (ETM+), and Operational Land Imager (OLI) sensors to monitor changes in the Bazoft River, Iran, from 1985 to 2015 to address the problem of riverbank erosion. A supervised classification approach.was for data processing. For each Landsat image the Modified Normalized Difference Water Index (MNDWI) was calculated to extract water bodies. To delineate the riverbanks manual digitization was used. For quantifying erosion and deposition over time changes in riverbank positions were analyzed. Major findings include significant erosion and deposition along the river, with the greatest changes observed between 62 and 84 km from the Karun-4 Dam. Net deposition was observed over the 30-year period. Manual digitization was one of the shortcomings since this is very time consuming and prone to human error. Future research could improve accuracy and efficiency in processing the Landsat imagery with the use of unsupervised machine learning techniques such as object-based image analysis (OBIA) for automated riverbank extraction.

The study [21] discusses soil erosion in the Siran River Basin,an ecological issue made worse by deforestation, climate change, and human activity. Its objectives are to identify areas that are prone to erosion and estimate yearly soil loss using the Revised Universal Soil Loss Equation, Geographic Information Systems and Remote Sensing. Works on the RUSLE model, deterioration anticipation strategies, and the effects of land use changes are important sources. The study maps and measures erosion risk parameters such rainfall, soil type, land cover, and terrain using GIS and satellite data, utilizing machine learning and remote sensing. It suggests that deep learning and AI-powered prediction models could enhance precision, and real-time monitoring sensor networks and higher-resolution remote sensing data may help comprehend soil erosion dynamics and mitigation methods

### 2.2.2 Riverbank Erosion Research in Bangladesh

Bangladesh is shaped by the dynamic forces of its major rivers like the Padma, Meghna, Jamuna, and Bishkhali. Through processes of erosion and accretion these rivers shape the landforms, influencing ecosystems, and impacting socio-economic conditions. For sustainable river management and disaster preparedness, understanding riverbank morphology using advanced remote sensing (RS) and geographic information system (GIS) techniques is critical. The following studies employ diverse geospatial methodologies to analyze riverbank erosion, sedimentation, and land cover changes over time, providing valuable insights into riverine dynamics.

Padma River Analysis: The paper [2] addressed the morphological changes of the Padma River along Naria Upazila The paper focuses on riverbank erosion, sedimentation, and land cover changes over 42 years (1977–2019). By using multispectral satellite images from the USGS Landsat program, the authors employed supervised classification with the Spectral Angle Mapping (SAM) algorithm in QGIS 3.8 for classification of land cover into water, built-up, vegetation, and bare soil. SAM was chosen for its robustness to illumination variations and topography. Key findings revealed that due to high sedimentation the river became more braided, with significant land cover changes like increased water bodies and decreased vegetation and built-up areas. Erosion shifted from the left to the right bank, with poorly vegetated areas being more vulnerable. In areas where there was reduced vegetation the surface temperature increased. This impacted the local climate and erosion. The study effectively compared changes in land cover, erosion patterns, and surface temperature over the 42-year period by combining quantitative data, visual maps, and thermal analysis. Further research is needed on anthropogenic activities, soil characteristics, and rainfall history. The small study area, lack of detailed temperature quantification (missing band 10 data), and insufficient exploration of river flow dynamics were some of the major limitations. Regardless of that the study provides critical insights for managing erosion near critical infrastructure like the Padma Bridge.

Meghna River Analysis: This paper, [22] also analyzes riverbank erosion and accretion in Hizla Upazila, Bangladesh, by utilizing a combination of remote sensing and GIS techniques. Landsat satellite imagery spanning 31 years (1989-2020), consisting of both Landsat 5 TM and Landsat 8 OLI data, was collected from the United States Geological Survey (USGS) Earth Explorer. These images were then processed on the Google Earth Engine (GEE) platform. To delineate water bodies the Modified Normalized Difference Water Index (MNDWI) was used. The Random Forest (RF) classifier was used to categorize land cover. Significant erosion in the central and western regions and substantial accretion in the eastern part were found in this study. The dynamic nature of the river system and its significant impact on land-use patterns were revealed by the spatial and statistical analyses as well as the significant impact on land-use patterns. Moreover the study highlighted the vulnerability of the region to riverbank erosion along with its associated environmental and socioeconomic consequences.

Jamuna River Analysis: The paper [9] studies riverbank erosion along the Jamuna River in Bangladesh by using geospatial and machine learning techniques to analyze historical patterns and predict future trends. Data was collected from Landsat-7 (2003, 2013) and Landsat-8 (2022) satellite imagery via the USGS Earth Explorer, focusing on Ulipur upazila. Both supervised and unsupervised classification methods were used to process the data. Supervised classification trained the model with previously known land cover types. On the other hand unsupervised classification was used for identifying erosion and accretion patterns without prior training. ArcGIS 10.8 and QGIS 2.18.15 were used for geospatial analysis which quantified changes in erosion, accretion, and unchanged areas over a period of 20 years. To predict future erosion trends an Artificial Neural Network (ANN) model was developed. This projected a significant reduction in erosion and accretion by 2042. Major findings include an increased amount of erosion from 2003 to 2002 (peaking at 4232.48 ha (hectare area) between 2013–2022) as well as a predicted decline to 132.60 ha (hectare area) by 2042. The study suggests a need for adaptive river management. However, this has limitations like data gaps, a narrow regional focus and insufficient exploration of anthropogenic factors. Despite these, the study gives valuable insights for sustainable river management and disaster preparedness.

The study [23] by Ahmed et al. (2012) discusses an investigation of long- and short-term riverbank migration and island development in the Jamuna River in Bangladesh by using multi-temporal Landsat imagery from 1973 to 2003. In this paper, advanced remote sensing techniques have been used to investigate erosion and accretion patterns in the banks of the river. The findings of this paper indicate that erosion on the right bank of the river is greater than on the left bank of the river; also, greater islands show greater stability than smaller islands. However, an important observation of this paper is that river width increases due to erosion and decreases due to accretion; also, the total area of islands increases over time, particularly in early 2000s. This paper also highlights the importance of river islands in overall river geomorphology; river islands usually indicate changes in river flow patterns and sedimentation patterns. Overall, this paper gives important insights into river geomorphology in the region, which is very important for river sustainability in the region.

Then, the paper [24] addresses the critical problem of riverbank erosion along the Jamuna River in Bangladesh. Rather than using any complex machine learning models, the study relies on a rule based, threshold driven classification approach grounded in radar backscatter characteristics. This study shows that Sentinel -1 SAR data can successfully detect riverbank erosion as early as one month after the monsoon season, which is significantly earlier than optical image based national assessments. Accuracy assessment against Sentinel-2 NDVI-based classification showed an overall accuracy ranging from approximately 87% to 91%, depending on the month analyzed. By focusing on the time series Sentinel-1 data and using cloud computing via Google Earth Engine, the authors have effectively explained an early warning capable erosion detection system. But, the study has some downsides: GEE does not provide SAR phase data which hinders the improvement by preventing the use of interferometric coherence; due to the large study area, ground-truth validation was limited; optical data use was restricted by cloud cover and required recalibration for other river systems which depend on empirical thresholds. Overall, this study is a valuable contribution to remote sensing applications in disaster risk management with strong potential for adaptation to other erosion-prone river systems worldwide.

Again, the paper [25] monitors and predicts riverbank erosion in the Jamuna river basin using an integrated framework combining satellite remote sensing and machine learning. The study uses Sentinel-2 Level-2A satellite imagery acquired from the COPERNICUS/S2 HARMONIZED dataset available in GEE. Sentinel-2 data were chosen due to their high spatial resolution and frequent revisit time which are well suited for monitoring rapidly changing river systems like the Jamuna. Its integrated and automated workflow using GEE enables scalable and reproducible analysis. Still, the extremely high values for linear regression suggests possible overfitting. Additionally, the absence of hydrological variables such as discharge and sediment load limits the physical interpretability of the models. In another paper [34], the authors have used a physically based approach for predicting fluvial erosion, rather than remote sensing or machine learning. This study applies hydrodynamic modeling and the excess shear stress method to estimate erosion rates with the aim of supporting river management and erosion mitigation planning in Bangladesh. By examining hydraulic forces and soil properties, it provides insight into the mechanisms of bank failure which is crucial for protecting communities in erosion-prone areas.

Moreover in the paper [26] satellite imaging and geospatial analysis are used to analyze the morphological changes that have occurred in Bangladesh's Bishkhali estuary during the last 25 years (1991–2015). By uncovering crucial erosion and accretion zones through indicating changers in channel area, length, width, and sinuosity it was uncovered that towns like Betagi and Bamna are at risk. Sediment processes were reflected in the noteworthy island development and fluctuating accretion rates. Using QGIS and Landsat imagery the study monitored changes in island growth and increase in channel area of 6.74 sq. km. Higher-resolution data, sediment and climate models expansion , and socioeconomic consequences can be taken into account for improved estuary management and policy planning.

### 2.2.3 Traditional and Numerical Modeling of River Erosion

The three papers herewith which didn't use any form of machine learning rather it utilized numerical models.

The main problem addressed in this [27] was the long-term impact of dredging on the fluvial geomorphology of the Jamuna River, focusing on erosion, sedimentation, and channel dynamics. The primary data was collected through field measurements (cross-sectional data, sediment concentration, water depth, and velocity) and satellite imagery (2000-2018) of mainly dry-season images (to maintain cloud/water variability) for consistency in analysis. Numerical modeling (not machine learning) was used to process the data. It was done with two methods: Method-I (depth-velocity relationship) and Method-II (depth-velocity-sediment concentration relationship). These are supervised approaches based on physical laws and empirical equations. The study revealed that dredging had a limited long-term impact. Moreover, with higher sedimentation (60-80) percent where dredging crossed sandbars and near the Sirajganj Hardpoint there were significant channel shifting was identified in this study. After flow-diverting structures were built the right channel became dominant.

Numerical models effectively predicted erosion-sedimentation patterns, aiding future river management was the major outcome for this study. The major limitation was the use of one-dimensional models, which may not fully capture the complex three-dimensional dynamics of braided rivers. It doesn't even use any RS to get images.

In this research,[28] emphasized riverbank erosion, channel relocation, and changes of LULC alongside the Arial Khan River between 1993 and 2024. The study analyzes time-series Landsat images from 1993, 2003, 2013, and 2024 that were collected from the USGS Earth Explorer through using GIS and remote sensing techniques. Geometric correction, band composite generation, and scan line error removal were used in the preprocessing of the data. For establishing LULC classes supervised classification with a maximum probability algorithm was applied. This was verified by ensuring (85-92) percent accuracy based on the confusion matrix. The quality vegetation was evaluated using NDVI analysis. This indicated that the quality was worsening with greater coverage. The study discovered that 5142.60 ha (hectare area) of land were lost to erosion with an average channel shift of 0.66 km over a period of 31 years compared to 4756.52 ha (hectare area) of anointed land. Higher erosion was detected in Muladi Upazila when the centerline displacement and sinuosity were analyzed with ArcGIS tools. The results demonstrate how the land has changed significantly and assist in the guidance of sustainable management. Because of the dependency of satellite data, the predictive power was inadequate. Through providing automatic classification, increasing accuracy, and providing dynamic erosion trend predictions as well as integrating machine learning or deep learning can significantly contribute towards much more reliable solutions.

The following paper did not use satellite imagery but used measurements from BWDB and then utilized regression models.

The study [29] predicted bed level changes and riverbank shifts in Bangladesh's Jamuna River using hydraulic modeling and machine learning (ML). Data acquisition relied on empirical field measurements from BWDB (2018–2019) which includes cross-sectional surveys, hydrological records such as discharge, water levels, and sediment concentrations. Bathymetry was reconstructed from cross-sections, while hydrodynamic variables (velocity, water levels) were derived via 1D/2D modeling (HEC-RAS, RIVERFLOW 2D). A supervised regression model in MATLAB linked to hydrodynamic inputs like overbank discharge, velocity to erosion rates, incorporating bed-level effects from 2D simulations. Key findings identified right-bank erosion up to 12m and left-bank deposition of 1–20m, with bed-level integration improving predictions ($R^2$=0.86). The study omitted satellite data (e.g., SAR, LiDAR), limiting spatiotemporal resolution and scalability. Future research should integrate multi-sensor remote sensing (Sentinel-2, InSAR) for enhanced morphodynamic monitoring as well as adopt advanced neural networks to address complex geomorphic interactions beyond traditional regression.

The study [24] proposes a radar based , cloud independent remote sensing approach to detect eroded land and settlements shortly after the monsoon season, overcoming the limitations of traditional optical-image based assessments. This study primarily uses Sentinel-1 SAR Ground Range Detected (GRD) imagery accessed through

Google Earth Engine (GEE). Sentinel-1 provides C-band SAR data in interferometric Wide Swath mode with VV polarization, a 10m x 10m spatial resolution and a 6-12 day revisit cycle, making it particularly suitable for cloud-prone regions like Bangladesh during the monsoon season. In addition , Sentinel-2 optical imagery was used only for validation through NDVI based land cover comparison, while all datasets were processed entirely within GEE without requiring local storage or high performance computing resources. The methodology consists of three major components: land cover classification, settlement detection and erosion detection. The authors have applied a deterministic threshold-driven classification approach based on statistical properties of SAR backscatters values. By utilizing the cloud computing through GEE and concentrating on time-series Sentinel-1 data, the authors effectively showed an erosion detection system with predictive features. The paper [30] adopts traditional, process based modeling rather than data driven AI approaches. Hydrodynamic simulations using the Surface Water Modeling System (SMS) and SRH-2D provide estimates of flow velocity and boundary shear stress along an 8.21 km reach of the Jamuna River. Erosion rates are computed using the excess shear stress process, that is a physically interpretable model linking applied shear stress with soil resistance. These models assume steady and quasi-unsteady flow conditions and treat the riverbank as a layered system, with erosion initiating in the weaker upper soil layer which highlights the role of flow hydraulics and soil mechanics in predicting riverbank retreat.

#### 2.2.4 Hybrid Physical-AI Models for River Erosion Prediction

Here's a few papers where both physics model and AI was used to predict erosion.

This paper [31] generated data using physics models and then used machine learning and deep learning to get the final output. Due to the limitation of real-world data a physics based model was used to simulate the erosion and generate the necessary training data for the AI model. By using equations like Shallow Water Equations (SWE) and Manning's equation, the numerical model simulates water flow as well as water velocity, depth, and discharge. It also simulates sediment transport (morphodynamics) using the Exner equation by considering sediment load due to secondary currents and bed slope effects, and accounts for sediment input from bank erosion. Lastly, it simulates the erosion of riverbanks itself by calculating erosion and deposition at the bank top to bottom. The output of this numerical model is simulated changes in river cross-sections, including vertical displacement of the riverbed (Dg), horizontal displacement of the riverbank (Dyb), and changes in channel width (Bb), which is then used to train the AI. The solution proposed is a novel AI-based method that incorporates this simulated data. The data was processed through a two-stage approach: 1) unsupervised Machine learning (Self-Organizing Map) categorized river sections based on geomorphology; 2) supervised deep learning (Long Short-Term Memory) (which is derived from RNN) trained a model to predict erosion using the categorized data and input factors like water flow and channel slope. The key finding is that this hybrid AI model significantly outperforms traditional methods when it comes to predicting riverbank erosion. However, a potential limitation is the possibility of bias in the training data, which could affect the model's applicability to broader scenarios. Overall, AI, through ML for data organization and DL for model building, paves the way for more accurate riverbank erosion prediction.

Apart from the studies on riverbank erosion, the following papers offer valuable insights into soil analysis, agricultural practices, and afforestation techniques relevant to our research on mitigating riverbank erosion through artificial afforestation.

Hybrid approaches that combine physical understanding with Ai techniques have emerged to address limitations of purely numerical models. In the paper [25], machine learning models such as XGBoost, LightGBM and CatBoost are trained on spatial, temporal and spectral features derived from Sentinel-2 imagery. By combining riverbank distance, lagged indices and water related spectral features, these models can predict riverbank changes more accurately than traditional models alone.

### 2.2.5 The Dynamics of Riverbank Accretion and Relevant Factors

In these papers ML and Remote sensing was used Riverbank Accretion and Relevant Factors.

Riverbank accretion, a deposition of soil along the banks of rivers, is a must in forming rivers and streams, affecting channel behavior, and helping to sediment economies. The concept of accretion across many river systems has been strengthened by recent research employing GIS and satellite imaging technologies. Using more than two decades of Landsat imagery along with Google Earth Engine, [4] constructed the first globally accessible dataset of riverbank accretion and deformation, which covered more than 370,000 km of rivers longer than 150 meters. Based on their outcomes, accretion rhythms overwhelmingly mimic changes in erosion, with width of rivers revealing up as the most reliable forecast. Land volume, plant life, mineral deposits, and habitation are secondary consequences. Compared to more robust systems in Europe and Canada, massive tropical rivers that included the Amazon and the Ganges-Brahmaputra-Meghna displayed high sedimentation ratios.Using multi-temporal Landsat photos from 1973 to 2015, [32] conducted an analysis of the region of the Dudhkumar river in Bangladesh. They discovered that active accumulation of sediment caused a boom in island (bar) existence over time, and that the left bank exhibited both higher long-term and short-term accretion. Additionaly, [19] investigated the Ramganga stream in India within a 91-year span through determined that bend emigration and stream disappearance prompted accretion to predominate throughout particular periods of time, specifically on the left bank. Accurate monitoring of changing river valleys and boundary lines have been rendered possible using imagery from space including the Modified Normalized Difference Water Index (MNDWI). In a similar way, [8] monitored the structure of the Barak River throughout 33 years and concluded that accretion sometimes overtook erosion, especially on convex meanders wherein lower velocity of water supported sedimentation. This research additionally emphasized the manner in which manufactured effects like building and agricultural practices, along with elemental characteristics like low gradient, microbes, and vegetation along rivers, regulated sediment processes. All of these studies demonstrate how vital continuous satellite imaging is to accurately measure the spatial and temporal characteristics of riverside accretion. The studies additionally address the socioeconomic consequences of accretion, especially shifts in cultivable land, the steady state of riverbanks, and the dangers of habitation. A potential strategy to anticipate future accretion-erosion movements is the integration of space imagery with machine learning models, for example Long Short-Term Memory (LSTM) systems. This is crucial for systems of early warning, efficient river management, and to minimize the hazards of lateral bank displacement in dynamic wetlands habitat.

In the paper [24], riverbank accretion is indirectly assessed by analyzing temporal changes in land cover derived from Sentinel-1 SAR imagery. Areas transitioning from water or sand to vegetated surfaces indicate accretion processes which are largely influenced by seasonal hydrological variations, sediment deposition and post-monsoon flow dynamics. Riverbank dynamics in the Jamuna are influenced by many factors such as monsoon floods, seasonal variation, and increased water flow. Key factors identified in the study [25] include spectral water indices (e.g., mNDWI), vegetation cover (NDVI, EVI) and distance from the riverbank. These findings highlight the complex interplay between hydrological, geomorphological and climatic drivers in shaping riverbank changes.

The study [30] identifies key factors influencing riverbank erosion dynamics along the Jamuna river. Hydraulic forces, particularly during peak monsoon discharges are the primary drivers of erosion. Soil properties, especially the composition of the upper sandy silt layer, determine bank susceptibility with weaker soils leading to rapid retreat once shear stress thresholds are exceeded.

### 2.2.6 Utilization of LSTM

In these papers Long Short-Term Memory (LSTM) Networks used to Predict Riverbank Erosion and Forecast Water Level.

The implementation of Long Short Term Memory (LSTM) networks systems for determining water levels along with modeling the erosion of riverbanks, has been rising in popularity subsequently because of the ability it has for recording sophisticated timelines and nonlinear connections between them. In order to enhance the exactness of riverbank erosion forecasting [33] designed a hybrid model methodology that utilizes LSTM with physics-driven computations. Hydrodynamic as well as soil transport scenarios have been recreated in their work using fake data sets created using Manning's equation, Shallow Water Equations (SWE), and also the Exner equation. The LSTM models that predict the changing position of riverbanks as time goes on were developed using these types of data. A two-step procedure was chosen: LSTM models have been utilized to represent temporal erosion behaviors after geomorphological processes were categorized at first using Self-Organizing Maps (SOM). Considering the findings, the combined approach performed noticeably better than conventional experimental and mathematical models, specifically when it came to locating zones that are prone to erosion and explaining the growth of pathways. In an associated research project, [33] analyzed continuous data from four hydrological stations including LSTM models to calculate short-term level of water in the Mekong River.With Root Mean Square Errors (RMSE) as little as 0.09 meters and Nash-Sutcliffe Efficiency (NSE) rates over 0.98, the model they developed displayed extraordinary precision in forecasting. The study highlighted the usefulness of LSTM for handling flood risks and agricultural development in the unstable Mekong Delta by focusing its potential to regulate dynamic waterway settings with only limited data. The benefit of LSTM in river level prediction in the Mekong Delta was further confirmed by [14], who once again reported large NSE amounts and determined that LSTM models need less testing and inputs than physically established algorithms, making them ideal for areas with insufficient tracking structures. On a different geographical scale, [34] conducted a comparative study on the Goose River in North Dakota, where LSTM models were benchmarked against the HEC-HMS hydrologic model. The LSTM approach demonstrated a strong ability to predict streamflow, especially during peak discharge and snowmelt events, with an NSE of 0.97 and low Percent Bias (PBIAS), despite some limitations in highly variable winter conditions. Collectively, these studies underscore the growing consensus that LSTM models, either standalone or in hybrid form offer a robust, data efficient, and scalable solution for riverbank erosion forecasting and water level prediction. They offer a helpful package of instruments to those in charge of water resources, particularly in the light of fluctuating hydrological systems, scarce field information, and global warming. The paper [24] does not utilize LSTM networks; however, it produces multi-year Sentinel-1 SAR time series that capture both seasonal and interannual riverbank dynamics. These temporally dense SAR datasets are well suited for LSTM based models, as they are designed to learn long term dependencies and temporal patterns. Therefore, the outputs and data structure of this study could be effective in future research for predicting riverbank erosion and forecasting river water levels in data driven frameworks.

## 2.3 Summary of Key Findings

The literature review points out key trends when it comes to research in the field of riverbank erosion. International studies tend to use remote sensing, GIS, and machine learning for analyzing river dynamics such as erosion, accretion migration with the use of satellite imagery and spectral indices. For instance, studies that utilized Landsat and Sentinel imagery with indices like NDWI and MNDWI have successfully mapped erosion hotspots and quantified land loss/gain across large river basins. The outcome of these studies highlights the effectiveness of these techniques for large scale analysis. Oftentimes they achieved high accuracy in land cover classification and change detection. Research on Bangladeshi rivers, mainly the Padma and Jamuna, demonstrates the applicability of similar geospatial techniques for assessing erosion vulnerability and predicting future trends in this dynamic environment. Traditional numerical models and field measurements often have limitations in handling the volume and complexity of data needed for comprehensive, long-term analysis. However these models are crucial for understanding river geomorphology.There is a trend of hybrid physical-AI models which combine equations with ML (e.g.,LSTM, SOM). The accretion of riverbank nearly resembles erosion patterns according to new studies integrating satellite images and GIS. River width has emerged as a key indicator of sediment growth. In particular high rises in deposition are seen in tropical rivers which are impacted by both natural and man-made factors like cover of vegetation, agricultural practices and flow rate. So, the continuous monitoring of accretion zones using remote sensing data has enhanced the knowledge of sediment pattern and its impacts. Furthermore, the pairing of accretion analysis song with Long Short-Term Memory (LSTM) networks is established as an effective technique to predict riverbank evolution. The LSTM-based models, especially those utilized together with physics-driven models, have displayed remarkable precision in modeling accretion–erosion changes, projecting water levels, and figuring out erosion-prone zones.These improvements suggest that LSTM approaches provides a comprehensive and flexible technique for managing water level fluctuation and minimizing the risk of flood and erosion. This shows promise for enhanced prediction accuracy by integrating process-based understanding with data-driven learning. Studies which incorporate soil data and land use practices utilizing remote sensing and ML (e.g., NDVI for vegetation monitoring) directly coincide with our research focus on relation between the aforementioned factors and erosion. Hydrodynamic and soil based modeling reveals the underlying mechanisms of erosion, particularly the critical role of peak monsoon discharge and bank material resistance in triggering rapid bank retreat. In contrast, optical remote sensing integrated with machine learning enables high resolution, automated detection and prediction of spatial erosion patterns over long time periods, while Sentinel-1 SAR time series analysis provides a cloud independent early warning capability for identifying erosion impacts shortly after monsoon events. These trends coincide with our research direction of integrating satellite/soil data with ML for targeted erosion detection as well as suggesting land management. Our objectives were to analyze erosion and accretion patterns, mapping susceptible areas as well as combining remote sensing indices with ML. This review addresses these objectives thoroughly.Many of the papers lack a certain comprehensive approach. They either focus on prediction or mitigation. Only a few integrate soil fertility with targeted interventions. Some rely on manual digitization or have limited resolution. Validation and transferability are often weak. Our research aims to address these gaps through a holistic approach, integrating soil fertility with targeted mitigation, using high-resolution data and automated ML, and emphasizing robust validation.

# Chapter 3

# Requirements, Impacts and Constraints

After establishing the erosion problem and research foundation in earlier chapters, this chapter presents the practical requirements, societal-environmental impacts, and strategic roadmap for the practical implementation of this study.

## 3.1 Final Specifications and Requirements

Our final system is a hierarchical Bidirectional LSTM-GRU architecture with attention that predicts riverbank erosion and accretion based on multi-year satellite time series and geometric features that are auxiliary. The model consumes bank-wise sequences of vegetation indices, water occurrence, land cover, elevation/ slope, and proximity measures, and provides annual or seasonal erosion and accretion indicators of each bank segment. The technical/methodological requirements will include:

- A time sequence of labeled bankline positions of erosion/accretion polygons based on multi-temporal satellite imaging like Landsat, Sentinel, which is already pre-processed in geometric and radiometric terms.
- Harmonized datasets of predictors such as NDVI, water occurrence, LULC, DEM derivatives, distance to chars and channels, assembled to a shared grid and time.
- An architecture Python-based sequence modeling pipeline, with training of the multi level hierarchical architecture of BiLSTM-GRU and attention layers.
- River/zone/bank level data segmentation and cross-validation to prevent spatial and time leakage and use of the most suitable classification.

**Data and software requirements:**

- Remote sensing sites: Google Earth Engine / QGIS / SNAP to gain access to the images, compose and extract bank lines.
- GIS tools: QGIS/ ArcGIS used to vectorize the banks, create the erosion/accretion polygons and spatial joins to the socio-environmental data.

- Numerical and ML stack Python, NumPy, Pandas, PyTorch/TensorFlow, scikit-learn, and Colab or local workstation with enough RAM and GPU.
- Hydrological and hydraulic datasets(For future work): discharge and water-level time series, gridded rainfall like IMERG, ERA5, and, where possible, outputs from 1D/2D hydrodynamic models.

Resource-wise, the project has to be connected to the internet by a good connection to download EO data and have some local storage to store multi-year images and labels and have reasonable computational resources to train the model and hyperparameter tuning.

## 3.2 Societal Impact

River erosion destroys thousands of people, land, habitats and livelihoods of char and floodplain people every year in Bangladesh. More proactive relocation, embankment strengthening and land-use planning can be facilitated by using predictive modelling frameworks that pre-delineate high-risk banks, which will reduce forced migration and livelihood disruption.

In terms of health and safety, the existence of more accurate erosion forecasts will help prevent sudden collapse of homes, roads and other critical infrastructure such as schools, markets, health centres, etc., reducing the risk of accidents and injuries caused by disasters. In terms of limited resource allocation, this model is socio-economically friendly, especially in terms of protective works, compensation and social protection programmes for affected families.

There are also legal and cultural aspects: river bank erosion changes administrative boundaries, land tenure and ownership, and it usually affects marginal char communities who have very little formal documentation. Transparent and data-based risk maps can facilitate evidence-based policy-making and reduce conflicts over land and rehabilitation as they provide a more objective basis for identifying affected households and prioritizing assistance to them.

## 3.3 Environmental Impact

The direct environmental impact of the project is quite small as it is mainly based on open-source satellite data as well as computing resources, without any new physical infrastructure. The advantage of remote-sensing-based monitoring is that it does not require large field campaigns and boat surveys which consume a lot of energy and cause disruption to the river ecosystem, unlike field-only methods.

But the indirect environmental impact of using model output is considerable. Accurate identification of erosion hotspots can contribute to the efficient placement and design of river training works, reservoirs and dams, and can reduce additional engineering and consequent environmental disruption. Meanwhile, structural interventions to repair eroded banks can alter sediment transport, aquatic habitats and floodplain connectivity; Therefore, implementation of the model should be incorporated into integrated river basin management that balances environmental, social and economic trade-offs. The modelling framework indicates areas where non-structural interventions such as buffer zones, afforestation, controlled use of floodplains would be more sustainable than strict engineering, and can encourage climate-resilient and environmentally friendly adaptation interventions.

## 3.4 Ethical Issues

The use and representation of data and the underlying decisions involve essential ethical concerns:

- **Privacy and fairness:** The model relies largely on satellite- and physical-based data; however, any incorporation of socio-economic or household-based data should not compromise privacy and stigmatize a particular community as being at high risk, in a manner that could reduce access to credit, land, or services.
- **Inequality in decision-making:** The erosion risk map may be used to determine the location of dams or to provide compensation; care should be taken to ensure that model-driven decisions are not biased against poor communities and in favor of better-connected individuals or the wealthy.
- **Transparency and explainability:** Deep learning models can be obscure and it is a professional's duty to disclose model assumptions, performance, and limitations, especially when the results justify decisions on extensive public spending or rehabilitation.
- **Responsibility and Abuse:** Model predictions should be made as probabilistic and uncertain rather than deterministic predictions, and not overconfident in individual numbers, to prevent overconfidence in single predictions and misuse in legal battles or political compromises over land and compensation. Researchers and practitioners should be cautioned to detail any uncertainties, engage local stakeholders where possible, and apply the model as an aid to decision-making, as opposed to alternative participatory and legal approaches.

## 3.5 Project Management Plan

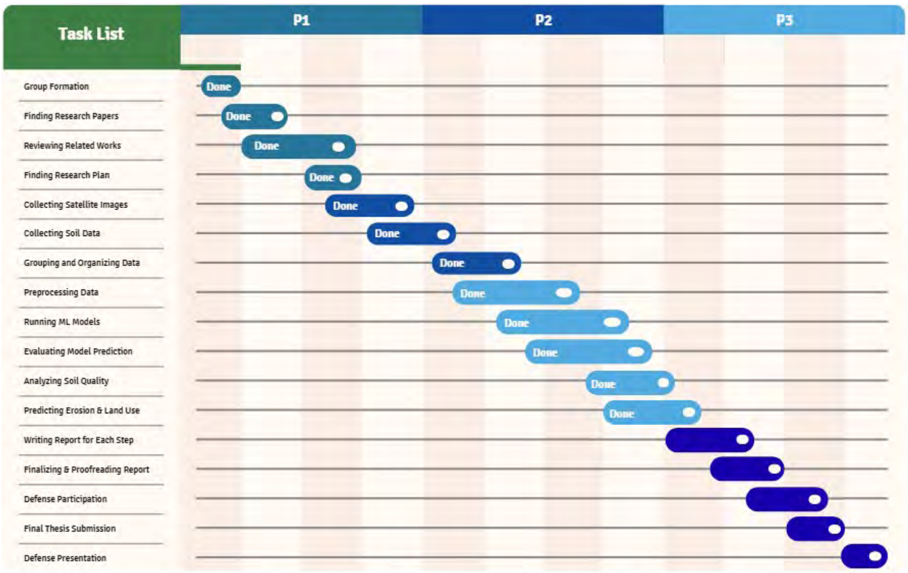


Figure 3.1: Project plan for one year.

The Gantt chart in Figure 3.1 depicts an outline of the project timeline which spans from P1 to P3.. The project initially focuses on group formation which starts on P1 and advances through key stages like literature review and research planning throughout P1. Data collection and processing from satellite imagery and soil data are also set to be in P1.The subsequent phase involves running machine learning models, evaluating model predictions, analyzing soil quality and predicting erosion and land use, which is anticipated to take place in P2.Finally, the project concludes with report writing, thesis preparation, and the defense presentation, scheduled for P3. This Gantt chart provides visual representation of the project timeline which allows for effective project management and progress tracking towards the final thesis submission and defense presentation.

## 3.6 Risk Management

Key project risks and mitigation strategies:

1. **Data quality and availability risk:** Lack of cloud cover, sensor gaps and gaps in hydrological records can interfere with the reliability of the predictor variables and the labeling of erosion and growth.

   **Mitigation:** Multi-sensor datasets, i.e., their integration (Landsat and Sentinel imagery) and optical data integration with SAR where necessary, will address this risk. Robust bankline extraction algorithms will be used and conservative quality masking will be used. Uncertainty will be explicitly factored into the training labels to reduce bias and further propagation will be used where applicable.

2. **Overfitting and poor generalizations:** Deep learning models fitted to a small number of river channel data may learn local patterns too strongly and fail to perform well when applied to unseen rivers or regions.

   **Mitigation:** Cross-validation will be conducted on other rivers and geomorphic regions to increase generalizability. Overfitting will be controlled by regularization methods, premature dissociation, and comparison with simple baseline models. Transfer learning and multi-task learning techniques will also be discussed when multi-river datasets are available.

3. **Computational limitations:** Classifier and sequence-based models, especially those with long-term inputs, can be computationally expensive and require extensive memory and training on GPUs.

   **Mitigation:** Model architectures will be optimized to provide a balance between performance and efficiency. Mini-batch training, mixed-precision computation, and test schedule-based care will be used. Heavy model architectures will be replaced by lighter model architectures in cases of computational limitations.

4. **Potential for misunderstanding by stakeholders:** Potential loss or increased risk maps may be mistaken by non-experts as a deterministic prediction, which may lead to inappropriate decisions.

   **Mitigation:** Outputs will be provided with clear legends, uncertainty indicators and explanatory notes. Maps will be supplemented with brief written or verbal descriptions that explain assumptions, limitations and appropriate use cases.

5. **Institutional and adoption risks:** It is possible that operational agencies may be reluctant to adopt machine-learning-based tools due to low technical capacity or familiarity with data-driven approaches.

   **Mitigation:** Project deliverables will be modeled so that they can fit seamlessly into existing GIS processes and they will be in standard formats, including maps and summary tables. Potential end-users will be consulted at the outset and extensive documentation will be provided to facilitate understanding and long-term adoption.

# Chapter 4

# Proposed Methodology

This chapter contains the overall methodology, which includes the selected Bidirectional LSTM-GRU hybrid model with attention mechanism and other models such as CNN-LSTM with attention mechanism, Multi Level LSTM, Random Forest, XGBoost, LightGBM, the entire multi-decadal satellite data collection pipeline, geospatial processing through spectral indices (NDWI, NDVI, NDBI, SAVI), and classifier training that transforms satellite data into a precise prediction of riverbank erosion and accretion.

## 4.1 Methodology:

The method used to find riverbank dynamics in several rivers in Bangladesh is meant to be accurate, repeatable, and scalable. It deals with the difficulties of defining riverbanks, identifying left and right banks, extracting shorelines, and measuring erosion and accretion processes. This method is mostly about finding and keeping track of changes in the shape of riverbanks over long periods of time, such as when char is found. The main goals are to accurately find the lines of the riverbank, always tell the left and right banks apart, and measure erosion and accretion at different levels. These goals are pursued despite practical challenges, including multi-sensor satellite data, extensive temporal coverage (1988–2025), cloud interference, and spatial variability in river width and morphology.

The methodology consists of several steps: defining Areas of Interest (AOIs), preparing satellite images, extracting water features, extracting riverbank lines, finding the best line, finding chars, classifying left and right banks, and analyzing area and change. Each step helps make a strong, stable model that can show the riverbanks at different times.

The first step began with selecting AOIs that were manually clipped from seven rivers -Baleswar, Bishkhali, Payra, Shibsa, Pasur, Karnaphuli and Surma. Baleswar, Bishkhali and Payra are Coastal rivers, Karnaphuli is in Southeastern hilly region, Shibsa and Pasur is in Sundarban Estuarine region and Surma is in Northeastern region. To visualize and use as a sample, 86 AOIs were clipped. Then, to collect data and pre-process them, Sentinel 2, Landsat 5, and Landsat 7 were used. The pre-selected AOIs were utilized to compute indices, raster vector water polygons, bank statistics per bank , Pink line, Best line detection ,Continuous line, Continuous bank, Orange line, char (river island), etc.

### 4.1.1 Spatial Zonation and Area of Interest Definition

This study incorporates river systems from multiple geomorphological regions of Bangladesh, including the southeastern hilly region (Karnaphuli), the coastal region (Payra, Bishkhali, and Baleshwar), the Sundarbans estuarine system (Shibsha and Pashur), and the northeastern floodplain (Surma). To represent the longitudinal and cross-sectional variation of the respective rivers and to facilitate uniformity in analysis of erosion and accretion at the zone-level, several spatial areas were outlined as spatial areas of interest (AOIs) to ensure that each chosen river is represented by multiple distinct areas of interest.


Figure 4.1: AOIs of the Southeastern Hilly Region River (Karnaphuli)

Figure 4.1 represents the spatial distribution of the multiple areas of interest along the Karnaphuli River which located in the southeastern hilly region of Bangladesh. A total of 17 sequential zones (AOIs) were delineated along the river course, starting from the downstream outlet as Zone 1 and progressing upstream to Zone 17 to capture longitudinal geomorphic variability.


Figure 4.2: AOIs of Coastal Rivers (Baleshwar, Bishkali, Payra

Figure 4.2 represents the coastal region and depicts three major river systems, including the Baleshwar River on the left, the Bishkhali River in the middle, and the Payra River on the right. The rivers were divided into sequential zones starting from the upstream end as Zone 1, where 10 zones were identified for the Baleshwar River, 13 zones for the Bishkhali River, and 14 zones for the Payra River to capture the spatial variability of coastal erosion and accretion processes.

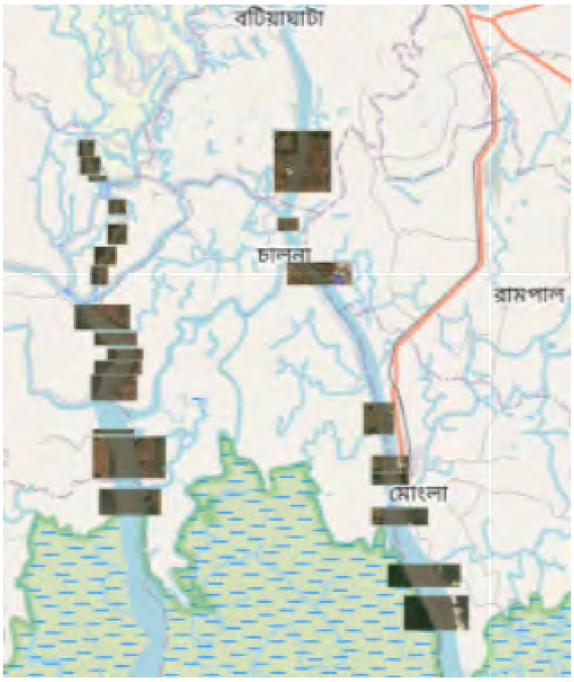


Figure 4.3: AOIs of Sundarban Estuarine Rivers (Shibsa and Pasur)

Figure 4.3 the Sundarbans estuarine region, where the Shibsa River (15 AOIs) on the left and the Pashur River (9 AOIs) on the right were segmented sequentially from upstream to downstream starting at Zone 1 to capture spatial variability in estuarine erosion and accretion processes.

Figure 4.4: AOIs of Northeasten River's (Surma)

From the map in Figure 4.4, it can be seen that sequential distribution of eight Areas of Interest (AOIs) along the Surma River in Sylhet, tracking the river's meandering flow from the upstream segments near the Sunamganj-Sylhet Highway (Zone 1) on the left to the downstream sections past the Sylhet-Beani Bazar Highway (Zone 8) on the right.

### 4.1.2 Data Visualization

**Flow Line Detection:**
To detect the AOIs and geometric left/right alignment, three attempts were tried. In the first attempt, the best line detection procedure has been established to generate a reliable geometric reference for distinguishing left and right riverbanks by recording the predominant flow direction inside each Area of Interest (AOI). First two types of trial lines are generated: vertical and diagonal lines, where the first one takes samples along the width of the AOI and the second one captures slanted river sections and joins the corners in a grid. Using the best line selection formula, the yellow line captures a dominant direction of the river flow, and that is used as a reference point for splitting AOIs and assigning banks. The continuous Purple Line joins the yellow lines and simply produces an unbroken and continuous line. It basically compensates for the limitations of the yellow line. For curved areas, purple lines work best to provide accurate geospatial left and right banks. The pink AOI marks a compact box that closely follows the yellow and purple shoreline lines. The orange AOI is drawn wider, stretching along the original limits to capture the full river path, including bends and nearby banks. The river polygon was enlarged by 500 m to create a buffer, and any sections beyond the study border were cut using the AOI. This process collects islands, Chars, and broken bank parts. A more precise and continuous portrayal of riverbanks is essential for identifying vast or multi-channeled river systems with varying widths.

$$\text{Bank}_{\text{continuous}} = \text{river.buffer}(500) - \text{river} \tag{4.1}$$

By expanding the river polygon by 500 m., this formula creates a buffer that captures the whole river route, including smaller landforms.

$$\text{Bank}_{\text{left}} = \text{river.split}(\text{left}) \tag{4.2}$$

$$\text{Bank}_{\text{right}} = \text{river.split(right)} \tag{4.3}$$

These formulas are used to detect the left and right bank of a river based on the river's centerline or best-fit reference line.

The interface between water and land defined the shoreline,

$$W(x, y) = \begin{cases} 1 & \text{if } NDWI(x, y) > T \\ 0 & \text{otherwise} \end{cases} \tag{4.4}$$

Where the threshold $T \approx 0$ was empirically derived as optimal for this region. This thresholding process ensures that pixels corresponding to water are classified as 'water' and the others as 'land'. In this study, erosion is measured by identifying areas where land that existed in 1988 is now underwater.

The spatial difference was computed as:

$$\Delta S = S_{\text{current}} - S_{\text{baseline}} \tag{4.5}$$

This yields two distinct zones: Erosion Zone– areas where historical land has been lost to water (purple line moved landward)- Accretion Zone– areas where new land emerged from water (purple line moved riverward). To compute the previous years, the following formulas are used:

$$\Delta S(1) = S_{\text{current}} - S_{\text{current-1}} \tag{4.6}$$

$$\Delta S(2) = S_{\text{current}} - S_{\text{current-2}} \tag{4.7}$$

$$\Delta S(3) = S_{\text{current}} - S_{\text{current-3}} \tag{4.8}$$

The erosion area is computed as:

$$\text{erosion} = B_{\text{w}} \cap B \ \setminus \ C_{\text{w}} \cap B \tag{4.9}$$

where $B_{\text{w}}$ is `baseline_water`, $C_{\text{w}}$ is `current_water`, and $B$ is `bank` Here the erosion is computed only for the baseline year, 1988

$$\text{erosion\_area} = \text{erosion.area}(1) \tag{4.10}$$

Accretion of the baseline year, 1988 was computed as:

$$\text{accretion} = C_{\text{w}} \cap B \ \setminus \ B_{\text{w}} \cap B \tag{4.11}$$

where $C_{\text{w}}$ is `current_water`, $B_{\text{w}}$ is `baseline_water`, and $B$ is `bank`.
Similarly accretion for any other year could be found using this formula.

$$\text{accretion\_area} = \text{accretion.area}(1) \tag{4.12}$$

For every time pair, the average NDVI, NDWI, and NDBI values within each AOI were computed to represent vegetation vigor, surface moisture, and urban or barren features. Additional indices such as SAVI, NBR, BAI, and MSI were also computed as needed to refine vegetation or moisture interpretation.

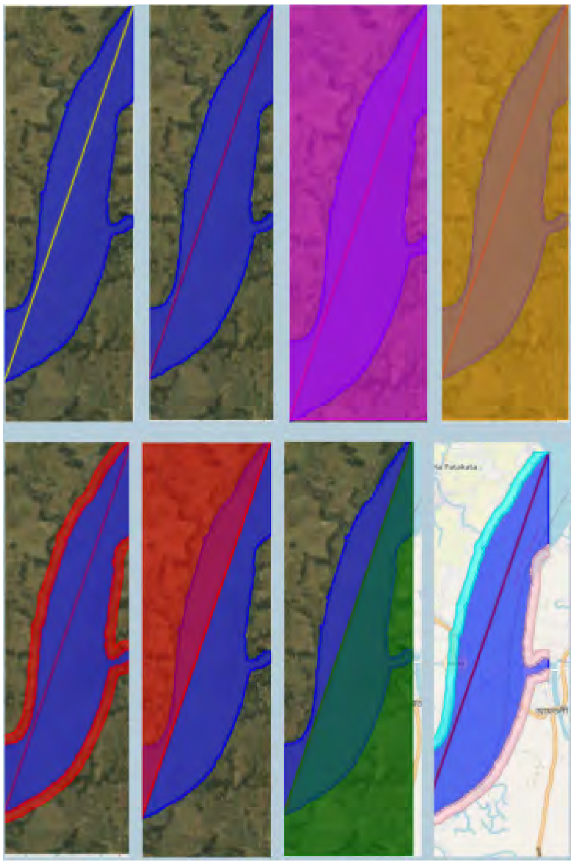

Figure 4.5: Best_Line_Detection_Analysis

This figure 4.5 shows the different stages of the best line detection. The process starts with a yellow line that has been refined to a continuous purple line, representing the principal axis of a river. This purple line is the base for detecting the banks. The algorithm uses a buffer (in the red zone) created around the river to determine a spatial extent to divide the surrounding landscape into what is called the "left portion" and "right portion" using this central purple line as a divider. Any char (river island) that is within the left portion is considered the left bank and any "char" that is in the right portion is considered the right bank. The line.intersection(water_geom,1) function will be used to locate the line that intersects with the most amount of char (river island), thus providing an accurate axis along the river's main channel which will subsequently be extended and simplified.

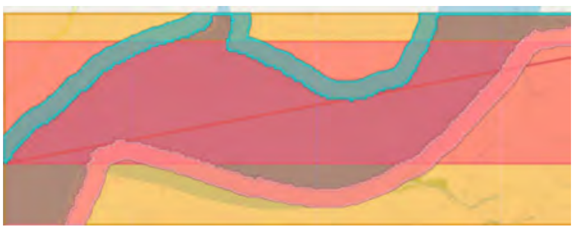

Figure 4.6: AOI adjustments

This Figure 4.6, shows the practical application of the best line detection. A comprehensive array of possible straight lines (both vertical and diagonal) are employed throughout the initial Area of Interest (AOI) to optimize the line and geometric left/right alignment. For each potential line, the code intersected it with the largest water polygon obtained from NDWI thresholding and vectorization (line.intersection(water_geom, 1)) and calculated the intersection length (clipped. length(). getInfo()).

The line with the greatest intersected length was designated as the "best line," presuming it represented the river's principal axis. The line was then extended into a continuous purple line through union and simplification. The left and right banks were delineated by partitioning a reduced Area of Interest (AOI) with a buffered variant of this line (another_aoi_3.difference(line_buffer, 1)), resulting in two polygonal segments.The geometry of each bank was categorized by comparing the intersection areas of the two segments (geom.intersection(left_portion).area() vs right_portion)

Although this method was effective for diagonally oriented rivers, it proved inadequate for exactly vertical or horizontal rivers due to the ambiguity in the AOI splitting logic. Furthermore, the exclusive use of the newly established AOI resulted in the exclusion of significant valid bank regions, causing some portion of the AOI to go to waste, and the left/right labels were determined by AOI geometry rather than the direction of river flow. Through the zone 4 of Bishkhali river limitations of trying to visualize this attempt are shown below:

zone_4=ee.Geometry.Rectangle([90.075, 22.265, 90.137, 22.305])

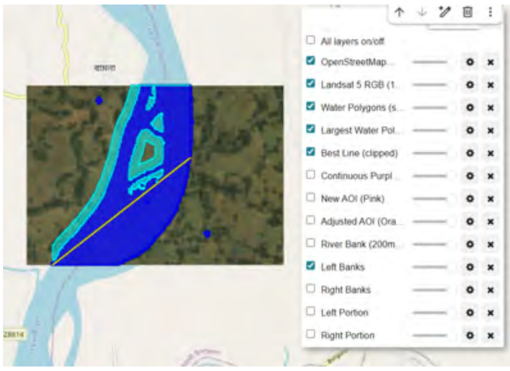


Figure 4.7: Char was detected as left bank part

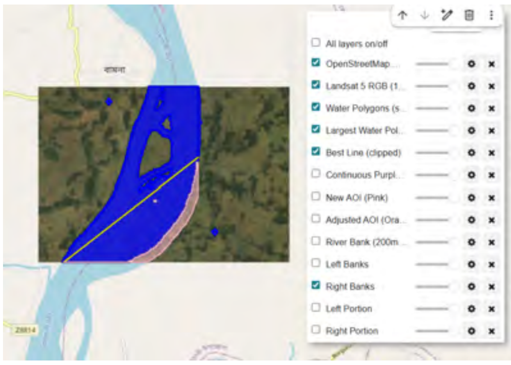


Figure 4.8: The right bank was not detected fully

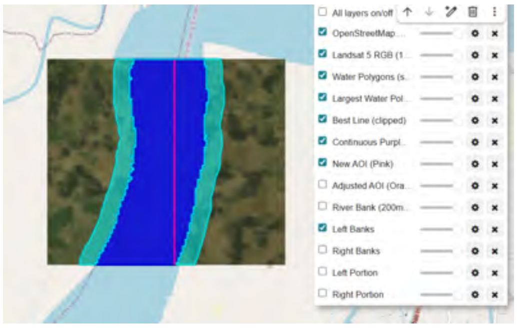


Figure 4.9: When the middle line goes vertically it only detects as left bank and no right bank

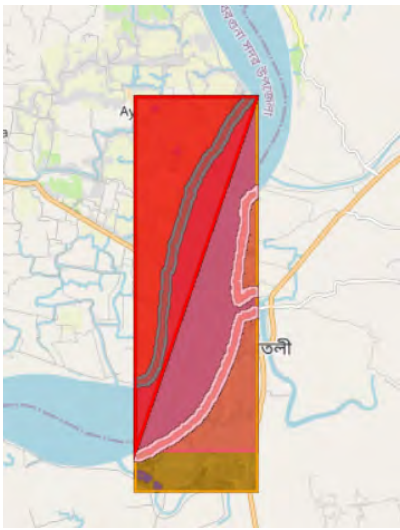

Figure 4.10: Payra zone 10 left/right bank detected perfectly as the river AOI is diagonal

In the 2nd attempt for multi-orientation line detection and centroid-cross-product flow logic,the code explicitly dealt with vertical, horizontal, and diagonal river alignments by making all three line families and choosing the one whose intersection length with the river polygon was the longest. This solved the problem of orientation dependency. This made sure that rivers were always found along any axis. More importantly, left/right classification was no longer based on slicing the AOI but on vector math. After choosing the best line, the code made sure that the flow direction was always north to south by putting the line endpoints in that order.As, in bangladesh, the sea lies to the south and river flow generally proceeds from upstraem regions toward the southern coast,this convention provides a convenient and robust basis for consistent left/right bank determination. The centroid was found for each bank polygon (bank.centroid(1)), and then the flow vector (dx, dy) and the vector from the line start point to the centroid (px, py) were crossed. The sign of this cross product directly told us if the bank was on the left or right side of the flow (cross.gt(0) $\rightarrow$ left). This got rid of the AOI dependency and made the classification make sense in the real world. However, since chars were still geometrically linked to land or banks in many instances, mid-channel islands were often incorrectly categorized as banks, and bank buffers still encompassed superfluous areas from adjacent water bodies.


Figure 4.11: Could detect left/right bank accurately when there is no char

Figure 4.12: Still detects char as part of the river bank

The 3rd and last attempt solves previous issues by implementing the bank-flow logic into a framework that is aware of its scale and is temporally consistent. A large 'Big AOI' is initially utilized to identify the actual primary river channel. This prevents side channels and adjacent bodies of water from influencing bank detection. Characters are distinctly delineated by removing the largest water polygon from land and the largest mainland polygon from land. The remaining land portions are integrated as a char geometry. To create a bank, one must first buffer the river geometry (utilizing `largest_water_geom.buffer()`), followed by sequential spatial filtering. This filter removes water and char geometries from the Big AOI, retaining only the actual riverbanks. The flow-line cross-product method remains employed to distinguish between the left and right banks. This approach is not getting affected by the direction of the river or the configuration of the AOI. Subsequently,it employs directionally accurate for example if the current year is 2017 water differentiation `water_2017` subtracted from `water_1988` for erosion and `water_1988` subtracted from `water_2017` for accretion to ascertain the extent of erosion and accretion. Subsequently, here the data is restricted to year-specific banks and characters to ensure its accuracy in both spatial and temporal dimensions. This initiative is robust as it disaggregates orientation detection, flow trajectory, landform classification, and temporal alterations into distinct, verifiable stages. Issues persist with NDWI's sensitivity to turbidity, Landsat's spatial resolution, and the approximation of geometric flow. The approach is orientation independent, char aware, spatial completeness, and hydrological consistent. This renders it ideal for examining riverbank dynamics and char formation over an extended duration.

In the previous attempts, the Bishkhali river zonal AOI was not being identified properly.Through the zone 4 of Bishkhali river the enhancements of trying to visualize the final code are shown below:


Figure 4.13: Flow line which indicates the left/right bank properly without any area loss

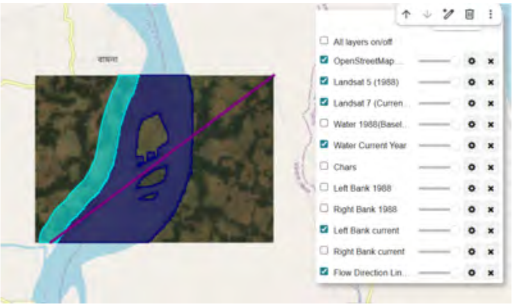


Figure 4.14: Could detect left bank without including Char in it

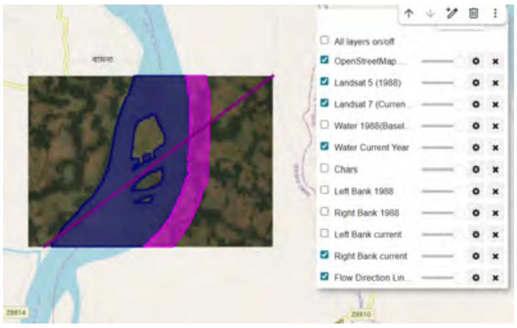


Figure 4.15: Could detect right bank without including Char in it

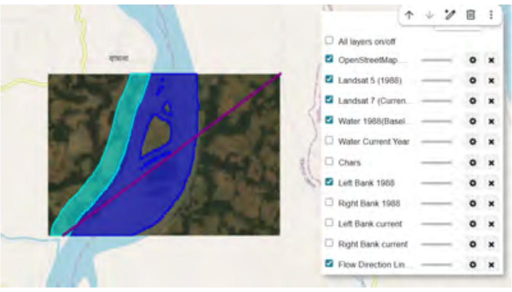


Figure 4.16: Left bank of base year 1988

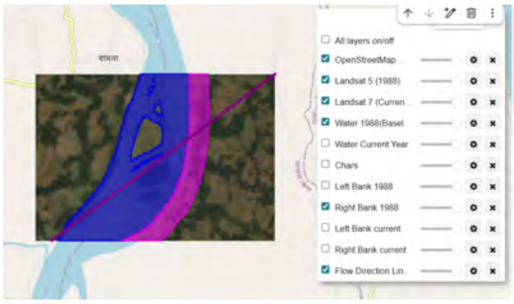


Figure 4.17: Right bank of base year 1988

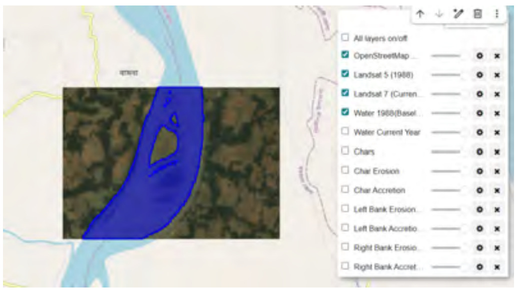


Figure 4.18: Water body of base year 1988

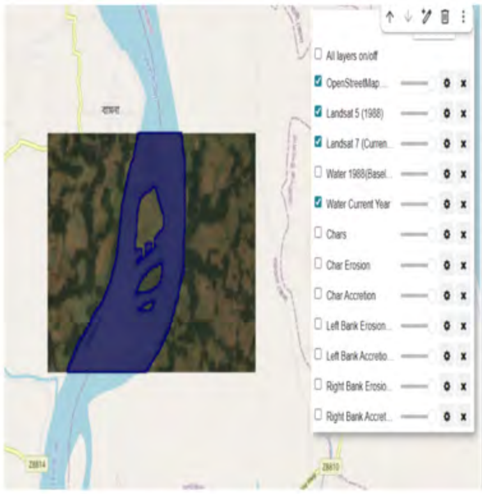


Figure 4.19: Water body of current year

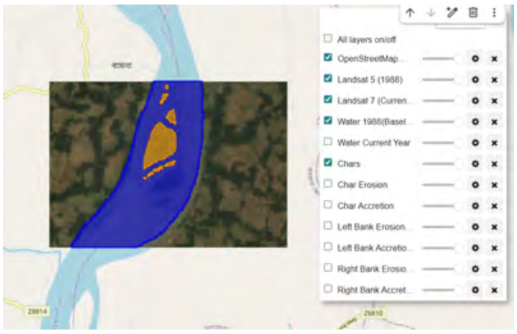


Figure 4.20: Char of base year 1988


Figure 4.21: The intersection between the water bodies of the current year and the base year is used to derive erosion and accretion.

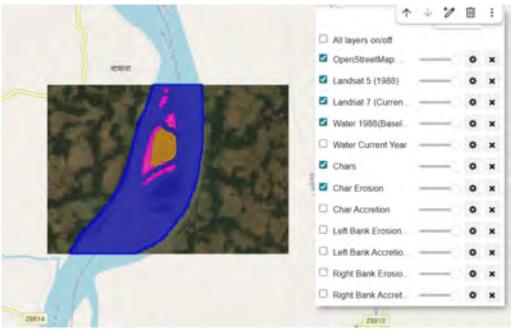


Figure 4.22: Char Erosion with Respect to the Base-Year (1988) Water Body

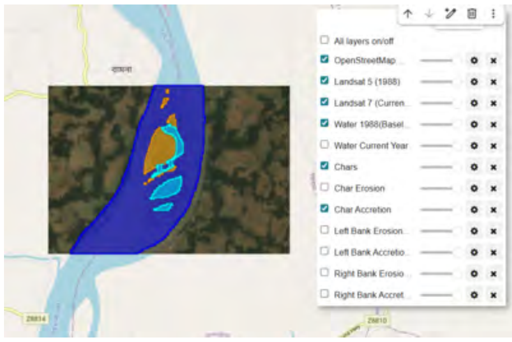


Figure 4.23: Char Accretion with Respect to the Base-Year (1988) Water Body

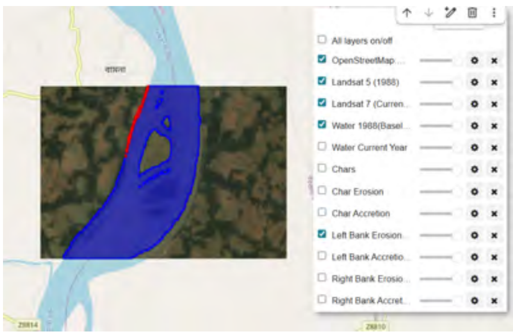


Figure 4.24: Left Bank Erosion with Respect to the Base-Year (1988) Water Body

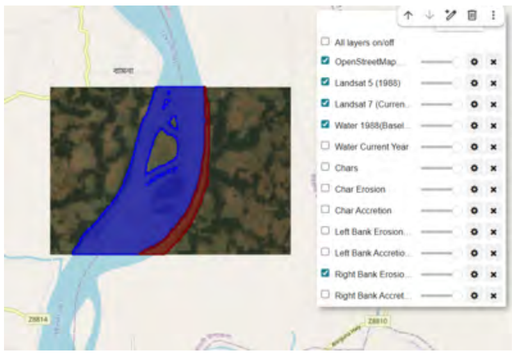


Figure 4.25: Right Bank Erosion with Respect to the Base-Year (1988) Water Body

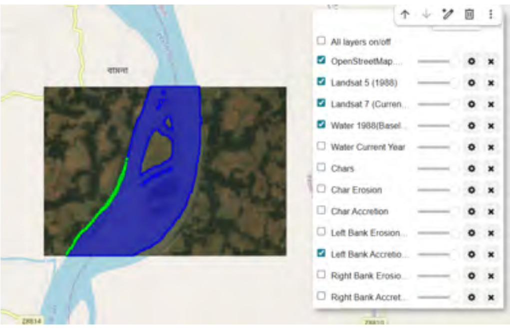


Figure 4.26: Left bank Accretion with Respect to the Base-Year (1988) Water Body

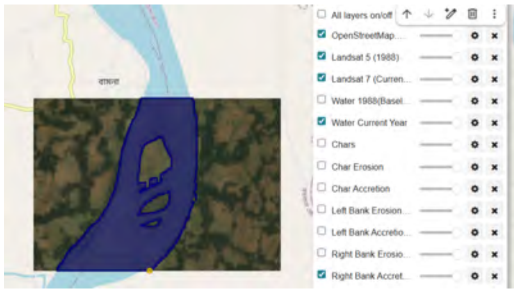


Figure 4.27: Right bank Accretion with Respect to the Base-Year (1988) Water Body

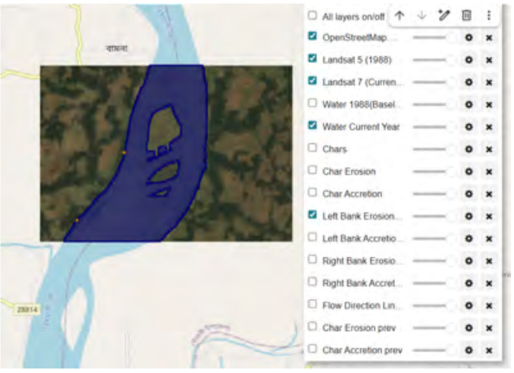


Figure 4.28: Current with previous year comparison shows Left Bank Erosion

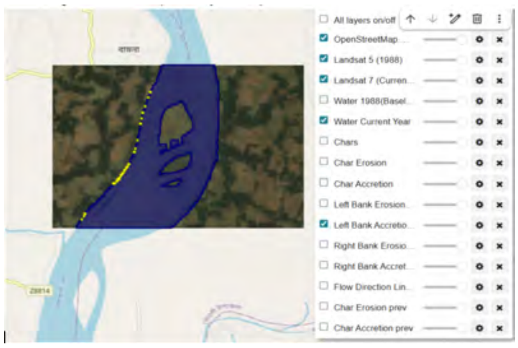


Figure 4.29: Current and previous year comparison shows Left Bank Accretion


Figure 4.30: Current and previous year comparison shows Right Bank Erosion

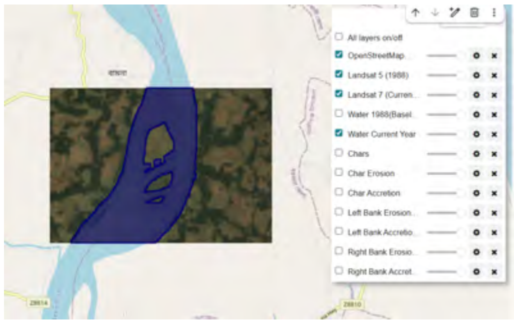


Figure 4.31: Current and previous year comparison shows Right Bank Accretion however, no visible accretion has occurred and therefore nothing is shown here.

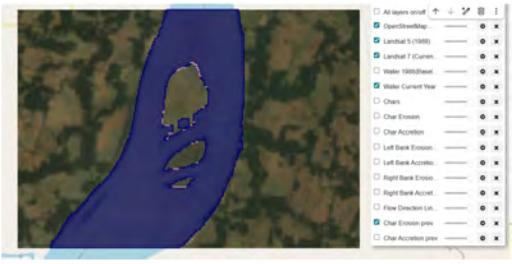

Figure 4.32: Current and previous year comparison shows Char Erosion

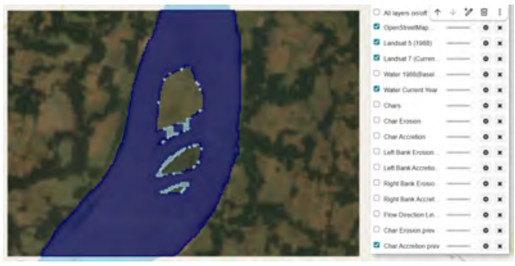

Figure 4.33: Current and previous year comparison shows Char Accretion

Similarly visualized erosion and accretion for both banks and chars for the current year compared to year two has been done, as well as the current year compared to year three. For instance, if the current year is 2017. The extent of erosion and accretion could be assessed by comparing the years 2016 (y-1), 2015 (y-2), and 2014 (y-3).

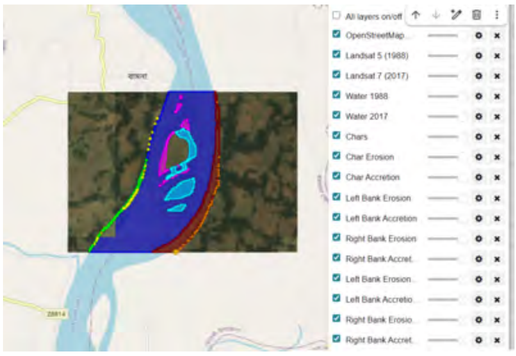


Figure 4.34: This is the AOI with all the labels on

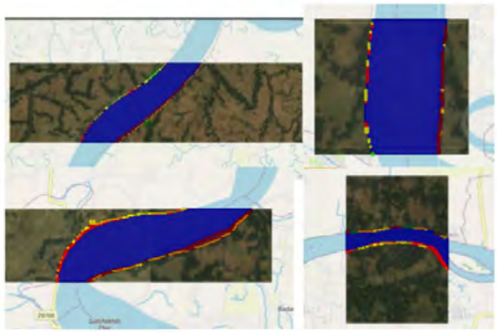

Figure 4.35: The final code works perfectly on these added conditions as well.So This method works in any orientation(diagonal, vertical, horizontal) of the river body in the aoi without any mistake.

## 4.2 Data Collection

The research started with the seven distinctive rivers from all over Bangladesh, covering the data from satellites, including Landsat (L5, L7, L8) and Sentinel-2 images from the timeframe 1988 to 2026. The Google Earth Engine (GEE) platform provides the computational methodology for accessing and processing these images over time and at scale. For geomorphological analysis to be successful, each river is segmented into 86 mature river segments or Areas of Interest (AOIs). The AOIs have been defined as to monitor the changes in erosion along riverbanks; the formation of chars; and the migration of channels over time. Each AOI contains a temporal window of data using Landsat 5 (1988-2001, 2003-2011), Landsat 7 (2002 and 2012-2017), and Sentinel-2 (2018-2026), with systematic preprocessing for cloud/bad pixel removal using cloud-free quality assessment bands and scene classification masks. Within each AOI, the active river channel and immediately adjacent bank regions have been isolated to reduce classification discrepancies during bank delineation processes.

### 4.2.1 Data Cleaning

Data cleaning is performed to ensure consistency and reliability in the multi-temporal data set. duplicates in the data set are managed by the unique composite keys (Year, River_Name, Zone_Number, Bank_Side) used in the data processing pipeline. River Name, Bank Side, and Soil Class, which are categorical variables, are standardized to ensure uniformity in the data set for all AOIs and years. The most significant data cleaning operations involve handling edge cases and ensuring mathematical consistency.

The data quality issue handled is the consistency of the data for soil textures. The USDA has a soil classification system with 12 classes for soil textures, with class 1 representing "Sand" and class 12 representing "Clay." However, the data set has zeros for some of the soil types at the edges of the AOIs, which is because of boundary effects and cloud cover interference. The zeros for the soil types are replaced by the most frequently occurring non-zero type of soil, which is identified by grouping the data by River_Name, Zone_Number, and Bank_Side, and then replacing the zeros with the most frequently occurring non-zero type of soil.

Another cleaning process is performed for land cover percentage consistency. Here, the three land cover classes are clipped to the range [0, 100] and then normalized to ensure they add up to exactly 100% for each observation. This is a mathematical normalization to correct for minor inconsistencies due to threshold-based classification methods.

### 4.2.2 Data Transformation

Transformation processes the satellite reflectance values into analytically geomorphic metrics.In this process counts are changed into area measurements in square meters to facilitate quantitative analysis of bank and char sizes. Percentages are used to represent land cover composition, which is generated from spectral index thresholds. These percentages are useful for comparing land cover composition among different years and satellite resolutions. The land cover classification is based on three mutually exclusive classes with known thresholds: Vegetation ($NDVI > 0.4$), Built-up ($NDBI > 0$), and Bare Soil ($NDVI \leq 0.4 \;\text{ AND }\; NDBI \leq 0$). These percentages are mathematically normalized to add up to 100%, and absolute area is recalculated from normalized percentages.

Seven spectral indices are calculated at the pixel level and then averaged for each geomorphic unit:

$$\mathrm{NDVI} = \frac{\mathrm{NIR} - \mathrm{RED}}{\mathrm{NIR} + \mathrm{RED}} \tag{4.13}$$

NDVI (Normalized Difference Vegetation Index) measures the vegetation density and health, ranging from -1 to 1 with higher values indicating denser vegetation.

$$\mathrm{NDWI} = \frac{\mathrm{GREEN} - \mathrm{NIR}}{\mathrm{GREEN} + \mathrm{NIR}} \tag{4.14}$$

NDWI (Normalized Difference Water Index) delineates water bodies and monitors char(river island) inundation patterns.

$$\mathrm{NDBI} = \frac{\mathrm{SWIR} - \mathrm{NIR}}{\mathrm{SWIR} + \mathrm{NIR}} \tag{4.15}$$

NDBI (Normalized Difference Built-up Index) identifies urban and developed areas, with positive values indicating built-up surfaces.

$$\mathrm{SAVI} = \frac{\mathrm{NIR} - \mathrm{RED}}{\mathrm{NIR} + \mathrm{RED} + 0.5} \times 1.5 \tag{4.16}$$

SAVI (Soil-Adjusted Vegetation Index) helps to reduce soil brightness interference in vegetation assessment, particularly valuable in sparsely vegetated riverbank areas.

$$\mathrm{MSI} = \frac{\mathrm{SWIR}_1}{\mathrm{NIR}} \tag{4.17}$$

MSI (Moisture Stress Index) indicates vegetation water stress, with values ¿1 suggesting moisture-deficient conditions.

$$\mathrm{NBR} = \frac{\mathrm{NIR} - \mathrm{SWIR}_2}{\mathrm{NIR} + \mathrm{SWIR}_2} \tag{4.18}$$

MBR (Normalized Burn Ratio) detects burned areas and vegetation stress, useful for identifying fire-affected bank vegetation.

$$\mathrm{BAI} = \frac{1}{(0.1 - \mathrm{RED})^2 + (0.06 - \mathrm{NIR})^2} \tag{4.19}$$

BAI(Burned Area Index) enhances identification of fire-affected regions in riverbank vegetation.

These indices collectively measure vegetation vigor, built-up presence, soil moisture, and surface water flow—each of which is a significant factor in bank stability and char formation. Topographic changes involve computing mean elevation from SRTM digital elevation models (with a resolution of 30m) and mean slope from terrain analysis, both of which are averaged on a per-bank and per-char polygon basis.

### 4.2.3 Feature Engineering and Temporal Dynamics

There are advanced features which are used to capture changes in geomorphic processes and how they vary over time. Erosion and accretion metrics can be produced by quantifying changes in bank area by comparing reference periods in a lagged-mode manner.

**1.Annual Change (Y–1):** it comparisons with the previous year
**2.Medium-term Change (Y–2, Y–3):** it comparisons with second and third recent years prior
**3.Long-term Baseline (1988):** it cumulative change since the initial observation year

To calculate these temporal comparisons, two complementary methods were utilized: Geographic Information System (GIS) for direct morphological change detection through geometric polygon differencing and Arithmetic Area Comparison in post processing for more stable, mass balanced estimates. The second method calculates erosion as a positive difference where a previous area is greater than the current area, and accretion as a positive difference where a current area is greater than the previous area.

$$\text{Erosion} = \max(\text{Areaprevious} - \text{Areacurrent}, 0) \tag{4.20}$$

$$\text{Accretion} = \max(\text{Areacurrent} - \text{Areaprevious}, 0) \tag{4.21}$$

Using these diffrences, erosion and accretion intensities are subsequently derived by normalizing change areas by current bank area:

$$\text{Erosion Intensity} = \frac{\text{Erosion Area}}{\text{Bank Area}} \tag{4.22}$$

$$\text{Accretion Intensity} = \frac{\text{Accretion Area}}{\text{Bank Area}} \tag{4.23}$$

These ratios are dimensionless and allow us comparisons between different scales; they range from 0 (indicating no difference) to possibly greater than 1 (when the changed area is larger than what currently makes up the channel, usually in major char formation events). Using char features to measure fluvial-landform interactions:

**1.Char (river island) Area Ratio:** Char (river island) areas are normalized by bank area, quantifying relative sediment deposition.

**2.Distance to Nearest Char (river island):** It euclidean separation between bank and char centroids.

**3.Char (river island) Presence Indicator:** It is the binary flag for char river island existence within the AOI.

**4.Char river island Count:** It counts the number of discrete char (river island) polygons within each AOI.

To support autoregressive analysis and predictive modeling, bank area is lagged three different ways (ie. Area_Prev, Area_2year_Prev, Area_3year_Prev) in order to detect trends, cycles, and persistence in bank morphological change over time.

### 4.2.4 Predictive Target Creation and Final Dataset Structure

To improve the process of preparing data for machine learning, a new prediction model has been established for erosion and accretion intensity (depending on the zone of the river or stream) through percentile-based classification. These intensities are then assigned to one of three classes (e.g., Class 1: Low; Class 2: Medium; Class 3: High).

**Class 0 (Low):** Intensity $\leq 33^{\text{rd}}$ percentile
**Class 1 (Medium):** Intensity $> 33^{\text{rd}}$ percentile and $\leq 66^{\text{th}}$ percentile
**Class 2 (High):** Intensity $> 66^{\text{th}}$ percentile

These current-year intensity classes are then temporally shifted forward to make the target variables for the subsequent year:

$$\text{TargetErosion, year } t = \text{ClassErosion, year } t+1 \tag{4.24}$$

$$\text{TargetAccretion, year } t = \text{ClassAccretion, year } t+1 \tag{4.25}$$

The presented framework provides a viable forecast model that utilizes year-to-year attributes in estimating the erosion/accretion class of the following year in a manner that reflects the methods used in actual river management practices. Because the last year of the model (2026) does not include any targets for the following year since no data for a year after 2026 exists, it will serve as a good testing ground for the model and for forecasting future years.
The model will produce three complete datasets:
**1.Erosion Training Dataset:** The dataset includes every year from 1988 through 2025 with complete feature sets and erosion targets, all of which have associated metadata (Year, River_Name, AOI_Name, Zone_Number, Satellite, Bank_Side), geometric features (Area_m2, Char_Count), vegetation cover composition (Veg_m2, Builtup_m2, Bare_m2 & corresponding percentages), spectral indices (mean NDVI, NDBI, SAVI, MSI, NBR, BAI), topographic features (Mean_Elevation, Mean_Slope), soil properties (Soil_Code, Soil_Class), char relationships (Char_Area, Has_Char, Dist_to_Char, Char_Area_Ratio), areas demonstrating historical change (Erosion_vs_1988, Erosion_vs_Prev, etc.), as well as intensity metrics (Ero_Intensity, Ero_Intensity_2yr, Ero_Intensity_3yr), and final output variable Target_Erosion.
**2.Accretion Training Dataset:** Similar to the structure of erosion dataset but focused on accretion processes. It contains accretion-specific intensity metrics and Target_Accretion as the predictive target.

**3.Testing Dataset (2026):** It contains only data from the latest year, 2026, all input features in the holdout test data match those in the training datasets but contain no target variables to allow you to validate the model. Also, because of the forecasting framework used, there is no way for you to generate true value(s) for the year 2026, as 2027 has not yet occurred to be used as ground truth.

It is mentionable that this framework haven't used any area in raw form because AOI could be of any size, so to maintain the same scale, area was divided to get the percentage (Build up, vegetation, bear land) and intensity (erosion, accretion) features. Moreover, the framework also generates features such as char (river island) erosion, char (river island) accretion, char (river island) build up vegetation, average distance of char (river island) from left bank, average distance of char (river island) from right bank which for the time being haven't been used in the research, but it could be used in the future char (river island) work to keep a track of the river and banks.

### 4.2.5 Data Integration

Data integration is the process by which multi-source geospatial information is integrated into one dataset for analysis. Satellite-based land cover information, spectral indices, topographic information such as mean elevation and slope, soil information, erosion and accretion information, intensity information, and char (river island) relation information are integrated into one dataset using a composite spatial-temporal key made up of AOI identifier, year, river name, zone number, and bank side.

This dataset is useful for analysis because it contains both spatial and temporal context information, such as bank side differentiation and char proximity information for spatial context, and multi-year change information and lag information for temporal context, which allows for analysis of the effect of short-term hydraulic and long-term climatic changes on river morphology.

### 4.2.6 Data Reduction

To minimize computational complexity and maximize the interpretability of the final model outcome, a dimensionality reduction technique was employed using a combination of correlation analysis and expert-oigzo_atiating the final model outcome. The final curated dataset illustrates the complex interactions between hydraulic forces, sediment dynamics, plant and soil interrelationships, and human activity upon these processes, which provides a firm foundation for predictive modeling of riverbank stability and char development in an altered environment.

The temporal aggregate data supports the identification of ten-year decadal trends of dominant types of changes, and is illustrated by the analysis of erosion and accretion rate changes from the baseline of 1988 to subsequent decades, which provide examples of gradual or rapid changes in riverbank morphology over time. The temporal reduction approach provides resolution for both long-term geomorphic change types and for examination of year-to-year variability of the geomorphic process.

### 4.2.7 Exploratory Data Analysis (EDA)

It performed an exploratory data analysis on the river erosion and accretion datasets to know temporal patterns of river erosion and accretion, net riverbank change over time, identify class imbalance, feature correlations, and potential outliers etc ensuring informed and reliable model development.

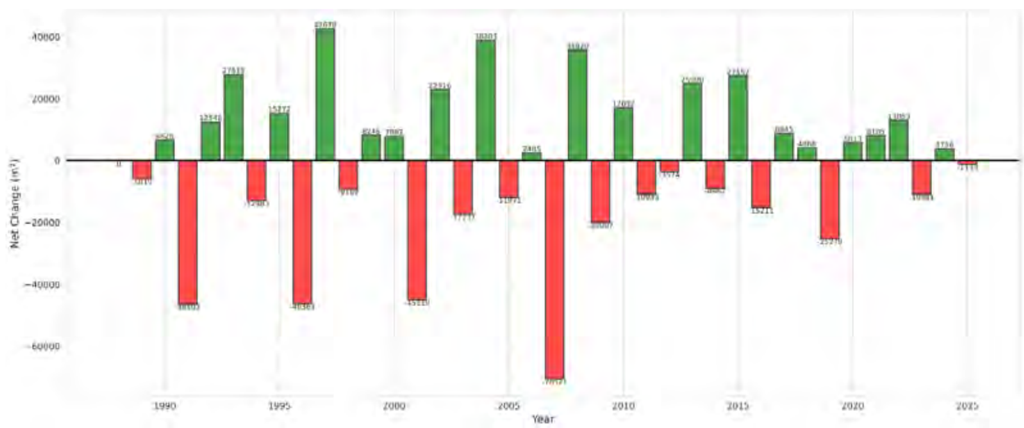


Figure 4.36: Net Riverbank Change Over Time

From this plot in Fig. 4.36,it can be seen the net riverbank changes over time. Here, the depth of the erosion bars is significantly higher than the height of the erosion bars, which indicates that when the river erosion is claiming land more aggressively than accretion can deposit it. The maximum annual erosion recorded was 70,521 m² in 2007, The maximum annual erosion recorded was 70,521 $m^2$ in 2007, which is approximately 65% higher than the maximum accretion gain of 42,678 $m^2$ in 1997. The section faced at least four major erosional events exceeding 45,000 $m^2$ (1991, 1996, 2001, and 2007), whereas accretion only crossed the 40,000 m² mark once. This clearly proves that erosion plays a dominant role compared to accretion, which is really alarming for Bangladesh.

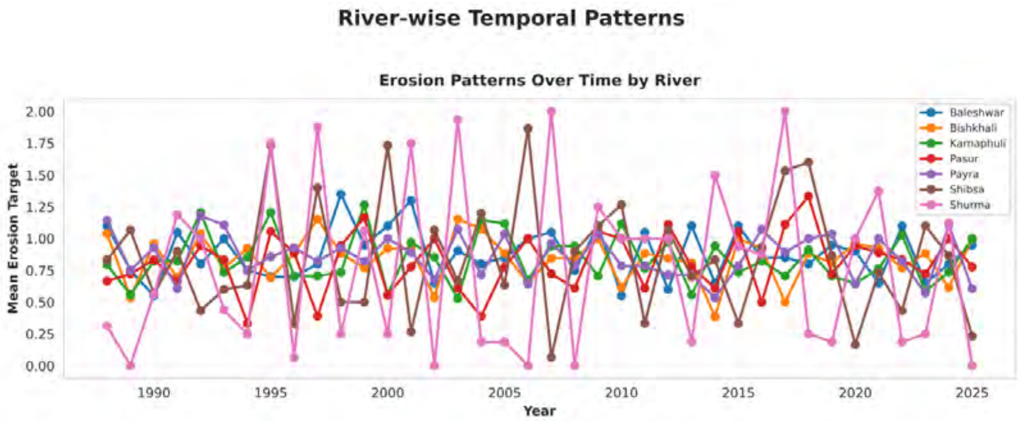


Figure 4.37: Erosion Patterns Over Time by River

The analysis of the temporal erosion patterns from 1988 to 2025 shown in Fig. 4.37 reveals that the Surma river and Shibsa river are the most volatile, frequently exhibiting extreme spikes in land loss that approach or reach the maximum target value of 2.00. On the other hand, the Karnaphuli river demonstrates a much higher degree of geomorphic stability, with its mean erosion target generally oscillating between a narrow and moderate range of 0.50 to 1.00. Other systems like the Baleshwar and Payra show intermediate fluctuations, while the entire plot highlights cyclical erosion peaks across most rivers around years like 1995 and 2007, indicating the impact of major regional environmental events.

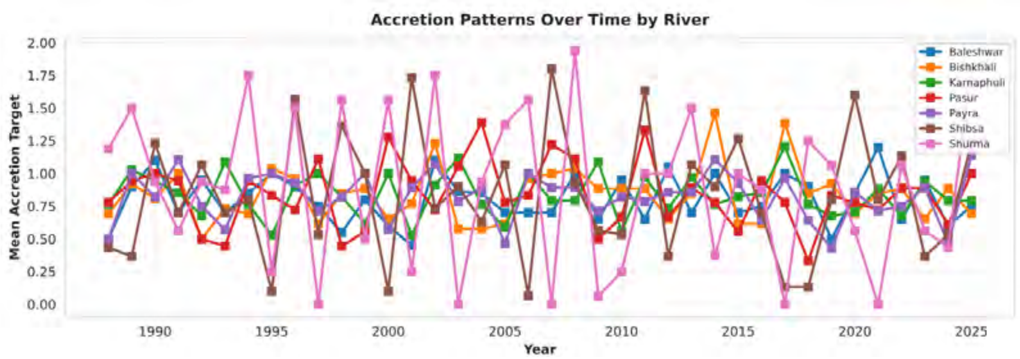


Figure 4.38: Accretion Patterns Over Time by River

This plot in the Fig. 4.38,shows how the average accretion patterns for seven rivers have changed over time. The colors and line styles for each river show how the accretion values changed from 1988 to 2025. Each river had its own high and low points at different times. The plot shows that the Surma and Shibsa rivers once more dominate the chart with high amplitude spikes implying that the erosive power of the rivers is frequently offset by extensive stages of land formation and siltation. The Pasur and Payra rivers appear to have a more regular and consistent accretion process with their targets around the 0.75 to 1.00 baseline but do not have the chaotic spikes of the more active meandering systems. Interestingly, in this plot the Karnaphuli river still possesses its stable reputation without diverse surges of deposition, which confirms that the geomorphological dynamics of the rivers of the coastal region of Bangladesh are extremely heterogeneous and basin-specific.

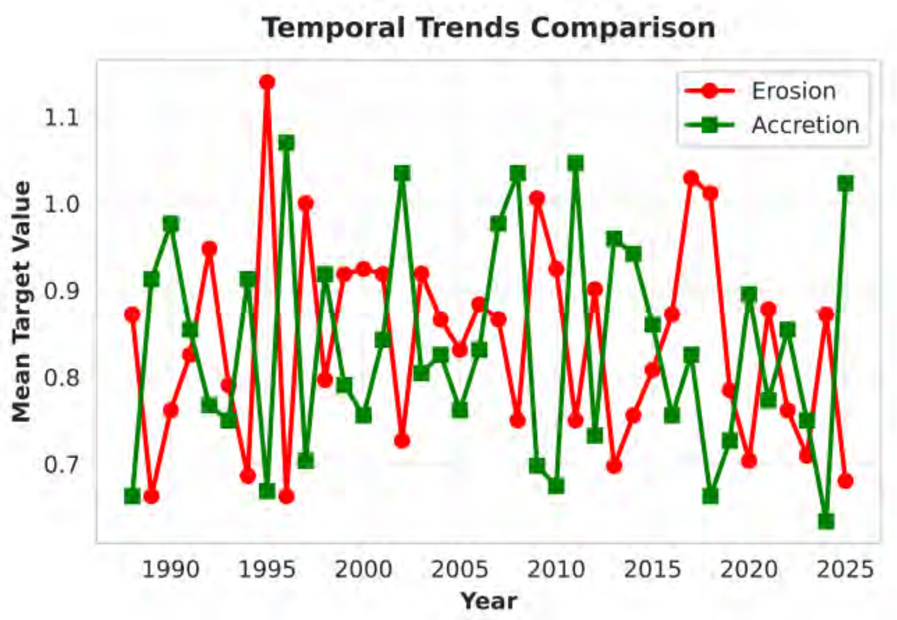


Figure 4.39: Temporal Trends Comparison

The graph in Fig. 4.39 is called "Temporal Trends Comparison" shows how erosion and accretion changes over time, from the years 1988 to 2025. The red line denoting the Mean Erosion Target and the green line denoting the Mean Accretion Target often exhibit an inverse effect, with a sharp peak in one of the two being regularly matched by a trough in the other. This is seen clearly around 1995 with the maximum in erosion recorded at 1.15 and a sudden increase in accretion in 1996 where the river systems tried to get into geomorphic balance. The plot between 2005 and 2012 shows that there was a phase where accretion tended to remain higher than erosion, meaning that there was a time-span where the sediment depositing processes and the growth of char predominated over the basins. Nevertheless, the final ten years between 2015 and 2025 show more regular and narrower swings, indicating that the riverbanks are getting more and more unstable whereby the year to year changes between losing and gaining of land are so swift. This volatility of the high frequency nature is one of the reasons why the predictive model is so challenging to use since the historical trends are ever being broken by these unexpected geomorphic shocks.

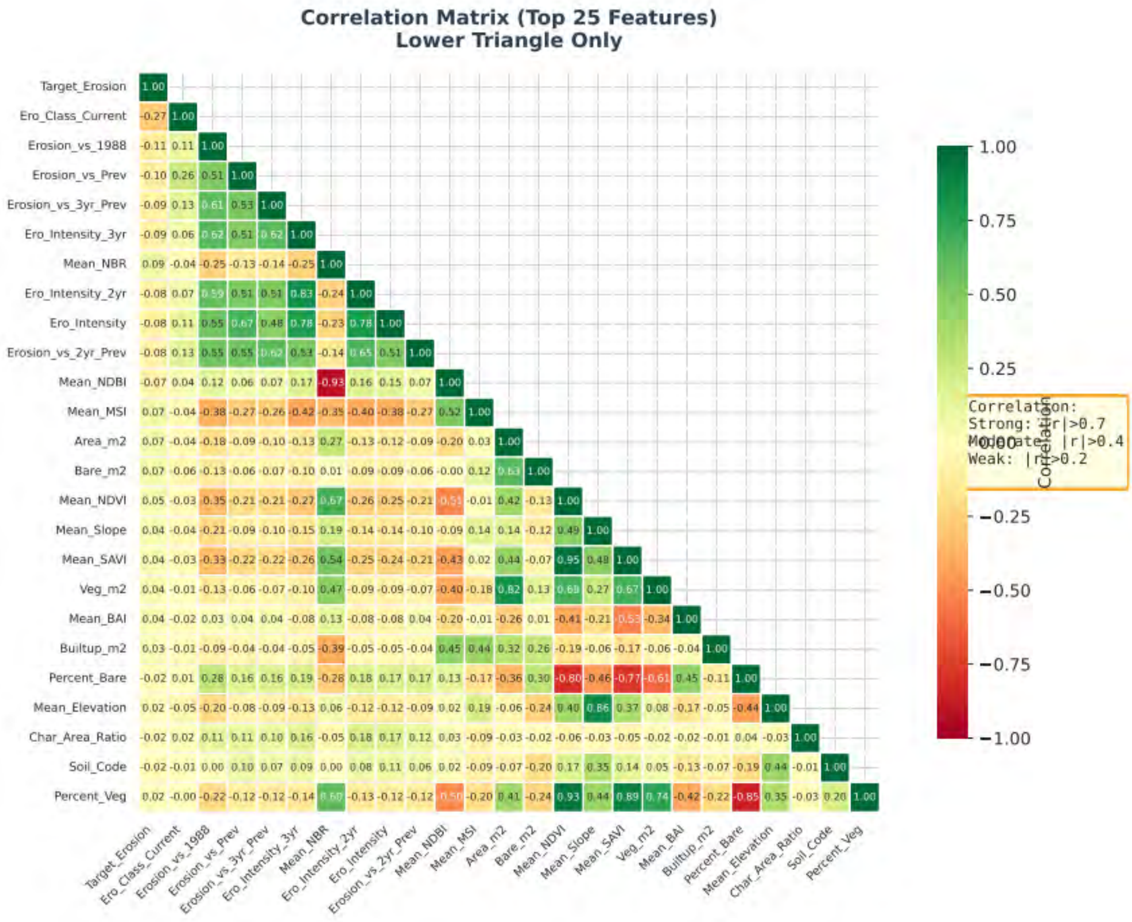


Figure 4.40: Correlational Matrix of top 25 features from Erosion Dataset

The heatmap in the Fig. 4.40, illustrates the correlation coefficients of the top 25 features associated with the Erosion dataset. The lower triangle has been chosen to avoid duplication. Darker shades of green represent positive correlations, which include the correlation between various temporal measures of erosion intensity and historical erosion data. Red colors represent negative correlations, which include the correlation between vegetation and built-up area.

**Intensity and Historical Correlations**

The positive correlations appear most significantly in the correlation of the historical geomorphological characteristics. Attributes like EroIntensity, EroIntensity2yr and EroIntensity3yr have highly positive correlation coefficients, usually above 0.75 with other attributes as well as historical standards like Erosionvs1988. Such a high correlation testifies to the idea that the erosion of riverbanks in these seven rivers is not an accidental phenomenon but a phenomenon with a high degree of temporal memory, in which the erosion of the past can be taken as one of the main predictors of the future.

**Spectral Relationships and Environmental Relationships**

It is also observed that the critical relationships between land cover indices and spectral markers have the critical inverse relationships as highlighted in the matrix. In one case, Percent_Veg (Vegetation) and Percent_Bare (-0.85) have a strong negative correlation, and PercentNDBI (-0.50) has a moderate negative correlation, which demonstrates that the decrease in vegetation cover leads to the increase of bare soil and built-up areas. Besides, the correlation of Mean_NDVI and Mean_SAVI (0.95) is very high thus showing that the two indices are offering almost the same information about the health of vegetation which is the reason why you are using numerous spectral inputs to be sure of the strength of the data.

**Topographic and Morphological Insights**

The morphological characteristics, such as the Mean_Slope and Mean_Elevation have a positive relationship of 0.86 which proves that as the elevation in the study areas is higher, the gradient tends to be steeper. Interestingly, Char_Area_Ratio exhibits relatively low correlations with most of the other features which shows that it is offering independent information to the model that cannot be explained by vegetation or slope only.

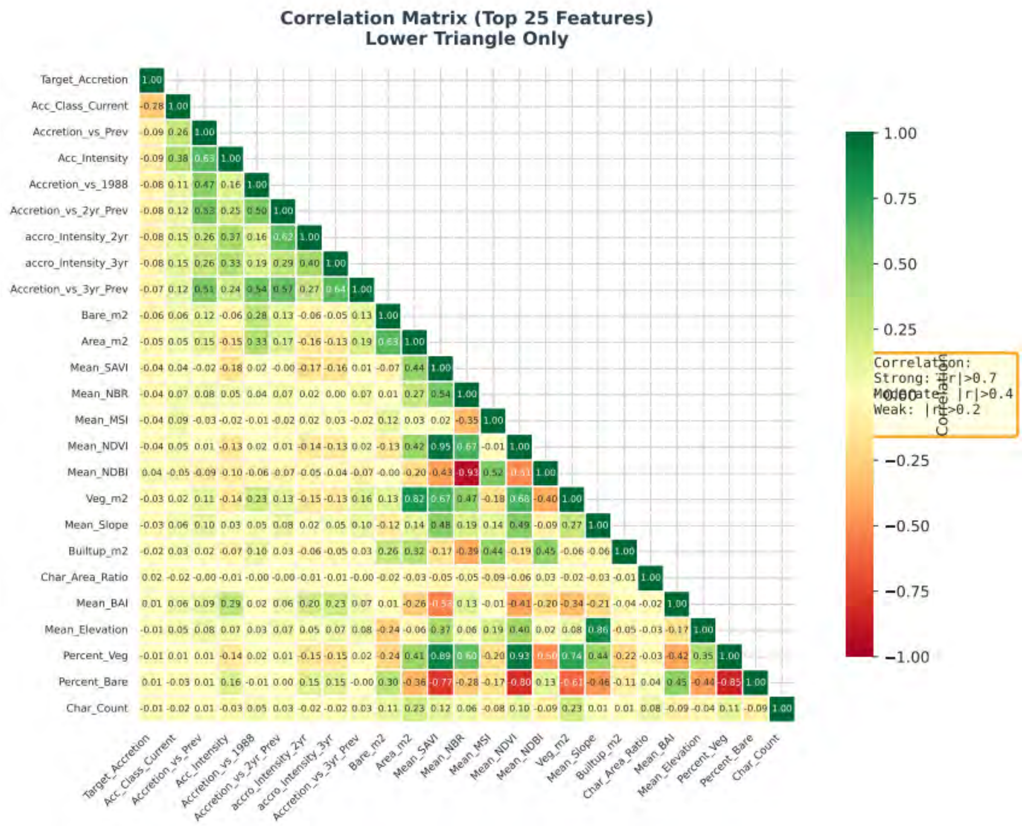


Figure 4.41: Correlational Matrix of top 25 features from Accretion Dataset

This heatmap in the Fig. 4.41 shows the linear relationships between the most important variables for the Accretion dataset, and it shows strong positive correlations between the accretion-specific intensity features and the area measures, as indicated by the high concentration of the green colors.

**Intensity and Historical Correlations**

Like erosion, accretion is also highly time-dependent, with past deposition having a strong impact on how trends can be changed at the present. Positive correlations are strong between Acc_Intensity and such historical variables as Accretion_vs_1988 (0.47) and Accretion_vs_Prev (0.63). This indicates that regions that are likely to experience siltation and char development are likely to be active in many years cycles, which enable the Bi-LSTM to train on such repetitive deposition patterns.

**Land Formation and Spectral Indices**
The matrix shows how special satellite markers determine the new land formation. Mean_NDVI and Mean_SAVI are virtually identical with each other (0.95), but both exhibited a close positive correlation with PercentVeg (0.93 and 0.89 respectively). This validates the hypothesis that with the process of accretion and stabilization of the new land, the health and the density of the vegetation increases rapidly and measurably. On the other hand, there is a strong negative relationship between PercentBare soil and Mean_NDVI (-0.80), which demonstrates the process of natural succession between sediment deposit and vegetated bank.
**Geomorphic Indicators and Area Indicators**
Area_m2 and Veg_m2 have a significant level of correlation (0.82) which suggests that bigger segments of banks or chars of these rivers tend to be vegetated and more geomorphologically complex. The relationship between MeanSlope and MeanElevation (0.86) is in line with the erosion data, which proves that the topographical structure of the basins is the same in both the processes. It is important to note that Char_Count indicates a weak, but independent correlation with accretion intensity and this gives the model distinct spatial data which spectral indices may lack.

### 4.2.8 Summary of Preprocessed Data

**Outlier Treatment of Dataset**

Both erosion and accretion datasets demonstrated considerable data quality concerns, characterized by numerous outliers in spectral indices, land cover attributes, and process-specific metrics (erosion/accretion intensity). The outliers jeopardized model stability and interpretability, requiring thorough preprocessing. Outliers were detected utilizing the Interquartile Range (IQR) method:

$$\text{Lower Bound} = Q_1 - 1.5 \times IQR \tag{4.26}$$

$$\text{Upper Bound} = Q_3 + 1.5 \times IQR \tag{4.27}$$

In contrast to outlier removal techniques that eliminate data points, IQR capping retains all observations while constraining extreme values to the determined limits. This methodology protects the original sample sizes, maintains temporal continuity for time-series analysis, and retains all geomorphic events. The treatment transformation:

$$X_{\text{treated}} = \begin{cases} \text{Upper Bound}, & \text{if } X > \text{Upper Bound} \\ \text{Lower Bound}, & \text{if } X < \text{Lower Bound} \\ X, & \text{otherwise} \end{cases} \tag{4.28}$$

The Interquartile Range (IQR) method found outliers. This method keeps the data safe. IQR capping, on the other hand, keeps all data points but limits extreme values to the calculated bounds. This is different from methods that remove outliers completely. This method keeps the original sample sizes, keeps the time-series analysis going, and lets all geomorphic events stay while fixing any differences in size.

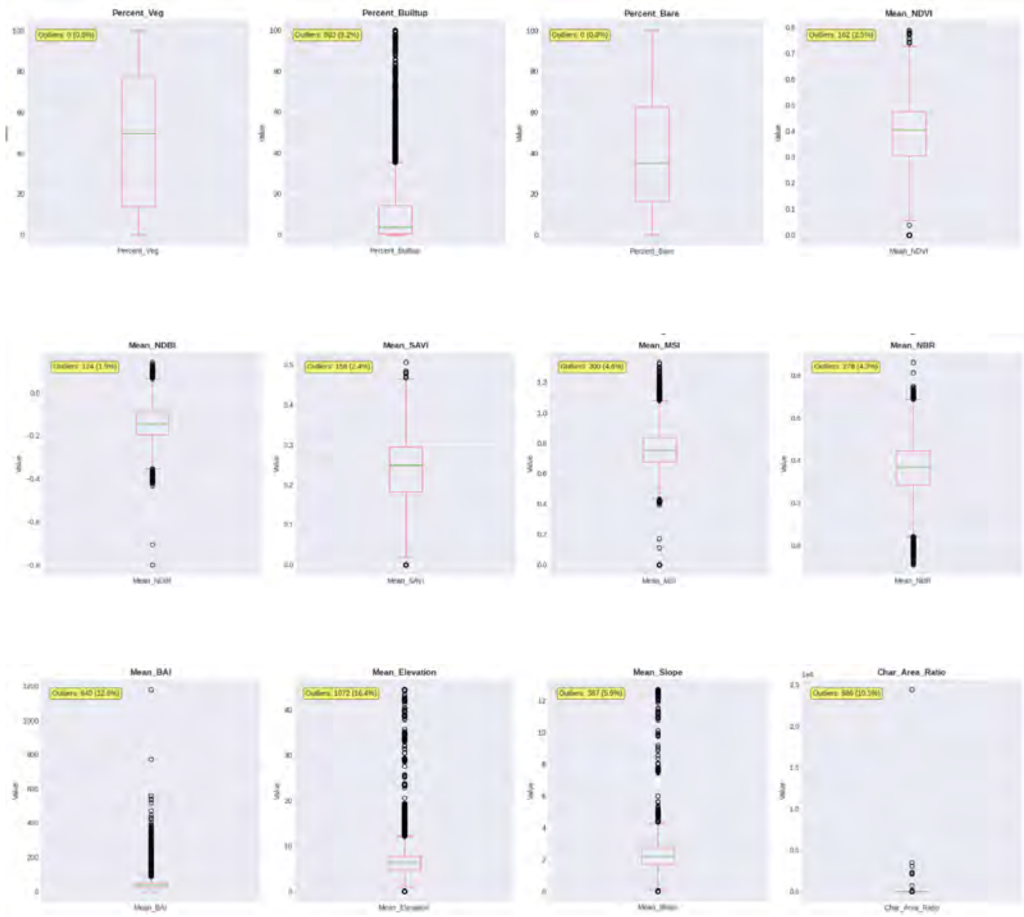

Figure 4.42: Before_Treatment_Boxplot

This image above in Fig. 4.42, is the original boxplot before limiting extreme values from the data points. Here, land cover and spectral indices show identical treatment results for both datasets as they share the same underlying remote sensing data.

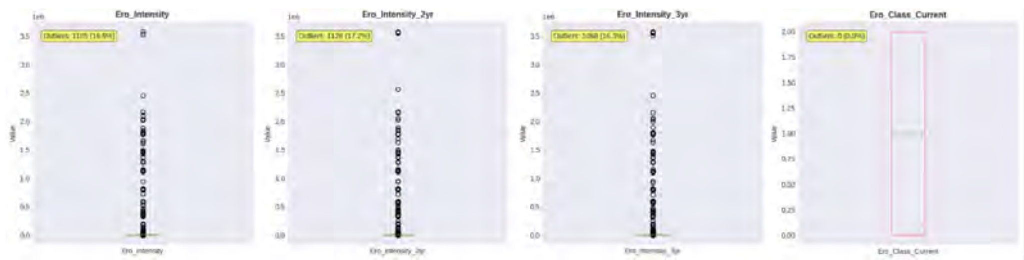

Figure 4.43: Before_Treatment_Boxplot FOR EROSION EXPLICITLY

The boxplot in Fig. 4.43, shows the distribution and variability of erosion related features like intensity over a period of time, prior to any kind of data preprocessing or treatment. The presence of a large number of black circles above the boxplot's whiskers suggests a large number of outliers in the dataset, particularly related to intensity features. The boxplot for "Ero_Class_Current" appears more concentrated, indicating a normalized distribution compared to the raw intensity features.shpws extreme data point values before capping.

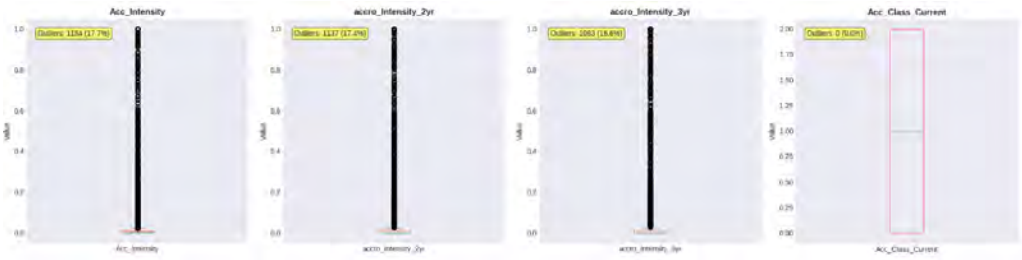


Figure 4.44: Before_Treatment_Boxplot FOR ACCRETION EXPLICITLY

This series of box plots in Fig. 4.44 shows the distribution of raw data for the features in the accretion dataset, which indicates a significant level of skewness in the "Acc_Intensity" feature. Like the previous plots for the erosion dataset, the long vertical lines of black dots in the box plots indicate extreme outlier values, which may need to be addressed in the scaling step of the data cleaning process.

## 4.3 Data Correction Analysis

In the erosion dataset, the 100% reduction in erosion intensity features points to the correction of measurement unit errors or data entry mistakes. The original values, which were in the thousands (e.g., 12,219.11 mean), were unrealistic for erosion metrics and reflected data collection artifacts rather than actual erosion events. Similarly, the accretion dataset showed an 89-95% reduction in accretion intensity metrics, indicating similar data quality issues. The original accretion metrics had extreme values (max=1.0) that surpassed physically plausible accretion rates for the study area. Common improvements involved ensuring physical validity by limiting percentage features to a range of [0, 100], removing any impossible values to enhance data quality, and applying the same adjustments across both datasets to ensure a fair comparison in later modeling.

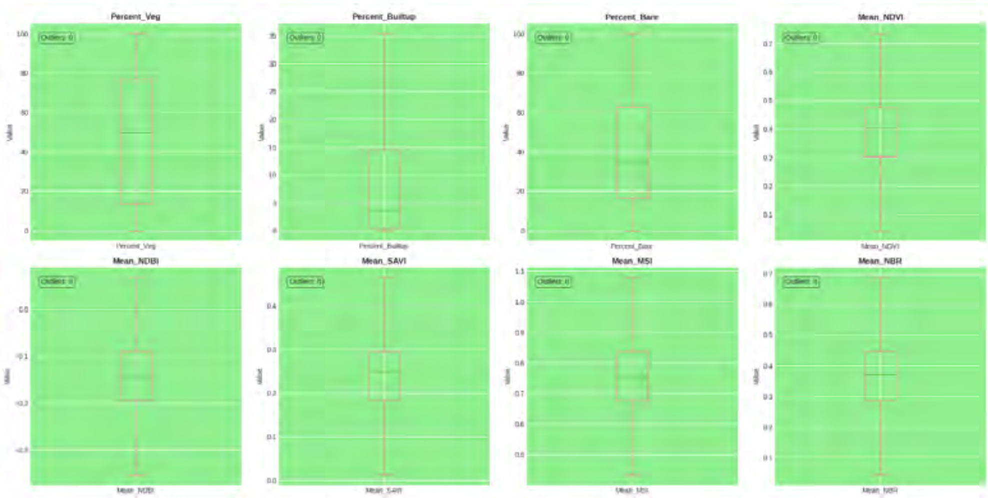


Figure 4.45: After_Treatment_Boxplot

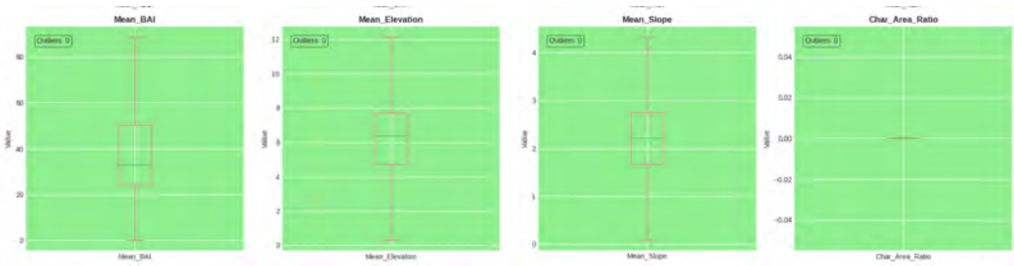


Figure 4.46: After_Treatment_Boxplot

This set of box plots in Fig. 4.46 represents the distribution of characteristics after applying data processing methods, for example, outlier capping, normalization, or scaling. Compared to the "Before Treatment" box plots, it can be noticed that the data distribution is now much tighter with very few extreme outliers, ensuring that the model is not biased by noise. This fine distribution of data is a better input for machine learning algorithms, thus providing improved predictions for erosion and accretion trends

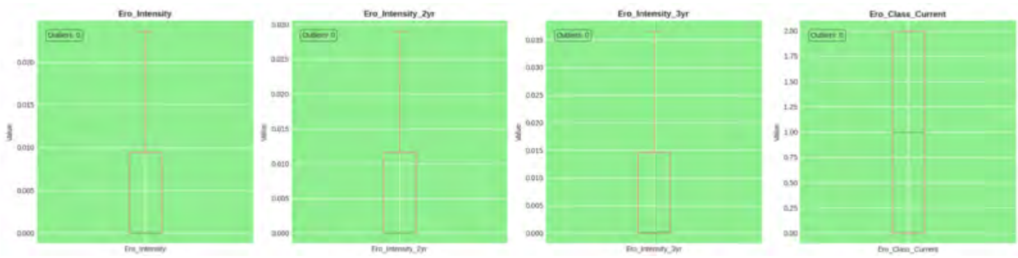


Figure 4.47: After_Treatment_Boxplot FOR EROSION EXPLICITLY

The figure in Fig. 4.47 demonstrates the distribution of erosion-related features after the data has been subjected to preprocessing operations such as outlier capping and data normalization. From the "Outliers: 0" labels on the above image, it can be seen that the extreme values in the data, which were dominant in the original data set, have been properly addressed in order to provide a uniform data distribution for features such as "Ero_Intensity" and "Ero_Class_Current". This is done in order to prevent the machine learning algorithm from being biased due to data noise.

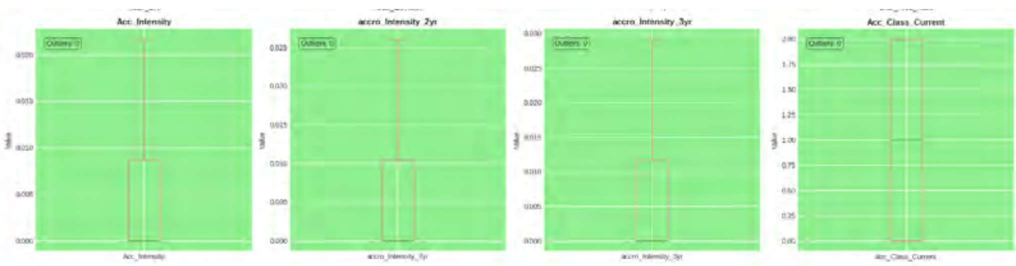


Figure 4.48: After_Treatment_Boxplot FOR ACCRETION EXPLICITLY

The figure in Fig. 4.48 shows the refined state of the accretion dataset after the treatment phase. The removal of the outliers for the various variables such as "Acc_Intensity" and "Acc_Class_Current" is evident, thus making the data distribution compact. By normalizing these features to a standard scale, the dataset is optimized

to be used for predictive modeling, with the importance of each feature determined by actual trends instead of their original magnitudes.
The treatment did not reduce the dataset sizes but instead corrected implausible values. All temporal, spatial, and relational structures were preserved throughout the process.

The consistent approach made sure that the feature ranges in both the erosion and accretion datasets were aligned, with the same physical constraints applied to each. This approach also provided standardized preprocessing, allowing for a fair comparison between the models, while ensuring that the transformations for both geomorphic processes were reproducible.

The IQR capping method addressed data quality issues in both the erosion and accretion datasets without altering their structure. It corrected errors in intensity metrics while preserving valid extreme events. Both datasets experienced similar data quality problems, and shared features like land cover and spectral indices were processed in the same way. The large drops in intensity metrics (100% for erosion and 89–95% for accretion) corrected measurement errors without eliminating valid extreme events. Both datasets showed similar data quality issues in the intensity metrics, and features like land cover and spectral indices were handled the same way. This approach ensured the erosion and accretion analysis could be compared fairly, restored physical plausibility to all geomorphic metrics, and transformed the datasets from unrealistic extreme values into accurate representations of river geomorphic processes.

After gathering the data, all processing was done with the real annual records, without any interpolation or creation of fake data. For each River–Zone–Bank combination, the riverbank data were cleaned and put in chronological order. The char data were then added to show how islands changed the shape of the land. We measured erosion and accretion by looking at changes in the area of the banks. We also calculated intensity ratios for classification, making sure that the data for erosion and accretion were kept separate for different classification models.

**Class imbalance handling:**

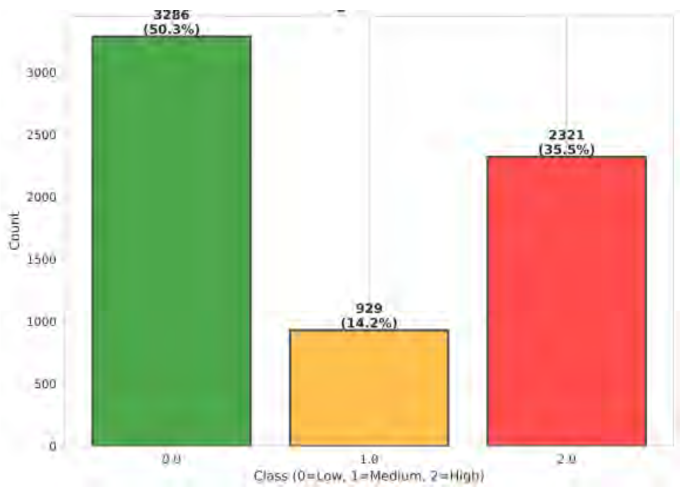


Figure 4.49: Target Erosion Distribution

This bar chart in Fig. 4.49 describes the class distribution for the target erosion feature, which is classified into different classes: Low (0.0), Medium (1.0), and High (2.0). From this dataset, it is evident that there is a class imbalance issue, with the majority belonging to the class "Low Erosion" at 50.3%, while "Medium Erosion" is the least frequent at 14.2%. The class distribution is a critical step for "Class imbalance handling", as it is important for determining specific machine learning techniques that must be employed to prevent the model from becoming biased towards a majority class.

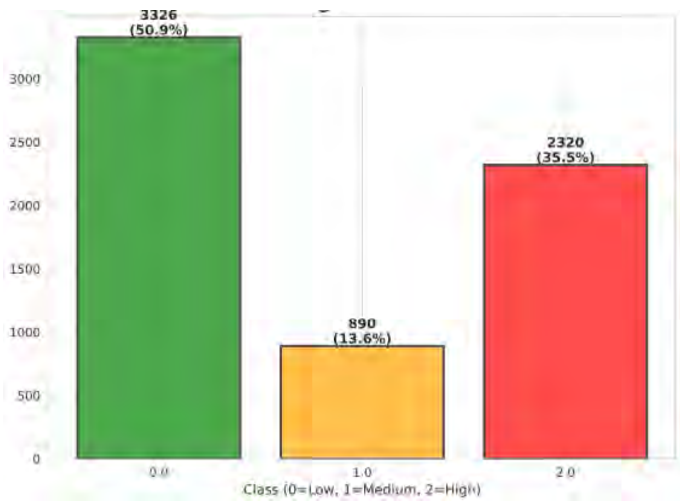


Figure 4.50: Target Accretion Distribution

The figure in Fig. 4.50, exhibits a similar imbalanced distribution pattern, with "Low" and "High" classes for accretion dominating the distribution while the "Medium" class is substantially underrepresented at only 13.6%. This visualization also confirms that both datasets demand specific sampling or weighting approaches for effective learning of patterns for moderate geomorphic changes.

We can see that the class distribution is imbalanced with the low and high erosion classes being the predominant ones in the dataset with the medium erosion class being greatly underrepresented. This can lead to the biasing of the model to the majority classes and minimize its capability to accurately learn the moderate pattern of erosion.

To solve the weighting of classes was done during model training which means that minority classes were given more weight in the loss function. Methods of oversampling, even SMOTE, were avoided deliberately in order to avoid the possibility of introducing artificial samples that can corrupt the actual dynamics of spatio-temporal erosion. On the same note, undersampling was not resorted to since it would lead to missing some important historical data on long time satellite measurements. This approach also makes sure that the model training is physically realistic and can reduce bias due to the imbalance between classes.

The final preprocessed dataset has a total 86 AOIs and seven rivers. It covers the years 1988 to 2025. The dataset has information about both the left and right banks, as well as their geomorphic, spectral, topographic, and soil-related properties. There are a total of 6,536 records, and each one is for a different combination of river, zone, bank side, and year.

This dataset is a good starting point for more research, such as modeling how riverbanks change over time and finding chars. It helps us understand erosion, accretion, and how temporary landforms like chars form. These are very important for keeping riverbanks stable.

## 4.4 Preliminary Designs:

This methodology's model combines geospatial and statistical techniques to examine riverbank dynamics. It comprises multiple tiers: an input tier, processing tier, classification tier, and output tier. The input layer comprises multi-temporal satellite images, confined to fixed Areas of Interest (AOIs), hence ensuring uniformity in spatial boundaries. In the processing layer, spectral indices are calculated, water masking is executed, and contours are delineated. A crucial component of this layer is the Best Line Detection algorithm, utilized to enhance the initially extracted riverbank lines. Char detection is integrated into this phase, utilizing variations in water coverage and moving boundaries to identify and monitor the emergence or dissolution of chars (temporary landforms created by sediment deposition in rivers).

The Best Line Detection technique enhances the riverbank line by identifying the best representative, continuous line through geometric filtering and distance-based optimization. This approach reduces fragmentation and enhances the continuity of the riverbank alignment, along with its distance from the river's centerline. The end product is a riverbank line that accurately depicts the steady, physically consistent bank across time. The process entails the following steps:

**Candidate Line Generation:** Initially, candidate lines are produced from the boundary pixels delineating water and non-water zones.

**Geometric Filtering:** Short, isolated, or excessively curved segments are eliminated. This aids in the removal of noise or transient features like sandbars.

**Distance-Based Optimization:** The proximity of each potential line to the river centerline is assessed. The actual bank line must be uniformly positioned on one side of the centerline, exhibiting a smooth contour in the direction of flow.

**Continuity and Smoothness Evaluation:** The remaining lines are assessed for spatial continuity, ensuring that the chosen line preserves a seamless flow and reduces sudden directional shifts. The best line is ultimately chosen, as it reduces fragmentation, maximizes continuity, and meets the criteria for distance consistency and smoothness.

### Implementation of Multi Level LSTM, XGBoost, LightGBM, Random Forest, CNN-LSTM-Attention Models

Multi-level Hierarchical LSTM model and baseline models are used (Random Forest, XGBoost, and LightGBM) in this research to predict riverbank erosion and accretion.

These models had been specifically tailored for the research model to work within multiple layers. For introducing a majority voting based ensemble model in order to optimize predictions and provide strong performance at any scale.

**Multi Level LSTM Model**

The LSTM model computes erosion and accretion along river banks by learning how both forms of water change over time using three years' worth of satellite images and other environmental data point information. The LSTM model takes advantage of 16 different features about the river banks including land cover types, topography, land use, etc. So it is able to identify sequential dependencies in the data and create a hierarchical model which can add accuracy for predictions at four different levels (global, river, zone and bank). To increase the accuracy of prediction, the model uses an ensemble strategy where majority votes are constructed on three random seeds (42, 123, 456) where the final prediction is made by the most common prediction of the three independently trained models.

**Multi Level LightGBM**

The LightGBM model is an example of using the gradient boosted model; it performs classification and regression using hyperparameters to train a model such as having 300 trees with maximum depth of the tree predicted to be 8 and learning rate set to 0.03 while accounting for class imbalance by weighting each class differently and utilizing regularization techniques to prevent overfitting. The model also uses ensemble majority voting where three models are trained with varying random seeds and the final choice of the class with the most votes is made which in turn lowers the variation in prediction and increases overall accuracy.

**Multi Level XGBoost**

The XG Boost Model employs a level of detail falling down the overall trends (global) to the bank level characteristics that constitute the most robust prediction basis since they have employed regularization techniques (L1 and L2), pruning (or removal of low performing prediction) and ensemble voting procedures to give rationales on data basis. The model applies 300 gradient boosted trees with a maximum depth of 8, learning rate of 0.03, and also advanced hyperparameters like minimum child weight (12), subsample ratio (0.7), column subsample ratio (0.7) and gamma (0.001) to restrain tree growth and overfitting. The framework also uses class balancing with sample weighting of frequency weights that are inverse and L1 (alpha=0.001) and L2 (lambda=1.5) regularization that limits the complexity of the model and improves generalization at all levels of the hierarchy. Besides making single model predictions, the framework also provides use of 3 seed ensemble with majority voting mechanism, where the model prediction of models with seed numbers 42, 123 and 456 are added together to form a better final prediction.

**Multi Level Random Forest**
The Hierarchical Random Forest model, works on predicting the erosion and accretion. It utilizes a level-based approach to increase precision with its hierarchical structure (Global, River, Zone, Bank). It also gives predictions by employing 300 decision trees trained on bootstrapped samples of data, with random feature selection to avoid overfitting. it also shows predictions based on the number of votes for each class and establishes features' importance based on impurity reduction. To deal with class imbalance it uses class weight. The model also makes use of ensemble majority voting to reinforce its predictions, in which three models are trained with distinct random seeds and results are independently predicted with each model with the overall result being determined by the majority of the votes, in effect, reducing the model variance. Last, the model develops hierarchical training to select the most specific model available for predicting erosion and accretion, producing variable essences among rivers and zones.

**CNN-LSTM with Attention Architecture**

**Introduction**
The physical nose and mouth of rivers continuously change with time through a combination of eroding and depositing materials, and these changes are an important part of many ecosystems, human development, and infrastructure. Being able to predict these changes requires a sophisticated model that accounts for the spatiotemporal complexity of how river systems develop over time. This research presents a new framework that employs a hierarchical deep learning method, using a CNN-LSTM architecture with Convolutional Layers and Multi-Head Attention mechanisms, to forecast both the processes of river erosion and accretion on all spatial scales, from global river systems to localized bank-scale changes. The research utilizes historical data derived from satellite imagery and topographic maps to develop a model for predicting river morphology and changes to river morphology with specific relevance to environmental resource management and disaster prevention.

**Data Description and Feature Engineering**
This study pulls together a rich set of geomorphological data from several rivers Baleshwar, Bishkhali, Karnaphuli, Payra, Shibsa, Surma, and Pasur. We broke each river down into zones, then split those into left and right banks, so you end up with a detailed map of each area. The dataset covers several years, which means you can actually see how things shift over time.
The model works with 16 features in five main groups. For land use and land cover, got vegetation coverage (Percent_Veg), built-up area (Percent_Builtup), and bare land (Percent_Bare) all key for understanding how stable the land is and how likely it is to change shape. Then, using remote sensing,the model presents spectral indices like vegetation health (Mean_NDVI, Mean_SAVI), built-up areas (Mean_NDBI), and other measures of environmental stress (Mean_MSI, Mean_NBR, Mean_BAI). These indicators really show what's happening ecologically and how people are changing the rivers. Topography matters too. We look at mean elevation (Mean_Elevation) and slope gradient (Mean_Slope), which play a big role in how fast water moves, how much sediment it carries, and how erosive the flow gets. Hydrological features—like

the channel area ratio (Char_Area_Ratio)reveal what's going on with the river's cross-section and how that affects flow and sediment movement.

Finally, historical changes are tracked: current intensity (Current_Intensity), two- and three-year trends (Intensity_2yr, Intensity_3yr), and the current classification (Class_Current). These give you a sense of how things have been shifting and help you spot patterns that stick around over time.

**Target Variables and Feature Adaptation**

This framework makes switching between erosion and accretion predictions pretty straightforward. All it takes is changing the feature names. For erosion, you stick "Ero_" in front of intensity features like Ero_Intensity or Ero_Intensity_2yr. For accretion, just swap in "Acc_" to get things like Acc_Intensity and Acc_Intensity_2yr. It's a simple trick, but it keeps the architecture the same across different prediction goals. No rebuilding is required; just rename the properties and then it's ready to tackle different problems. This makes the whole setup flexible and easy to use in all kinds of situations.

**Temporal Data Configuration**

One thing that really sets this framework apart is how it handles time. The temporal validation strategy is strict no sneaky data leakage here. The data gets split into three chunks. The Training Set has everything up to 2016, which gives a solid base for learning how rivers have changed. The Validation Set covers from year 2017 to 2021, so it shows more recent river conditions and helps with fine-tuning the model. The Test Set is for 2022 to 2025, which means the model gets tested on data it hasn't seen, just like a real forecasting challenge.

When it comes to building sequences, the framework grabs three years at a time. It slides a window over the data, each time grabbing three years in a row. Each sequence looks at three consecutive years of features, and the model's job is to predict the class of morphological change at the last year in the sequence. This setup lets the model pick up on patterns over a medium time span without bogging things down. It's a good balance enough history to spot trends, but not so much that the system gets unwieldy. In the end, the model learns from the past and makes solid guesses about what's next.

### Model Architecture

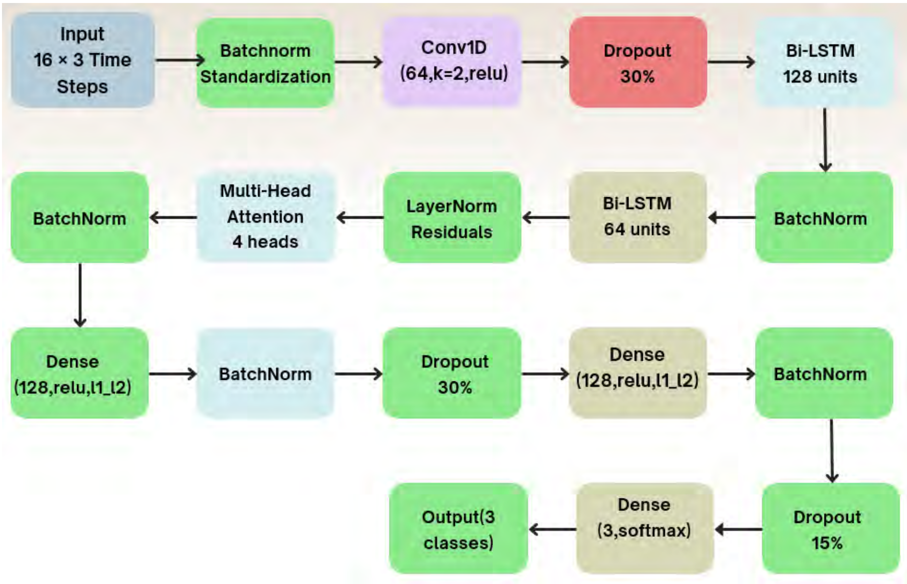


Figure 4.51: CNN-LSTM Attention Architecture

This Fig. 4.51 shows how the model architecture comes together. It's built to handle river morphological data in a way that really digs into the details. First up, there's the Bidirectional Processing Mechanism. Most models only move from past to future, but this one does something different. This network model is composed of two parts, a forward LSTM directionally from past to future, as well as the reverse LSTM moving from future to past. This is important because the actions for example, volume change that occur in a river are responding to events that happened in the past and events that will occur in the future. Therefore, in order to develop an understanding of an event like how a river's flow changes, the forward LSTM analyzes the past; and, the reverse LSTM provides information on the future event which provides context to the past like providing information to the past LSTM about a change in river flow before it occurred.

Next, it've got the Convolutional Layer for Temporal Feature Extraction. This part uses a 1D convolutional layer with 64 filters and a small kernel (size 2) to catch short-term patterns in the three-year data sequences. It picks up on sharp changes or local quirks that a regular LSTM might miss if it was just chugging through the sequence step by step.

Then there's the Multi-Head Attention Mechanism, which brings in four separate attention heads. Each head hones in on different details maybe one's catching seasonal plant shifts, another's watching rainfall, a third is tracking elevation changes, and the last one's following historical patterns. Processing all these angles at the same time lets the model zero in on what matters most, making predictions about complex river changes a lot sharper.

Finally, the Hierarchical Processing Strategy ties it all together. The model uses two LSTM layers, one on top of the other. The first layer, with 128 units, picks up the big-picture patterns. Then the second layer, which has 64 units, takes what the first layer found and turns it into features that make classification easier. Stacking the layers lets the model go deeper and understand the subtle ways river conditions shift over time.

**Hierarchical Training Framework**
This framework incorporates a four-layer spatial hierarchy, designed to model river dynamics at progressively finer spatial resolutions.
The Global Model Layer (Layer 1) was developed with all available data from rivers throughout the world and the entire spatial extent of the examined rivers, representing global trends, patterns, and relationships among the morphological changes identified for each river across the world. The River Models Layer (Layer 2), consists of a unique model for each river system, identifies individual river systems' characteristics and behaviors according to their unique watersheds and hydrologic regimes. Zone-Specific Models (Layer 3) focus on individual river reaches or zones of rivers, where spatial variation of the morphological processes occur within individual rivers. Bank-Specific Models (Layer 4) provide the finest spatial granularity by creating separate left and right bank models for each zone in a river to account for the asymmetrical nature of erosion and deposition in each river's banks.
Each level of the hierarchy is trained independently of one another based on their respective data set, thus avoiding transfer learning from one layer of the hierarchy to another. As a result, each hierarchical level develops spatially independent learning characteristics and does not influence each other. The training of each hierarchical level uses the Adam optimizer with a combination of learning rate scheduling and early stopping as means of developing a strong generalization while minimizing overfitting.

**Model Training and Evaluation:**

**Training Configuration:**
In order to create a training configuration that allows for both efficient learning and enough capacity for generalizing, the Optimization process will use the Adam optimizer with a learning rate of 0.001, and will use ReduceLROnPlateau Scheduling to reduce the learning rate when there is no longer improvement in the performance of validation. The Regularization process also provides various forms of regularization including 30% dropout after all convolutional and dense layers and L1_L2 Weight Regularization on all convolutional and dense layer weights, and Batch Normalization is utilized in all areas of the Architecture. Inverse frequency weight has been applied fo class balancing to ensure all morphological change classes are properly represented during training. Early Stopping is applied with a patience of 15 epochs to prevent overfitting while still allowing for sufficient training. To further enhance the robustness of prediction and lowering the model variance, an ensemble majority voting strategy is used in the framework, whereby three models are trained using varying random seeds (42, 123, 456) and the final prediction is assigned to the most voted class by the three models. This combination strategy is useful to reduce the effects of random starting points and represent a wide range of decision limits to make more stable and trustworthy predictions at all levels of hierarchy.

**Evaluation Metrics:**
The model's performance is evaluated by using various metrics. The primary metrics

used to evaluate the Model will be Overall Accuracy, Weighted F1 Score, Macro F1 Score, and Cohen's Kappa which will indicate the correctness of the predicted values and the precision and recall of the predicted values for each of the morphological change classes. Each morphological change class will also have its performance reviewed using the per class analysis which will include precision, recall, and F1 score for each morphological change class while the Analysis of AUC-ROC and Confusion Matrix provides additional indications of the performance of the Model.

**Overfitting Detection and Prevention:**
The framework implements a dual-threshold overfitting detection system, which flags overfitting when the training F1 - validation F1 gap exceeds 0.10 or when the validation loss / training loss ratio exceeds 1.50. Multiple prevention mechanisms, including early stopping, learning rate reduction, dropout, and weight decay, work together to maintain model generalization.

**System Innovations and Advantages:**
**Architectural Innovations:**
This model brings together a Hybrid Temporal System with Bidirectional Temporal Processing, blending Convolution and Attention in its layers, plus Multi-Level Spatial Modeling.Not only does the network explore the less obvious aspects of the data, but it also provides insight into the larger scale of what's happening by utilizing both the bidirectional LSTM to read information from previous and subsequent points in time, but can also provide insight into how to use convolutional and attention layers to help identify which part(s) of an input set will provide valuable information.

**Methodological Advantages:**
The framework keeps Temporal Integrity tight by using time-based splits. This setup blocks any old training data from sneaking into predictions, so you get results that actually reflect real-world scenarios. Feature Adaptability allows the model to easily switch between erosion and accretion prediction capabilities. Comprehensive Regularization provides a strong foundation for the model to exhibit strong generalizability across a variety of data sources.

**Practical Benefits:**
The use of Attention Mechanisms provides excellent Interpretability with respect to how the model arrived at its predictions, while also providing Scalability via Hierarchical Structures; additionally, each level of the model will be trained independently which eliminates the ability to propagate errors throughout the model.

**Conclusion:**
This bidirectional LSTM framework blends convolutional and attention mechanisms to tackle river morphological change prediction in a pretty smart way. It pulls together advanced neural networks, detailed spatial modeling, and strict checks on time-based data, which really boosts both accuracy and real-world usefulness. The model doesn't just handle one thing Rather it predicts both erosion and accretion, and it manages all those messy, complicated spatiotemporal patterns that usually trip up other systems. That makes it a solid choice for environmental work and river management. Plus, the focus on keeping the timing right, regularizing the model, and actually checking its results means you get predictions you can trust when making decisions.

## 4.5 Implementation of selected Design

**Bidirectional LSTM-GRU Hybrid with Attention Mechanism:**

**Introduction**

This research introduces an advanced system for forecasting alterations in river geomorphology, utilizing deep learning to identify trends across various spatial and temporal dimensions. The model has a unique four-layer ensemble architecture that is designed to systematically capture river dynamics, from global river trends to the specific behaviors of each individual riverbank. What makes this model unique is that it can capture both general river dynamics and specific bank-level behaviors. It does this while keeping strict time-based validation that is split up to protect the data's temporal integrity.

**Overall Architecture Overview**

A cascading learning approach will be implemented by the proposed framework that consists of four different learning layers, whereby the granularity of learning increases through each successive layer. The Global Model is the first layer where the overall river data sets are combined to derive general river dynamics and create a baseline for modeling purposes. The River-Specific Models layer then uses each river data set independently to characterize and represent that specific river's distinct characteristics and behaviors. The third level, Zone-Level Models, is implemented to represent rivers as zoned locations with defined geographic features; thus modeling more precisely by taking into consideration geographic features that affect flow of water within rivers. Finally, the Bank-Level Models predict changes at a river bank level; thus allowing for symmetric and asymmetric modeling of both banks of a river. The proposed layered approach to learning will provide a broad-based, global understanding of rivers while also providing localized predictions for river banks, thereby improving both precision and quality of river predictions and interpretability of river models.

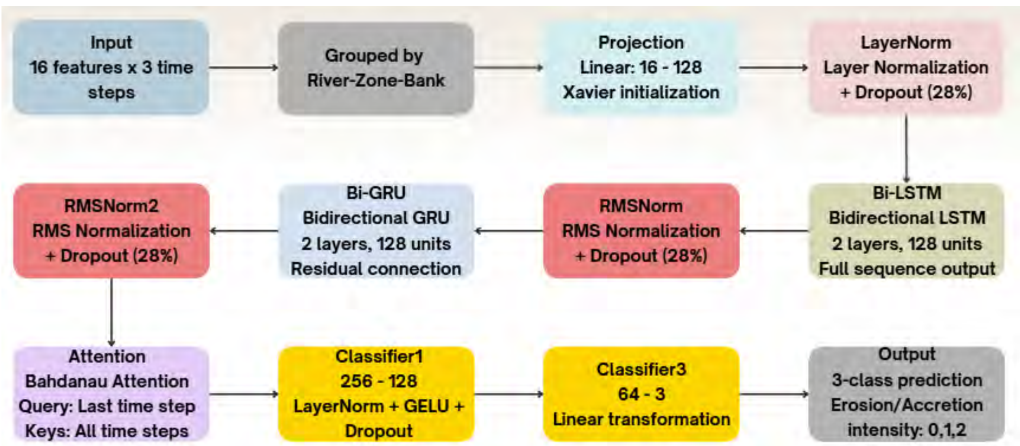


Figure 4.52: Bidirectional LSTM-GRU Hybrid with Attention Mechanism architecture

The flowchart in Fig. 4.52, represents the architecture of a Bidirectional LSTM-GRU Hybrid model, which has been developed for classifying the intensity of river erosion and accretion. The process starts with the input features, which are categorized according to the river zone and bank. These features are then subjected to projection, normalization, and a sequential dual-layer of Bi-LSTM and Bi-GRU layers. A Bahdanau Attention mechanism is also incorporated to emphasize the importance of key time steps before the data is fed into the multi-stage classifiers. The final output is a three-class classification (0, 1, or 2), which identifies the intensity of geomorphic change.

### Core Model Architecture Components

The Bidirectional LSTM-GRU model is a hybrid model that can effectively manage temporal geomorphological data using the attention mechanism. The model's input layer processes 16 features over two time steps, representing one year of historical data. This makes the model computationally efficient

### RMSNorm Layer

One of the major components of the architecture is the RMSNorm layer, as it helps achieve better gradient flow compared to other normalization techniques like LayerNorm. The formula for the RMSNorm is given by

$$\mathrm{RMSNorm}(x) = \frac{x}{\sqrt{\mathrm{mean}(x^2) + \varepsilon}}\gamma \tag{4.29}$$

Such a formula helps achieve better stability during the training process, especially for recurrent networks.

### Bahdanau Attention Mechanism

The system uses an additive attention mechanism based on Bahdanau's work. This lets the model focus on important temporal patterns in the data. The mechanism of this model is made of three parts: query transformation (Wa), key transformation (Ua), and scoring (Va). By calculating alignment scores between the query and each time step, it identifies the historical periods most relevant for predicting geomorphological changes

### Bidirectional LSTM-GRU Hybrid

The basic temporal model is a combination of both LSTM and GRU architectures. The first layer is a Bidirectional LSTM with 128 hidden units. This layer is used to identify long-term dependencies in both directions. The second layer is a Bidirectional GRU with 128 hidden units. This layer provides more computational efficiency without compromising long-term dependencies. A residual connection is added to maintain the flow of information in both directions to avoid vanishing gradients.

### Multi-Layer Classifier

The network used in the classification has a three-layer feedforward configuration using GELU activation functions. The network has 256 input features and reduces to 128 hidden units and then 64 intermediate features before outputting 3 classes for the intensity of geomorphological change. The network uses 28% dropout regularization in all layers to avoid overfitting.

### Temporal Sequence Configuration of Sequence Length Selection

To obtain the best possible prediction using the model, it uses two years' worth of historical data. This was specifically chosen to allow the use immediate most recent previous experiences but at the same time provide computational performance. Also, using a sliding window approach will result in overlapping sequences, so all data is used and all appropriate temporal dependencies are learned.

### Temporal Sequence Configuration of Split Strategy

An innovative aspect of the framework is the strict temporal split scheme of the data; i.e. ensuring the training/validation/test data do not overlap, thereby preventing possible data leakages. The training data set will include data prior to the end of 2016, while the validation dataset will include all of 2017 through 2021, and the test dataset will include 2022 through 2025. The forward-looking configuration of the model will predict conditions from historical data, similar to how real-world forecasts are created.

### Input Feature Categories

The 16 features used to develop the model consist of 5 major feature categories. A land-use/land-cover (LULC) category consists of features such as Percent_Veg, Percent_Builtup, and Percent_Bare and is used to provide details about the stability of the land and its potential for erosion. The spectral indices category consists of features in which remote-sensing data are used to measure vegetation health (Mean_NDVI) and detect built-up areas (Mean_NDBI) and indicate plant stress (Mean_MSI). Topographic category includes features such as Mean_Elevation and Mean_Slope which help in determining water velocity and transportation capacity of sediment. Hydrologic features, such as Char_Area_Ratio, represent channel geometry and its effect on sediment transport. The last category of features, Historical Change, provides multi-annual trend data to allow the model to learn how the changes occurred and whether or not there is autocorrelation over time.

### Feature Scaling Methodology

All of the features have been standardized using the standard scaler (z-score normalization) to ensure that the gradients would flow smoothly and that there would be no possible confounding variables owing to the differences of the scales and distributions of the features used as inputs to the model. Furthermore, by normalizing each feature at each of the hierarchical levels independently, consistency is assured, and any spatial domain specific differences will not cause any biases in the model

### Training Configuration

Optimisation Parameters uses AdamW for the weight decay of 4e-5 to form a properly weighted optimised algorithm by providing the ability for the learning rates to be adjusted as the input data adapts through using L2 (weight decay) regularisation. A learning rate of 8e-5 is paired with the Cosine Annealing learning rate scheduler to gradually decrease and optimise performance over time through proper convergence; this will ensure that the output of the model converges smoothly during training as well as improve model convergence. In addition, a batch size of 16 to provide the right balance for efficient computing with stable gradient estimates is used. The training is performed for at most 150 epochs using the early stopping criteria (patience = 20 epochs) to prevent overfitting of the later epochs when training has concluded.

Regularisation Strategies allow us to generalise from the data through using multiple regularisation techniques such as dropout 28%, weight decay 4e-5 and label smoothing 8%. We are also augmenting data through the use of noise, by injecting Gaussian noise (standard deviation = 0.012) across features, to be used as a feature add for reducing overfitting. We are also implementing gradient clipping at a maximum gradient of 1.0 to continue to provide smooth gradient estimations to maintain stable training.

To combat class imbalances inverse frequency weighting method is used to ensure that each class (less frequently changing geomorphologically) receives the necessary attention while training. This reduces the likelihood that a model is biased to the majority class and provides for a consistent level of performance for all change classes during evaluation.

**Hierarchical Training Process**

The Global Model, or Layer 1, is based on a complete dataset and provides a reference point for what constitutes universal geomorphological features, or patterns, that will help build future models (it will extract features and help us to understand the rivers and river dynamics at a very high level).

The River-Specific Models, or Layer 2, take segments of data based on individual rivers and provide models that capture river-specific characteristics. Because they can be initialized from the Global Model, uses transfer learning to converge the models more quickly while making sure they are specific to their respective/rivers. The Zone-Level Models (Layer 3) capture river-specific variations within specific river zones (not just at the river level) but require a minimum of 10 sequences in order to ensure reliability while still allowing for the fact that river data will be variable in terms of how much is available.

The Bank-Level(Layer 4) Models provide predictions for each river bank (left and right). In cases where there is no sufficient data for a single bank, the model will be adjusted for the bank by using a fine-tuned version of the respective parent zone models; this allows us to provide reliable predictions for banks even when insufficient data exists.

**Ensemble Model and Majority Voting**

To improve prediction robustness the framework uses an ensemble majority voting scheme in which three models are trained on separate random seeds (42, 123, 456) and the overall prediction is made by choosing the class that is voted by majority of the three models. This collective strategy is effective in reducing the effects of randomization of the initializations and exploring a variety of decision limits, leading to more consistent and dependable forecasting at all the levels of the hierarchy. The predictions are then aggregated across the world, so that the consensus based classification can make use of the advantages of each model whilst ameliorating the disadvantages, and thus obtain excellent generalization accuracy on temporal data that have not been seen before.

**Evaluation Metrics**

Primary Metrics (accuracy and weighted F1 score) are evaluated from several primary metrics (i.e. accuracy and weighted F1 score - both of which measure precision/recovery) as well as one macro metric (macro F1 score) which gives an unweighted average across all classes; Cohen's kappa provides a measure of how well the model/observer agrees beyond random chance (chance).

In addition to primary metrics, Non-Primary Metrics (per-class metrics) include the same detailed per-class metrics (i.e., precision, recall, and F1 score) for each of the No/Minimal/Mild/Moderate/High Change; they allow one to gain deeper insights into the performance of the model.

Advanced metrics (e.g., AUC-ROC curves and confusion matrix analysis) are used to evaluate the model's capability to discriminate among classes and to provide information with respect to errors. In addition, F1 gap and loss ratio thresholds will be used to detect overfitting.

**Overfitting Detection and Prevention**

Detection of overfitting is based on two criteria in the Overfit Detection Criteria. The first criterion is a significant difference between the F1 score of training and validation (greater than 0.15) and the second criterion is a train/validation loss ratio greater than 1.2. Using this double threshold for detecting overfitting limits the amount of false positives and allows for better identification of true cases of overfitting.

The use of early stops on validation loss when it reaches a plateau, the use of a learning rate schedule, and extensive regularization are all used to prevent overfitting and together they help ensure that the model remains generalizable across a wide range or set of inputs.

**Model Innovations and Advantages**

Innovations in Architecture's system are architecturally innovative, including being able to process in both forward and reverse directions (using FFRD) by capturing both the past and the future context and providing a memory-efficient means of processing data by incorporating a hybrid of LSTM and GRU networks. The use of attention mechanisms is very effective for orienting to the most important time patterns, and RMS Normalisation provides extra stability when training.

In addition to being methodologically innovative, the combination of effective temporal splits, hierarchical model learning that gradually generates compound-dependent versions of the model, multiple layers of performance evaluation effectiveness, and many layers of robust regularisation works together to guard against overfitting are other advantages of this methodology.

The primary practical advantages of the Practical Benefits Model include greater interpretability as a consequence of its hierarchy, scalability (in three different spatial dimensions), transferability (via parent model initialization), and robustness from a multitude of regularisation techniques.

**Implementation Details**

Deep learning with a technical stack developed using PyTorch 2.0+ supplemented by NumPy, Pandas, Scikit-Learn, and Matplotlib for data processing, visualization, and assessment. The system uses CUDA-capable GPUs for efficient computation due to hardware acceleration.

Reproducibility Measures for the Reproducible System include the use of fixed random seeds, the use of deterministic CUDA operations, maintaining extensive logs throughout the entire process and saving the state of the model to allow for complete reproducibility of the process.

**Conclusion**

The hierarchical deep learning system represents a new way to predict changes in rivers by using a combination of improved accuracy and usefulness. A hybrid of bidirectional long-term memory networks, gated recurrent units with attention mechanisms, validation over strict time intervals, and meaningful evaluation, gives an indication of whether the predicted values would be reliable, interpretable and useful for managing rivers. The system is designed to easily accommodate erosion and accretion predictions, providing researchers and land managers with a flexible resource for geomorphological research and management.

# Chapter 5

# Result Analysis

This chapter presents the experimental results of the proposed models for erosion and accretion intensity classification into three classes: Low (0), Medium (1), and High (2). The performance of the Bidirectional LSTM–GRU hybrid model is systematically compared with several baseline models using standard evaluation criteria. The analysis covers global model performance, river-specific performance, confusion matrices, receiver operating characteristic (ROC) curves, and spatial risk heat maps, which together provide actionable insights for riverbank management in Bangladesh.

Model performance is measured to have a rigorous and reproducible evaluation with **Accuracy**, **Macro F1-score**, and **Weighted F1-score** and **Cohen Kappa**, All of these are derived from the confusion matrix. Let $TP_i$, $FP_i$, and $FN_i$ denote the true positives, false positives, and false negatives for class $i \in \{0, 1, 2\}$, and let $N$ be the total number of samples.
The overall **Accuracy** is defined as:

$$\text{Accuracy} = \frac{TP_0 + TP_1 + TP_2}{N} \tag{5.1}$$

The **F1-score** for each class $i$ is computed as:

$$\text{F1}_i = \frac{2TP_i}{2TP_i + FP_i + FN_i} \tag{5.2}$$

The **Macro F1-score**, which treats all classes equally, is given by:

$$\text{F1}_{\text{macro}} = \frac{\text{F1}_0 + \text{F1}_1 + \text{F1}_2}{3} \tag{5.3}$$

The **Weighted F1-score**, which accounts for class imbalance by weighting each class according to its support, is defined as:

$$\text{F1}_{\text{weighted}} = \frac{n_0\text{F1}_0 + n_1\text{F1}_1 + n_2\text{F1}_2}{N} \tag{5.4}$$

where $n_i$ denotes the number of true samples belonging to class $i$.
Finally, **Cohen's Kappa** ($\kappa$) measures the agreement between predicted and true labels while correcting for chance agreement:

$$\kappa = \frac{p_o - p_e}{1 - p_e} \tag{5.5}$$

where the observed agreement $p_o$ is:

$$p_o = \frac{TP_0 + TP_1 + TP_2}{N} \tag{5.6}$$

and the expected agreement by chance $p_e$ is computed as:

$$p_e = \sum_{i=0}^{2} \left( \frac{n_i}{N} \cdot \frac{\text{pred}_i}{N} \right) \tag{5.7}$$

with $\text{pred}_i$ denoting the number of samples predicted as class $i$.
These metrics provide a comprehensive assessment of both overall classification accuracy and class-wise balanced performance, which is particularly important for evaluating erosion and accretion intensity prediction under class imbalance conditions.

## 5.1 Result of All Model

### 5.1.1 Model Result for Erosion

Table 5.1: Global Model Results for Erosion Prediction:

| **Model** | **Accuracy** | **Weighted F1** | **Macro F1** |
|---|---|---|---|
| Multi Level LSTM | 0.3198 | 0.3123 | 0.2554 |
| CNN-LSTM with attention mechanism | 0.3939 | 0.3981 | 0.3488 |
| Multi Level Random Forest | 0.5523 | 0.4886 | 0.3060 |
| Multi Level XGBoost | 0.5872 | 0.4962 | 0.3061 |
| Multi Level LightGBM | 0.5349 | 0.4604 | 0.2783 |
| **Bidirectional LSTM-GRU Hybrid with Attention Mechanism** | **0.5116** | **0.4911** | **0.4256** |

This table 5.1,contains the global-level (Level 1) accuracy results of all models which compares the results of six machine learning architectures to predict the intensity of erosion. Multi Level XGBoost model was the most accurate with a value of 0.5872 showing better classification ability on a global basis. CNN-LSTM with attention mechanism achieved an accuracy of 0.5939, and Multi Level LightGBM had a competitive performance with the accuracy of 0.5349. Even though the Bidirectional LSTM-GRU Hybrid with Attention Mechanism had a relatively lower accuracy of 0.5116, it had much better scores in Macro F1 (0.4256) and Weighted F1 (0.4911) scores, which means that it is more capable of dealing with an imbalance of classes and making more balanced predictions in all classes of erosion intensity, especially in underrepresented classes. The tree-like models (XGBoost, LightGBM and Random Forest) proved to be accurate all the time whereas hybrid neural networks with attention mechanisms have more balanced results when dealing with minor categories and thus is better suited to situations where fair prediction of all erosion categories is required.

### 5.1.2 Model Result for Accretion

Table 5.2: Global model results for Accretion prediction:

| **Model** | **Accuracy** | **Weighted F1** | **Macro F1** |
|---|---|---|---|
| Multi level LSTM | 0.3488 | 0.3483 | 0.3274 |
| CNN-LSTM with attention mechanism | 0.3648 | 0.3670 | 0.3499 |
| Multi Level Random Forest | 0.3895 | 0.3723 | 0.3266 |
| Multi Level XGBoost | 0.4419 | 0.3836 | 0.3294 |
| Multi Level LightGBM | 0.3895 | 0.3427 | 0.3337 |
| **LSTM-GRU Hybrid with Attention Mechanism** | **0.4128** | **0.4340** | **0.4022** |

The table 5.2 contains the global-level (Level 1) accuracy results of all models ,which presents the comparative performance of six models for predicting accretion intensity. The CNN-LSTM with attention mechanism achieved the highest accuracy of 0.3658, followed by Multi Level XGBoost (0.4419) and Multi Level LightGBM (0.3895). Notably, while the Bidirectional LSTM-GRU Hybrid with Attention Mechanism showed an accuracy of 0.4128, it demonstrated the highest Macro F1 (0.4022) and Weighted F1 (0.4340) scores among all models, indicating exceptional ability to provide balanced predictions across all accretion classes and effectively handle class imbalance. This superior F1 performance suggests that the BiLSTM-GRU model is particularly effective in correctly identifying minority classes, making it the most reliable choice for scenarios requiring balanced classification despite slightly lower overall accuracy. The relatively lower accuracies across all models for accretion (0.3488-0.4419) compared to erosion reflect the inherently more complex and unpredictable nature of sediment deposition processes.

## 5.2 Result Analysis of Bidirectional LSTM-GRU Hybrid with Attention Mechanics

### 5.2.1 Model Result for Erosion

**Global:**

The Global Hierarchical Model for erosion, utilizing a Bidirectional LSTM–GRU hybrid with attention, has an accuracy of 51.16% on an independent global test set of 344 samples, with a weighted F1-score of 0.4911 and a macro F1-score of 0.4256. It signifies a notable enhancement over the 33% random baseline for a three-class problem and surpasses the worldwide performance of the associated accretion model, suggesting that erosion signals are relatively more discernible from the available feature set at this scale. The non-overfitting flag, along with a moderate F1-gap of 0.0736 and a validation-to-training loss ratio of 1.08, indicates that the Bidirectional LSTM–GRU hybrid with attention model generalizes adequately without significant overfitting.

#### Learning Dynamics: Loss, F1, and Accuracy Trends and Class-wise Behavior from the Confusion Matrix

The model performed best at predicting or representing Class 0 (minimal erosion) - F1-score = 0.6340, precision = 0.636, and recall = 0.632. Thus, the model is able to identify stability and little erosion on banks, which have clear spectral and geomorphic signatures and are the most common types in the dataset.

Class 2 (high erosion) also does pretty well, with an F1 score of 0.488, a precision of 0.497, and a recall of 0.487. It finds almost half of the high-erosion cases. This is very important for managing risk because these areas are most likely to lose land and banks. The ROC-AUC for Class 2 (about 0.633) shows that the model always tells the difference between areas with a lot of erosion and areas without a lot of erosion.

But Class 1 (moderate erosion) is still the hardest category, with an F1-score of 0.155, a precision of 0.267, and a recall of 0.110. Many samples of moderate erosion are incorrectly labeled as either low or high erosion. This is probably because the class boundaries are not clear, especially when there is class imbalance. This means that the model can't tell the difference between moderate erosion patterns on a global scale.

In general, the Global BiLSTM–GRU with Attention model is a good starting point for predicting erosion in all rivers. With a 51.16% accuracy rate and a weighted F1-score of 0.49, it is fairly adept at distinguishing between low and high erosion classes, and its ability to pick out high erosion areas may be key to setting up critical risk areas with those measurements. However, there is a significant disconnect with moderate erosion classifications, suggesting that it is very difficult to classify moderate erosion globally; therefore, this supports a hierarchical approach that utilizes localized models based on specific rivers and riverbanks to consolidate prediction accuracy, improve separation of the overlapping classes, and aid in distinguishing moderate erosion from other classes.

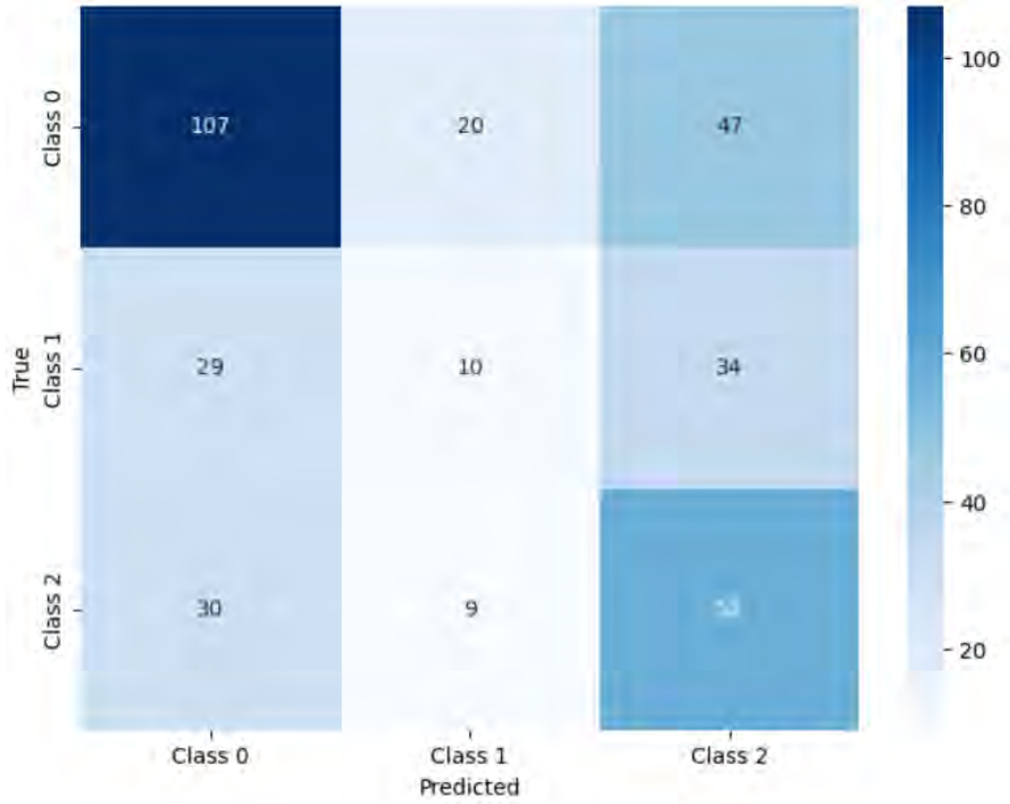


Figure 5.1: Confusion matrix for the Global layer

The confusion matrix plots in Fig. 5.1 shows the performance of the classification model for three classes of intensity levels. The diagonal lines represent accurate classifications for Class 0, Class 1, and Class 2. Although the model possesses high prediction accuracy for Class 0, as indicated by accurate classifications for 107 samples, it also presents a major challenge for Class 1 samples, where only 10 samples were classified accurately. This problem, which occurs during the classification of Class 1 and Class 2 samples, relates to the problem of class imbalance discussed earlier.

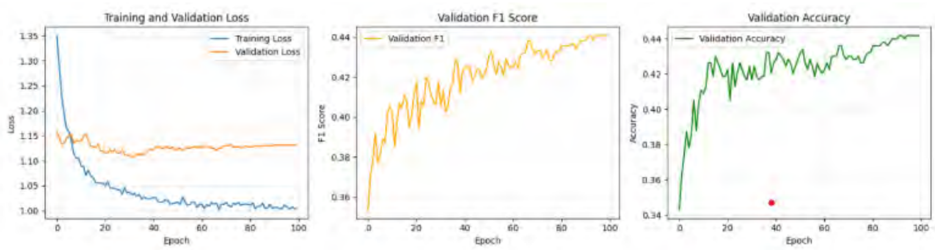


Figure 5.2: Loss, F1 Score and Accuracy Graph

This series of training plots in Fig. 5.2 shows the model's learning process throughout 100 epochs, where it can be seen that the model is constantly learning, indicated by the decrease in training loss and the increase in validation accuracy and F1 scores. The validation loss also plateaus early on, which indicates that the model achieves its maximum predictive power early on without much overfitting. These metrics affirm the effectiveness of the model's architecture, which is a combination of LSTM and GRU, in learning the underlying temporal patterns of river geomorphology.

**River:**

Table 5.3: River wise Result:

| River | Accuracy | Weighted F1 | Macro F1 | Test Samples |
|---|---|---|---|---|
| Baleshwar | 0.50 | 0.4552 | 0.4347 | 40 |
| Bishkhali | 0.3077 | 0.3370 | 0.2809 | 52 |
| Karnaphuli | 0.3235 | 0.3354 | 0.3201 | 68 |
| Pasur | 0.50 | 0.5200 | 0.4931 | 36 |
| Payra | 0.4643 | 0.4332 | 0.3761 | 56 |
| Shibsa | 0.3667 | 0.2924 | 0.2478 | 60 |
| Surma | 0.25 | 0.2192 | 0.2483 | 32 |

The table 5.3 shows how well the model performed on these particular rivers, which indicates that different rivers have different levels of accuracy. For example, the Baleshwar and Pasur rivers have the best accuracy at 0.50, while the Surma river is the most difficult to make predictions on, with an accuracy of only 0.25. This is an indication that different rivers have different characteristics that influence their rate of flow, which in turn influences the intensity of erosion or accretion.

The Baleshwar model hits 50% accuracy, with a weighted F1 of 0.455 and a macro F1 of 0.435 on 40 test samples. It stands out when it comes to high erosion (Class 2), pulling in an F1-score of 0.621. It also does a decent job with low erosion (Class 0). But when moderate erosion (Class 1) comes into play, things fall apart a tiny sample size and lots of overlap with other classes drag its F1-score all the way down to 0.091.

The Shurma model performs poorly, achieving only 25% accuracy and a weighted F1-score of 0.219. It predicts Class 0 with high precision but low recall, and its Class 2 performance appears inflated due to frequent false positives. The loss curves fluctuate considerably, indicating unstable training caused by the small sample size. The AUC values for all classes are close to random.

Among the other rivers, Bishkhali and Karnaphuli show moderate performance, with substantial confusion between erosion classes. Pasur performs best (50% accuracy; weighted F1-score = 0.520), capturing both low and high erosion cases. Payra performs reasonably for low erosion but struggles with moderate and high erosion, while Shibsa performs better for moderate erosion but misses most high-erosion cases. Overall, Baleshwar achieves the highest accuracy (50%) among the evaluated rivers.

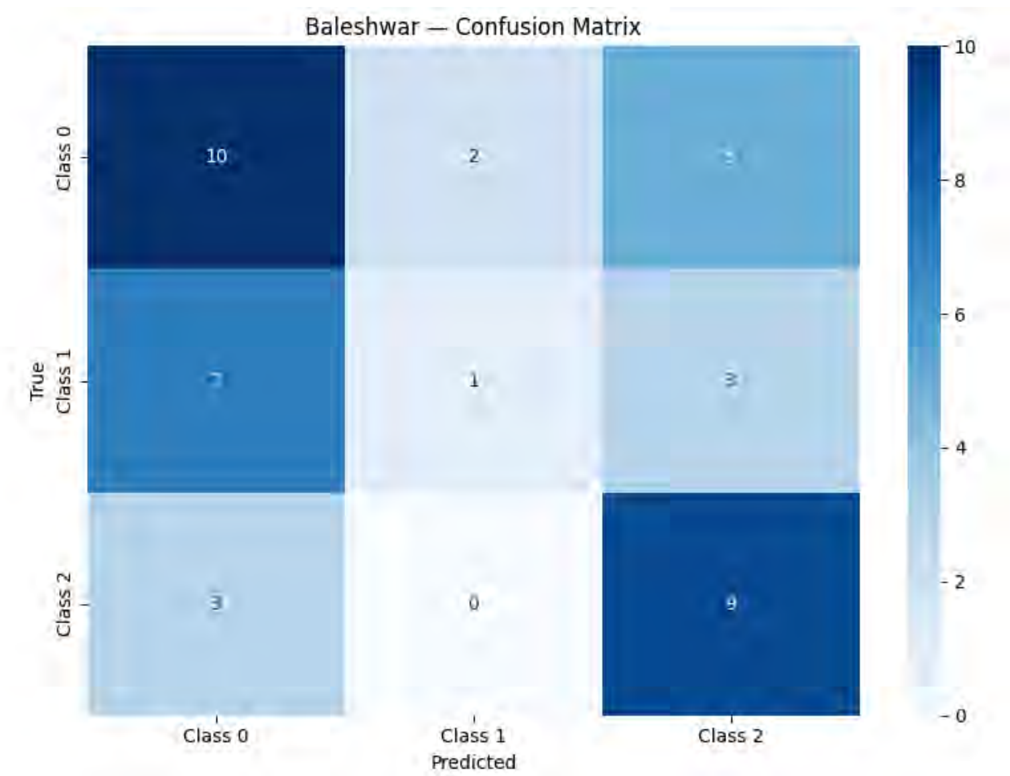


Figure 5.3: Confusion matrix for the Baleshwar River

This matrix in Fig. 5.3 gives a precise description of the classification results for the model in relation to the Baleshwar River dataset, which recorded a top accuracy rate among all datasets at 0.50. The model demonstrates a high capacity for correctly identifying the Low (Class 0) and High (Class 2) classes of intensity changes, as it correctly predicted 10 and 9 samples, respectively. Nevertheless, the challenge of correctly identifying the Medium (Class 1) category still persists in this dataset as well.

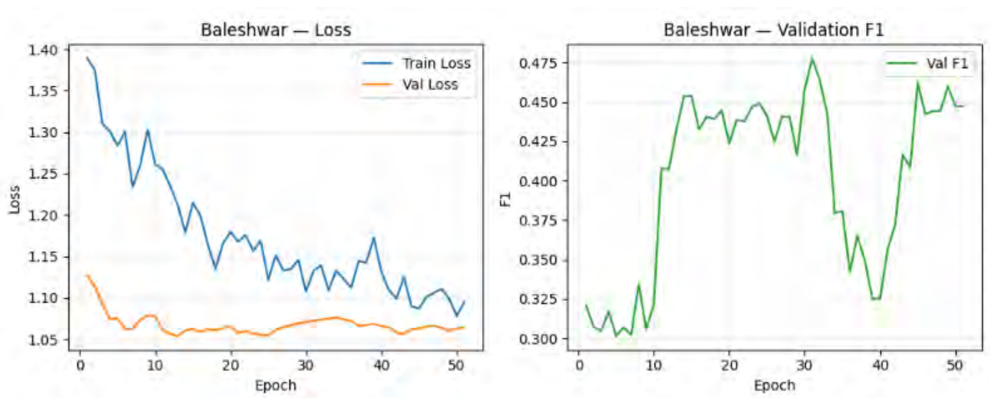


Figure 5.4: Loss and F1-score for the Baleshwar River

These curves in Fig. 5.4 are specific to the training progress of the Baleshwar River model and show a steep decline in training loss in the initial 20 epochs, followed by stability. The validation F1-score has significant fluctuations, with the maximum value at around 0.475 at epoch 32. This indicates that the model is sensitive to the temporal patterns in this particular river. The validation loss has low and constant values, indicating that the hybrid model has managed to avoid overfitting in any significant manner and has tried to generalize the geomorphic patterns.

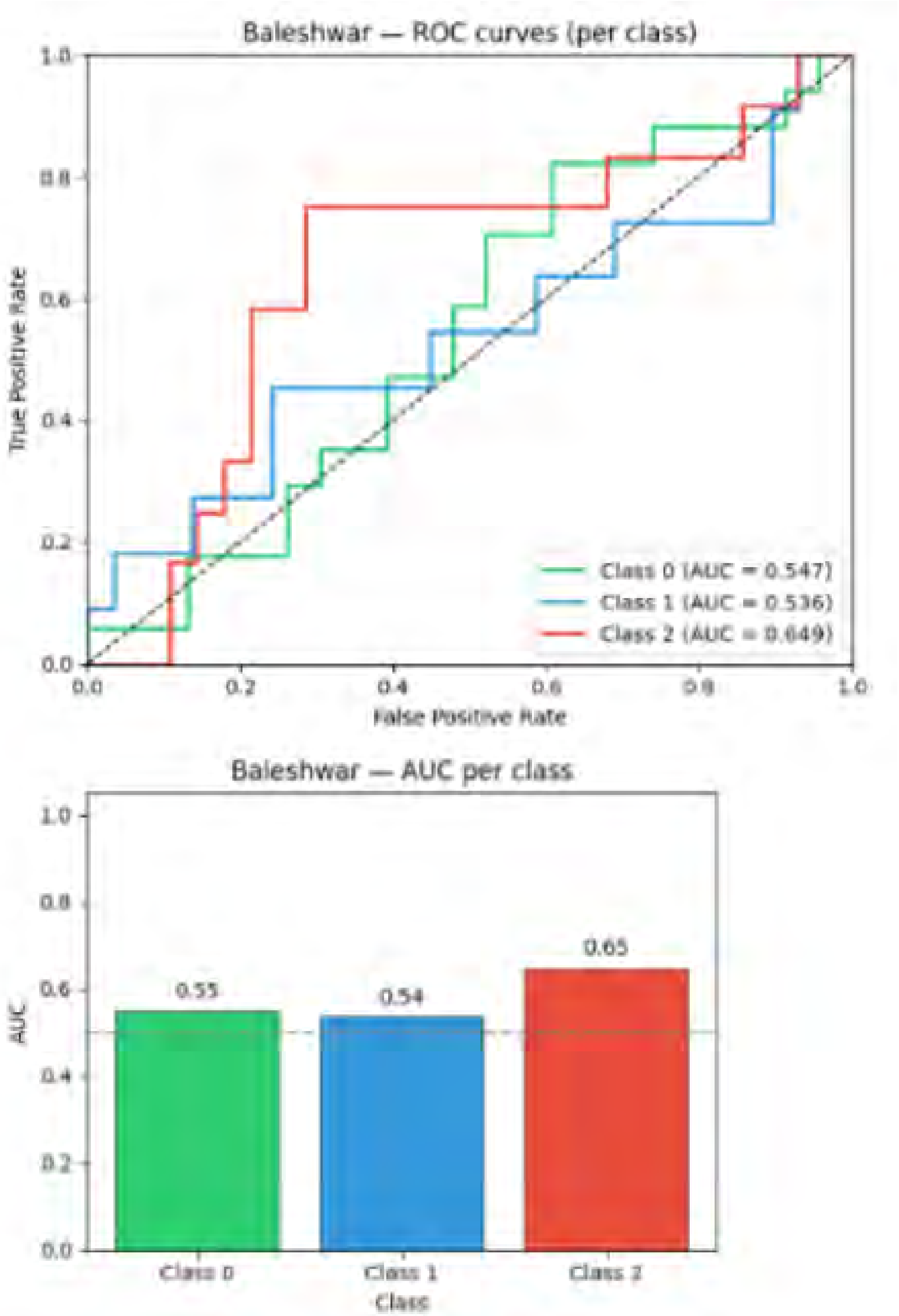


Figure 5.5: ROC curves and AUC for the Baleshwar River

The Receiver Operating Characteristic (ROC) curves and Area Under the Curve (AUC) in Fig. 5.5 values for the Baleshwar River model, based on three different classes, are shown in Figure 5.5. The model performs best on Class 2 (High Intensity) with an AUC of 0.65, followed by Class 0 with an AUC of 0.55 and Class 1 with an AUC of 0.54. Each of the three curves is above the diagonal dashed line, showing that the model performs better than a random classifier for all classes. This shows that although the model performs best on high-intensity geomorphic changes, it has a consistent level of predictive ability for the entire imbalanced dataset.

**Zone:**

Table 5.4: Zone-wise result of some rivers:

| Zone | Accuracy | Weighted F1 | Macro F1 | Test Samples |
|---|---|---|---|---|
| Pasur Zone 4 | 0.75 | 0.73 | 0.73 | 4 |
| Surma Zone 5 | 0.75 | 0.77 | 0.73 | 4 |
| Bishkhali Zone 3 | 0.00 | 0.00 | 0.00 | 4 |
| Baleshwar Zone 5 | 0.00 | 0.00 | 0.00 | 4 |

The table 5.4 shows two zones having very high performance (Pasur Z4 and Surma Z5) both did achieve approximately 75% accuracy and a Macro F1 of about 0.73, with promising goodness of fit for all three classes of erosion (low, moderate, and high). The model in Pasur Z4 also did a good job of separating moderate and high erosion (Class 1 with an F1 score of approximately 0.67; Class 2 with an F1 score of approximately 0.80). Surma Z5 demonstrated similar characteristics and performance for both the majority and minority classes. Conversely, the two Zones (Bishkhali Z3 and Baleshwar Z5) with the lowest performance achieved F1's of 0% and 0 respectively, as they had an extreme class imbalance or excessive label noise, which caused the model to mis-classify all samples, thus preventing the model from learning any differentiating patterns. This suggests that data scarcity and class imbalance dramatically impact the model's performance; in this case, the model over-fitted on the small test set. Based on these results, it appears that although the hierarchical BiLSTM–GRU model is performing well on Zones that have abundant and well-distributed data, there is a dramatic reduction of performance when classes are underrepresented, which suggests that zone-level performance should only be evaluated qualitatively in conjunction with river-level performance statistics.

**Bank:**

Table 5.5: The results of selected banks

| Bank (River_Zone_Bank_Side) | Accuracy | Weighted F1 | Macro F1 | Test Samples |
|---|---|---|---|---|
| Baleshwar_zone_6_bank_right | 1.00 | 1.00 | 1.00 | 2 |
| Baleshwar_zone_8_bank_left | 0.00 | 0.00 | 0.00 | 2 |
| Karnaphuli_zone_15_bank_left | 1.00 | 1.00 | 1.00 | 2 |
| Karnaphuli_zone_2_bank_left | 0.00 | 0.00 | 0.00 | 2 |
| Pasur_zone_5_bank_left | 1.00 | 1.00 | 1.00 | 2 |
| Pasur_zone_7_bank_left | 0.00 | 0.00 | 0.00 | 2 |
| Payra_zone_2_bank_left | 1.00 | 1.00 | 1.00 | 2 |
| Payra_zone_1_bank_left | 0.00 | 0.00 | 0.00 | 2 |
| Shibsa_zone_7_bank_left | 1.00 | 1.00 | 1.00 | 2 |
| Shibsa_zone_3_bank_left | 0.00 | 0.00 | 0.00 | 2 |
| Surma_zone_3_bank_left | 0.50 | 0.33 | 0.33 | 2 |
| Surma_zone_1_bank_left | 0.00 | 0.00 | 0.00 | 2 |

The table 5.5 represents that two out of three categories at the local level, some of the banks, such as the "Baleshwar_zone_6_bank_right" and the "Pasur_zone_5_bank_left," attain a perfect score (F1 = 1.0) by correctly classifying both of the test samples that belong to the same class. Nonetheless, this does not imply that the model has "solved" the predictions associated with these particular banks. Instead, it reflects a significant degree of overfitting by the model to the patterns exhibited by both of the very small sample test sets because there are more parameters in the complex model than there are observations at that specificity level. On the flip side, the "Baleshwar_zone_8_bank_left" is misclassified with an overall score of zero due to class size issues, the infrequency of some classes, as well as the geometric noise associated with them. Generally, the classification model tends to find "globally" common patterns while ignoring small local anomalies. Models that produce intermediate results, like "Surma_zone_3_bank_left," are unstable, so a single correct misclassification can cause the score to drop by 50 percent. The unreliability of short sequence lengths or the low number of labels results in the model's failure to learn effective temporal signatures due to the limits and discrepancies of its attention mechanism. Overall, whether banks are producing results at the bank level is influenced by random variation, class imbalance as a whole, and noise associated with the labels, so bank-level results are best interpreted as overall statistical values and qualitative spatial patterns; however, river- and zone-level models produce more reliable quantitative assessments.

### 5.2.2 Model Result for Accretion

**Global:**

The Global Hierarchical Model, which uses a bidirectional LSTM–GRU hybrid with attention, provides a baseline for predicting river geomorphological change. It achieves a global accuracy of 41.28%, exceeding a random baseline and highlighting the difficulty of global-scale prediction. The training loss decreases consistently, indicating good convergence, while the validation loss plateaus at approximately epoch 20, suggesting limited generalization at the global scale due to complex inter-river variability. Validation accuracy and F1 improve steadily, with the F1 reaching 0.44, indicating that temporal weighting was effective, while dropout and label smoothing helped stabilize the model's predictions. The confusion matrix shows that Class 0 (minimal change) is classified with high accuracy but is sometimes confused with Class 2 (high change); Class 1 (moderate change) remains difficult to separate due to overlap with Classes 0 and 2. Overall, the model is reliable for Class 0 but exhibits low recall, and it performs reasonably for Class 2, which is important for detecting extreme geomorphological change events. Performance for Class 1 is comparatively weak (F1 = 0.25). The weighted F1 score of 0.4340, indicates that while the global model captures large-scale trends, additional hierarchical layers are required to refine predictions at smaller spatial scales.

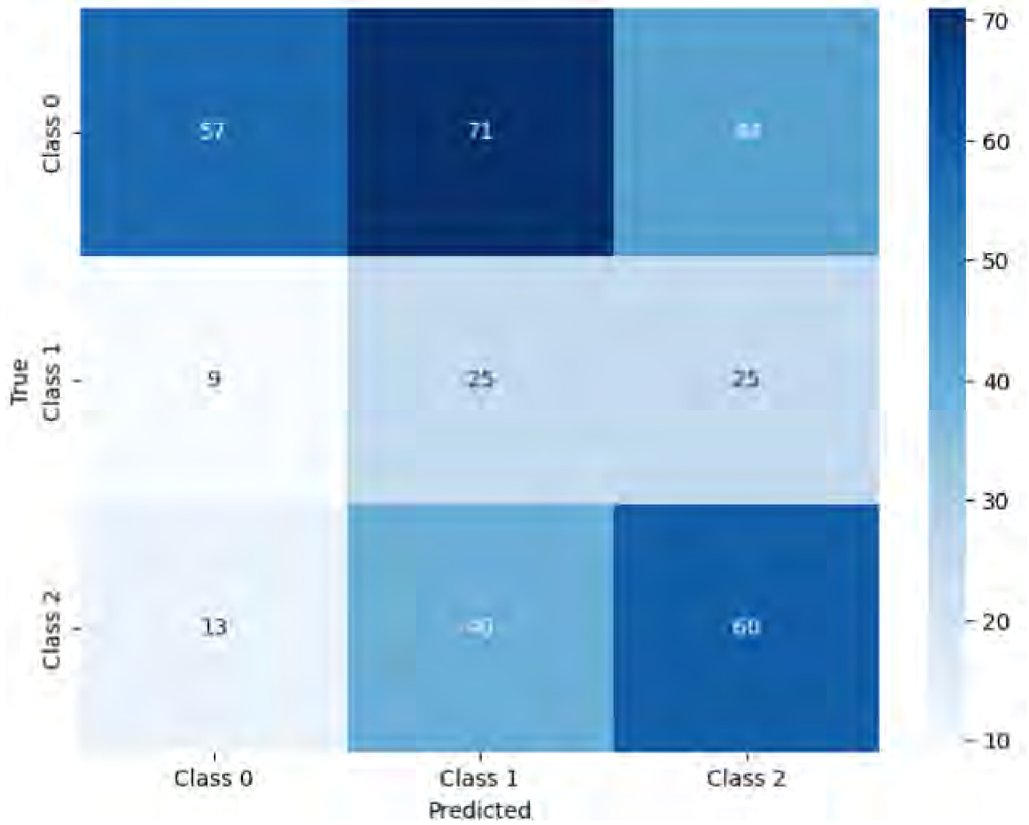


Figure 5.6: Confusion matrix for the Global layer

This confusion matrix in Fig. 5.6 describes the level of classification accuracy of the global model over three levels of intensity, with a high degree of success in accurately classifying Class 2 with 60 correct classifications. Nevertheless, there is a considerable amount of overlap between the classes, especially in the 71 instances of Class 0 being classified as Class 1. This would indicate that the model is able to accurately classify the trends of high intensity, but not the low and medium intensity geomorphic changes.


Figure 5.7: Loss, F1 Score and Accuracy Graph

Fig. 5.7 are learning curves for the global model, where the performance of the model goes through about 20 epochs. There is a sharp initial decline in the loss before it levels off. For validation F1 score and accuracy, the high volatility before they start to increase. Accuracy reaches a peak at about 0.43. Validation loss is stable, which states that it is able to generalize fairly well without much overfitting.

**River:**

Table 5.6: River wise Accretion:

| River | Accuracy | Weighted F1 | Macro F1 | Test Samples |
|---|---|---|---|---|
| Baleshwar | 0.175 | 0.083 | 0.140 | 40 |
| Bishkhali | 0.327 | 0.327 | 0.315 | 52 |
| Karnaphuli | 0.441 | 0.407 | 0.352 | 68 |
| Pasur | 0.306 | 0.243 | 0.279 | 36 |
| Payra | 0.179 | 0.149 | 0.169 | 56 |
| Shibsa | 0.367 | 0.325 | 0.358 | 60 |
| Surma | 0.469 | 0.438 | 0.324 | 32 |

Table 5.6, indicates the river-wise accuracy of the accretion performance, where the highest localized accuracy of 0.469 and 0.441 was recorded for the Surma and Karnaphuli rivers, respectively. However, the accretion performance of the Baleshwar and Payra rivers was found to be more challenging for the model, resulting in the lowest accuracy of 0.175 and 0.179, respectively. The significant variation in the Weighted F1 scores, ranging from the highest of 0.438 for the Shurma river and the lowest of 0.083 for the Baleshwar river, further explains the impact of the unique river dynamics on the accuracy of the model for the prediction of land gain. The above-mentioned accuracy values clearly indicate that the accretion phenomenon is highly complex and challenging for the model.

For Bishkhali, the model does a decent job separating Class 0 and Class 2, with AUC scores of 0.61 and 0.58. But when it comes to Class 1, it's basically guessing AUC drops to 0.48. The confusion matrix tells the story: it keeps mixing up most samples, tagging them as Class 1, so recall looks okay for that class, but precision falls apart. The model just can't get a handle on moderate accretion, which makes the F1 score swing all over the place.

Karnaphuli does a bit better. The AUC hits 0.66 for Class 0, though it slips to 0.53 for Class 1 and 0.58 for Class 2. It picks out low accretion (Class 0) pretty well, but stumbles with high accretion (Class 2), and can't really tell moderate erosion apart from the rest. Baleshwar is rough. Accuracy drops to just 0.175, and the F1 scores are just as bad. The model basically collapses here it keeps predicting moderate erosion and ignores the stable or highly eroding spots. Pasur isn't great, but it's slightly better. Accuracy climbs to 0.31, and it has a fair shot at catching high accretion (Class 2). Payra scores low, especially for Class 0. in both Recall and F1 scores

Shibsa holds up okay for Class 1, but the model gets confused with the other classes. Surma lands the second-best accuracy at 0.469. It's pretty good at spotting high accretion (Class 2), but can't predict moderate erosion (Class 1) at all. In short, the model's results are all over the place. It keeps running into trouble with class imbalance, not enough data, and telling the difference between intermediate erosion levels. It's clear that better feature engineering and a more refined model are needed, especially for the finer details. For accretion Karnaphuli has the best accuracy then any other implemented rivers in the model.

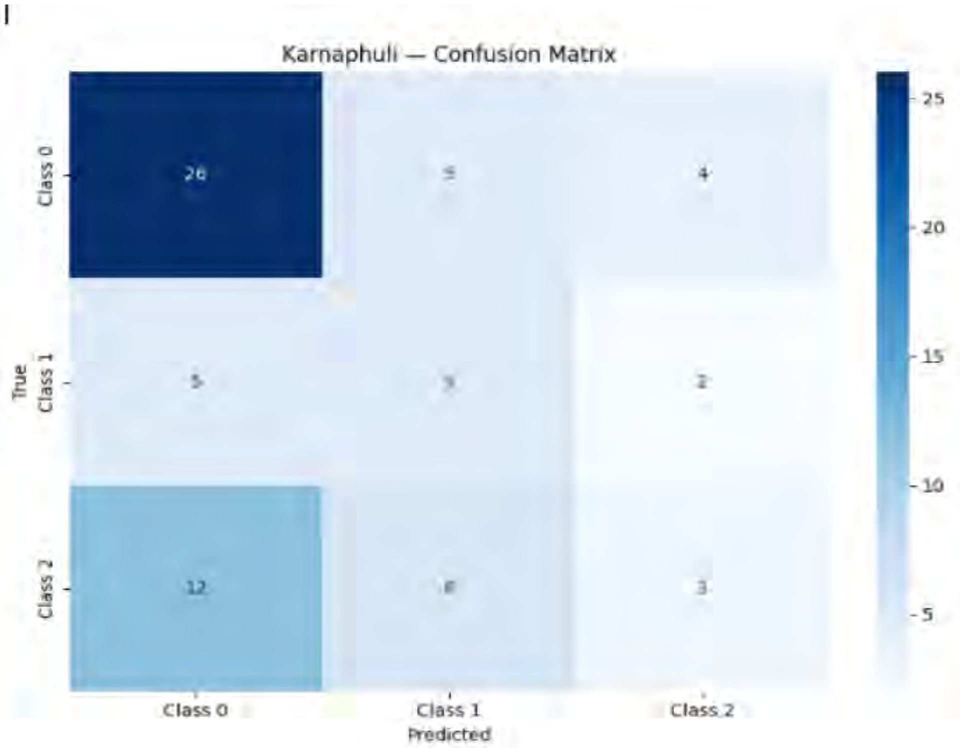


Figure 5.8: Confusion matrix for Karnaphuli River

The confusion matrix for the Karnaphuli River in Fig. 5.8, indicates that the model performs best in classifying Class 0 (Low intensity), where it accurately classifies 26 out of 35 samples. But it performs poorly in classifying Class 2 (High intensity), where it incorrectly classifies 12 out of 21 actual High-intensity samples as Low-intensity. The model also performs poorly in classifying Class 1, where it accurately classifies only 5 samples.

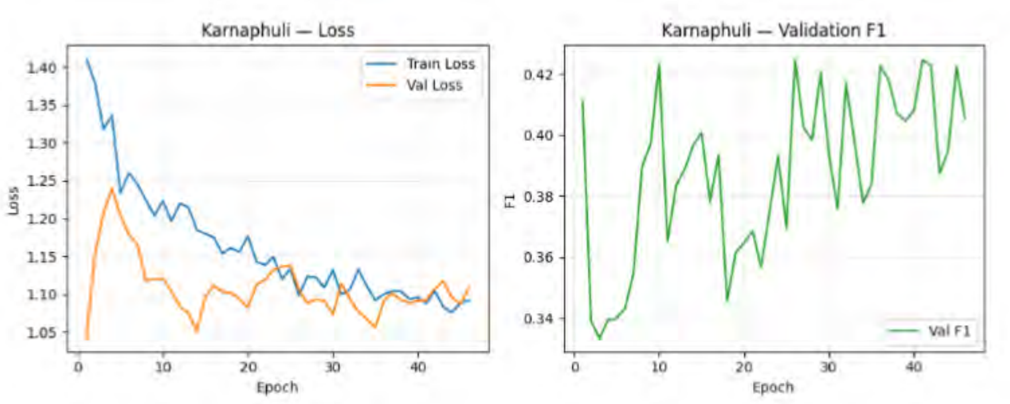


Figure 5.9: Loss and F1 Validaation of Karnaphuli River

The training plot in Fig. 5.9 for the Karnaphuli River displays a training loss with a decreasing and stable trend after 30 epochs. Conversely, the Validation F1 score displays a highly fluctuating trend over the 50 epochs, ranging from 0.33 to 0.42. This high fluctuation in the validation performance suggests that the model is having difficulties in generalizing the non-linear accretion patterns specific to the Karnaphuli River.

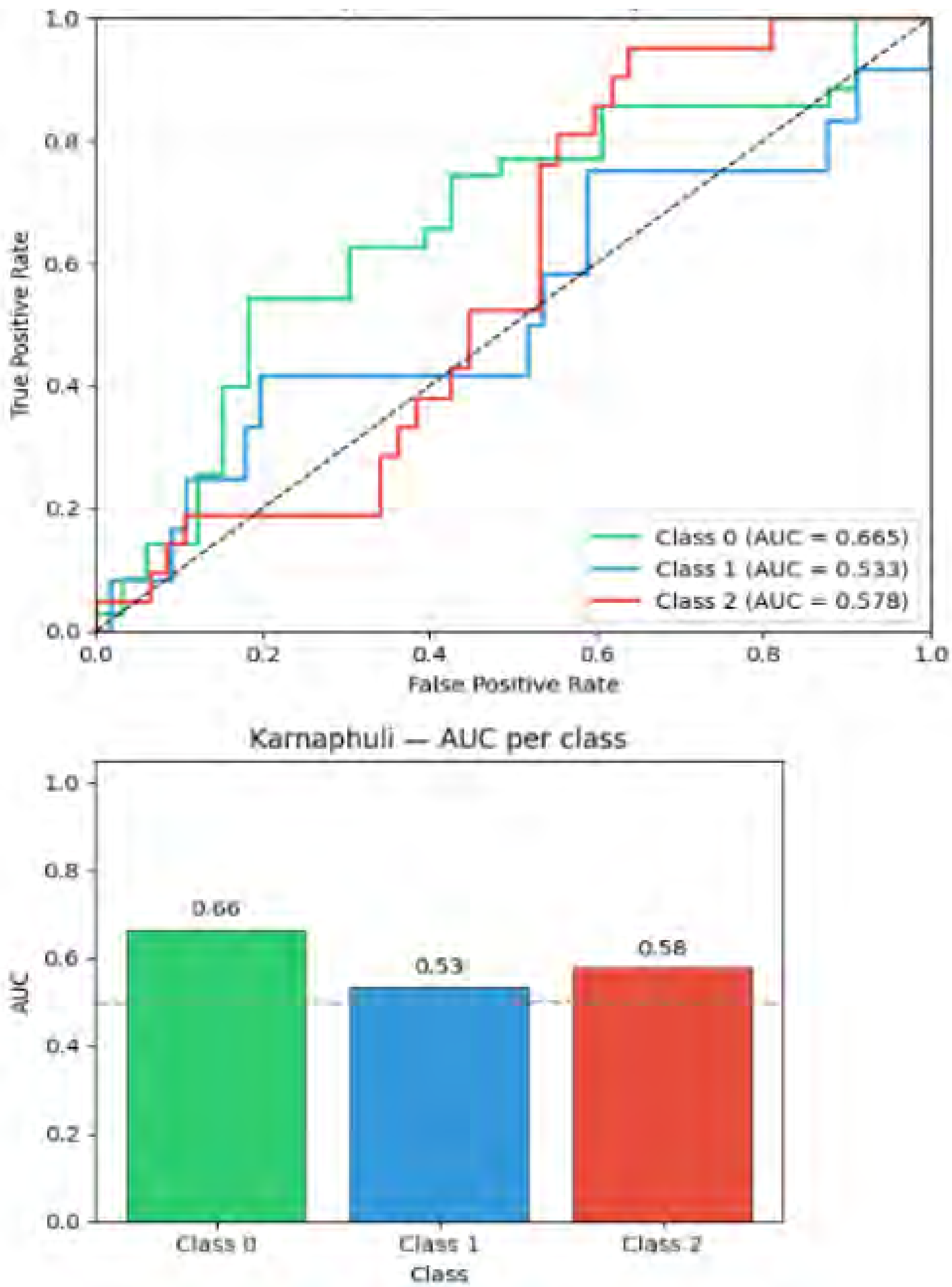


Figure 5.10: ROC and AUC of Karnaphuli River

As shown in Fig. 5.10, the ROC curves and their corresponding Area Under the Curve (AUC) values for the classification of the intensity of accretion in the Karnaphuli River are given below. The model performs best at identifying Class 0 (Low intensity) with an AUC of 0.66, followed by Class 1 and Class 2, which have a moderate predictive ability of 0.53 and 0.58, respectively. It, therefore, suggests that the model has a moderate ability to distinguish between different classes of land gain, but the most challenging task is the prediction of moderate accretion, i.e., Class 1.

**Zone:**

Table 5.7: Zone-wise Accretion Results

| Zone | Accuracy | Weighted F1 | Macro F1 | Test Samples |
|---|---|---|---|---|
| Baleshwar Zone 8 | 1.00 | 1.00 | 1.00 | 4 |
| Karnaphuli Zone 10 | 1.00 | 1.00 | 1.00 | 4 |
| Baleshwar Zone 1 | 0.00 | 0.00 | 0.00 | 4 |
| Pasur Zone 4 | 0.00 | 0.00 | 0.00 | 4 |

Extreme variations in the predictability of river segments are revealed in Table 5.7 for Zone-wise Accretion Results. Although Baleshwar Zone 8 and Karnaphuli Zone 10 have shown perfect results for all metrics at 1.00, there are zones such as Baleshwar Zone 1 and Pasur Zone 4 where accuracy is zero at 0.00. Although this is due to a small sample of 4 test cases per zone, this again reveals that geomorphic patterns can be extremely predictable in some river zones while completely elusive in others.

Good accretion zones like Baleshwar Zone 8 and Karnaphuli Zone 10 achieve perfect accuracy and F1, correctly classifying all test samples into the three accretion classesAdequate temporal-spatial signals are available to this setting to establish clear dependencies between the training dataset's stable/moderate/high levels of accretion (even with only a few short sequences), which enables to generate near-perfect labels. However, it is possible that these nearly perfect scores were generated in part because of the small sample size of the training dataset; therefore, the predictions that are made based on the training dataset may have been a coincidence and not strong enough to support generalization of the training performance to other datasets.

In those areas of the world where poor rates of accretion are found – specifically, Baleshwar Zone 1 and Pasur Zone 4 – has obtained a zero F1 score for all of the test examples such as all test examples were incorrectly predicted. A common issue seen within data is an overwhelming presence of one class or too many label fluctuations, which will usually cause the model to fall into using the most common class and become unaware of otherwise rare patterns from the dataset. Because of missing at least one of the minority classes in the data such as missing at least one of the poor rates of accretion, the macro F1 score drops to zero; therefore, when looked at the overall result of the performance measure it will usually reflect a poor level of performance.

The model was not able to learn about future accretion rates at the zone level because of only having four samples for each zone made the model sensitive to noise; therefore, if just one of the predictions was incorrect, the overall accuracy would increase or decrease by 25%. In addition, the model overfits to global patterns and fails to learn about zone-specific behaviors in the accretion rate for each zone. Additionally, models usually learned best for those zones with very high levels of class imbalance (i.e., very little high level of accretion), thus causing the models to fail with a high accuracy within the dominant class and have poor accuracies for the other classes in the data.

**Bank:**

Table 5.8: The results of selected banks for Accretion:

| Bank (River_Zone_Bank_Side) | Accuracy | Weighted F1 | Macro F1 | Test Samples |
|---|---|---|---|---|
| Baleshwar_zone_10_bank_left | 1.00 | 1.00 | 1.00 | 2 |
| Baleshwar_zone_1_bank_left | 0.50 | 0.33 | 0.33 | 2 |
| Karnaphuli_zone_2_bank_left | 1.00 | 1.00 | 1.00 | 2 |
| Karnaphuli_zone_1_bank_left | 0.00 | 0.00 | 0.00 | 2 |
| Pasur_zone_3_bank_left | 1.00 | 1.00 | 1.00 | 2 |
| Pasur_zone_1_bank_right | 0.00 | 0.00 | 0.00 | 2 |
| Payra_zone_13_bank_right | 1.00 | 1.00 | 1.00 | 2 |
| Payra_zone_3_bank_left | 0.00 | 0.00 | 0.00 | 2 |
| Shibsa_zone_12_bank_right | 1.00 | 1.00 | 1.00 | 2 |
| Shibsa_zone_5_bank_left | 0.00 | 0.00 | 0.00 | 2 |
| Surma_zone_7_bank_right | 1.00 | 1.00 | 1.00 | 2 |
| Surma_zone_3_bank_left | 0.00 | 0.00 | 0.00 | 2 |

In table 5.8, banks with perfect accretion scores such as `Baleshwar_zone_10_bank_left` and `Karnaphuli_zone_2_bank_left` achieve 1.0 precision, recall, and macro F1, with both test samples correctly assigned to the observed accretion class. The model's accuracy will be unrepresentative based on the accuracy of the model matching the primary detected bank pattern. However, due to the small number of observations (2), any perceived accuracy is inaccurate; thus, the matrix exhibiting the greatest deviation between expected and observed will also exhibit the least amount of matrix accuracy.

There are some banks with poor performances, such as `Karnaphuli_zone_2_bank_left` and `Pasur_zone_1_bank_right`, scored zero for both accuracy and F1 values. In addition, all samples associated with these banks were classified incorrectly. Problems arise when banks demonstrate unusual or varied classes of accretion that are under-represented in the training data. As a result, during the testing of the model, the model will classify to a class that was learned with more frequency among all bank point locations along the river.

It should also be noted that when testing against complex models (bank level), there are only 2 test samples associated with each bank; therefore, any misclassifications will produce a higher percentage of accuracy measures. Also, since the LSTM–GRU model was not designed for shorter sequences and less complex temporal behaviors specific to banks, it is prone to overfitting noise and has been unable to develop unique temporal behaviors for the various banks. In addition, the very limited data used to train the model at the bank level and the model being developed using river-level phenotypes has all contributed to the lack of predictive accuracy for banks. Therefore, it is important to interpret the results from the banks with caution and rely more on the accuracy of results based on the river-level or zone-level behaviors.

## 5.3 Ensemble Majority Voting Results

Since ensemble majority voting was implemented across all model architectures (LSTM, CNN-BiLSTM-Attention, BiLSTM-GRU-Attention, Random Forest, XG-Boost, and LightGBM) to improve prediction robustness, the results of this aspect are included in this section.

### 5.3.1 Ensemble Results for Erosion

#### Ensemble Majority Voting System Performance Analysis of BiLSTM-GRU Hybrid Model for Erosion Prediction

The 4–layer hierarchical ensemble voting system that combines the predictions of global, river-specific, zone-specific, and bank-specific models reached the final test accuracy of 46.22% of 344 temporal sequences, with the weighted F1-score of 46.01. The macro-average of the F1-score of 41.18% and Cohen Kappa value of 0.1345 suggest minimal to fair levels of agreement other than a random chance, and shows the relative lack of overall discriminatory strength in the model. As opposed to the desired advantage of model stacking, the ensemble performed worse than the individual global model, indicating a 9.7 percent drop in accuracy and a 6.3 percent drop in weighted F1-score. This breakdown implies that the addition of more granular, localized modeling provided conflicting information and noise on majority votes, as opposed to the complementary, specialized information. The confusion matrix showed that performance in the three classes of erosion severity had a very imbalanced performance. The model showed moderate performance in Class 0 (No Erosion) appropriately classifying 98/174 (56.3% recall). The worst performance was observed with Moderate Erosion (Class 1) where the count of correct predictions amounted to 16 out of 73 correct predictions (21.9 recall), which suggests that there is a fundamental challenge in discerning slight erosion cues at an early stage. Class 2 was determined as High Erosion with intermediate success and obtained 45 correct predictions of 97 (46.4% recall). That trend indicates that the ensemble framework is the best one to differentiate the two ends of the severity spectrum but struggles to capture the subtle transitional category, which is particularly imperative in the planning of proactive intervention.

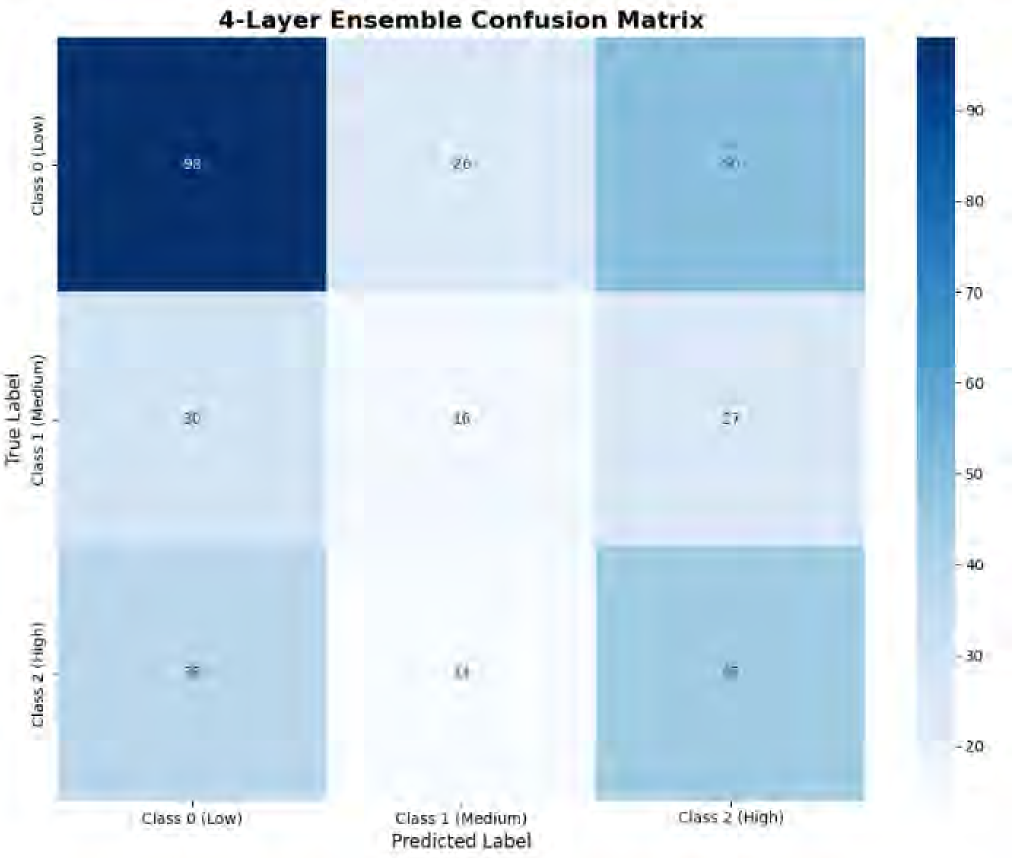


Figure 5.11: Confusion matrix of BiLSTM-GRU for the Ensemble Majority Voting for Erosion Prediction

This confusion matrix in Fig. 5.11 shows that the system is most effective at identifying Class 0 (Low) erosion, correctly predicting 98 instances in that category. But the model faces challenges with Class 1 (Medium) and Class 2 (High), often misclassifying high intensity events as low-intensity, which reflects the difficulty of predicting rare, extreme geomorphic changes.

**Ensemble Majority Voting System Performance Analysis of CNN-BiLSTM-Attention Model for Erosion Prediction**

The CNN-Bi-LSTM-Attention ensemble achieved an overall accuracy of 42.15% (Weighted F1-Score: 38.08%) across the test set, representing a significant positive improvement over the global model's performance, with an accuracy increase of 11.48% and a weighted F1 gain of 7.49%. However, despite this improvement, the model's discriminatory power remains very low, as evidenced by a Cohen's Kappa of only 0.0014, indicating performance barely above chance. The confusion matrix reveals the core limitation of this architecture: it demonstrates a pronounced bias towards predicting Class 2 (High Erosion), severely compromising its ability to correctly identify the other classes. The matrix shows a high count of false positives for Class 2, meaning many instances of Class 0 and Class 1 are being misclassified as severe erosion. This bias inflates the recall for Class 2 but catastrophically reduces precision for that class and devastates the performance metrics for Class 0 and Class 1, leading to the low macro F1-score of 30.82%. The model's architecture, while capturing complex spatio-temporal patterns, ultimately fails to balance class predictions, resulting in an ensemble that is significantly more accurate than the global baseline but not reliably discriminative across all erosion severity levels.

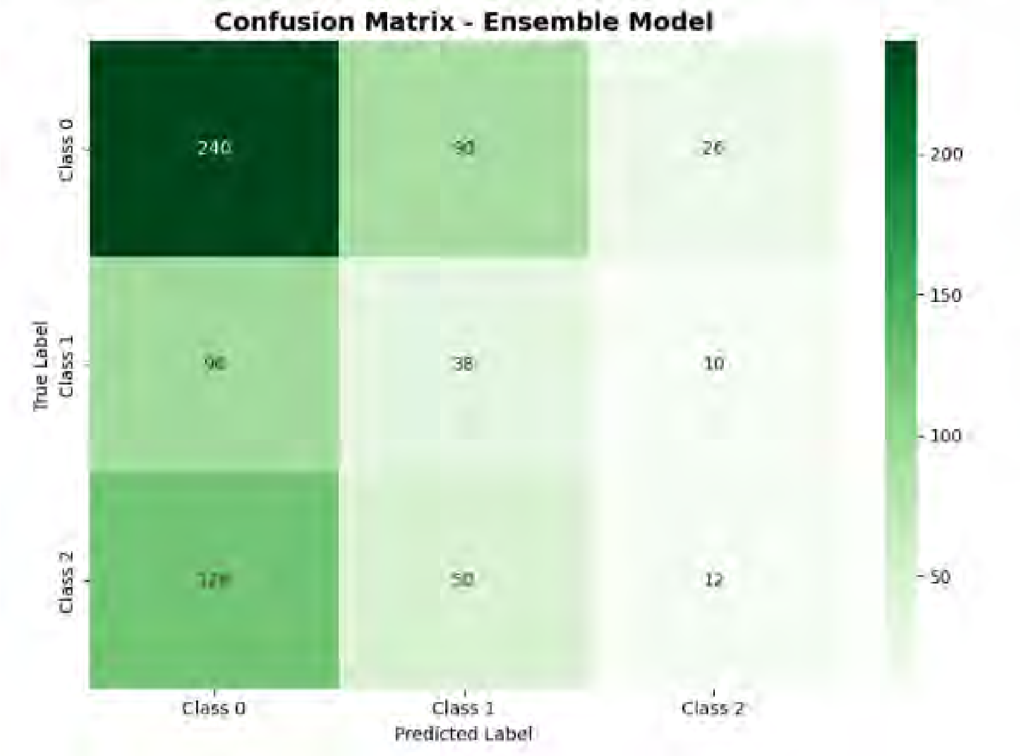


Figure 5.12: Confusion matrix of CNN-BiLSTM for the Ensemble Majority Voting for Erosion Prediction

From the confusion matrix in Fig. 5.12 it could be seen that while the system is highly proficient at correctly identifying Class 0 instances with 240 true positives, it significantly struggles with Class 2, misclassifying 126 of those high-intensity cases as low-intensity.

### Ensemble Ensemble Majority Voting Results of All Models for Erosion Prediction

Table 5.9: Ensemble Majority Voting Results for Erosion Prediction (All Models)

| Model | Accuracy | Weighted F1 | Macro F1 | Cohen's Kappa |
|---|---|---|---|---|
| Multi-level LSTM | 0.4826 | 0.4858 | 0.4314 | 0.0000 |
| CNN-LSTM with Attention | 0.4215 | 0.3808 | 0.3082 | 0.0014 |
| Multi-level Random Forest | 0.5756 | 0.4872 | 0.2953 | 0.0256 |
| Multi-level XGBoost | 0.6047 | 0.5066 | 0.3129 | 0.0618 |
| Multi-level LightGBM | 0.5233 | 0.4477 | 0.2664 | -0.0672 |
| **Bi-LSTM-GRU Hybrid** | **0.4622** | **0.4601** | **0.4118** | **0.1345** |

The table 5.9 presents the performance metrics of various ensemble majority voting models used for erosion prediction, evaluated across Accuracy, Weighted F1-score, Macro F1-score, and Kappa. While the Multi Level XGBoost achieves the highest raw accuracy (0.6047), the Bidirectional LSTM-GRU Hybrid with Attention stands out as the superior overall performer. Despite its slightly lower accuracy of 0.4622, it demonstrates the most robust predictive reliability by securing the highest Kappa score (0.1345), indicating that its predictions are significantly less likely to be the result of random chance compared to the other models.

### 5.3.2 Ensemble Results for Accretion

#### Ensemble Voting System Performance Analysis of BiLSTM-GRU for Accretion

The 4-layer ensemble voting system of accretion prediction was much more poorly performing than a matching system of erosion, and had an ultimate test accuracy of just 31.69% (weighted F1-score: 31.83) on the same 344 test sequences. The ensemble is a significant degradation of the performance of the standalone global model (accuracy: 41.28%, weighted F1: 43.40, macro F1: 40.22), indicating a 6.0% absolute drop in accuracy, and a 4.5% drop in the weighted F1-score. Such a reduction shows that the special river, zone, and bank-level models did not offer complementary data on accretion classification but they put forward contradictory forecasts that would prove detrimental to the consensus. The overall reliability of the model is also doubted by the coefficient of Cohen Kappa of 0.0544 that corresponds to the insignificant agreement beyond chance. The confusion table is very poor and inverted in terms of the number of classes compared to the erosion scores: the system had the worst performance in recognizing the “No Accretion” (Class 0), with a correct prediction of only 33 of 172 cases (19.2% recall). It had the highest (although still moderate) performance on Low Accretion (Class 1) with 33 of 59 (55.9% recall) and High Accretion (Class 2) was detected in 43 of 113 cases (38.1% recall). This trend indicates that the ensemble structure is deeply troubled by the inability to identify non-accreting, non-time-varying conditions and its power to identify events of sediment deposition is only fairly strong, which reflects a major issue with the modelling of geomorphic accretion events, as opposed to erosion.

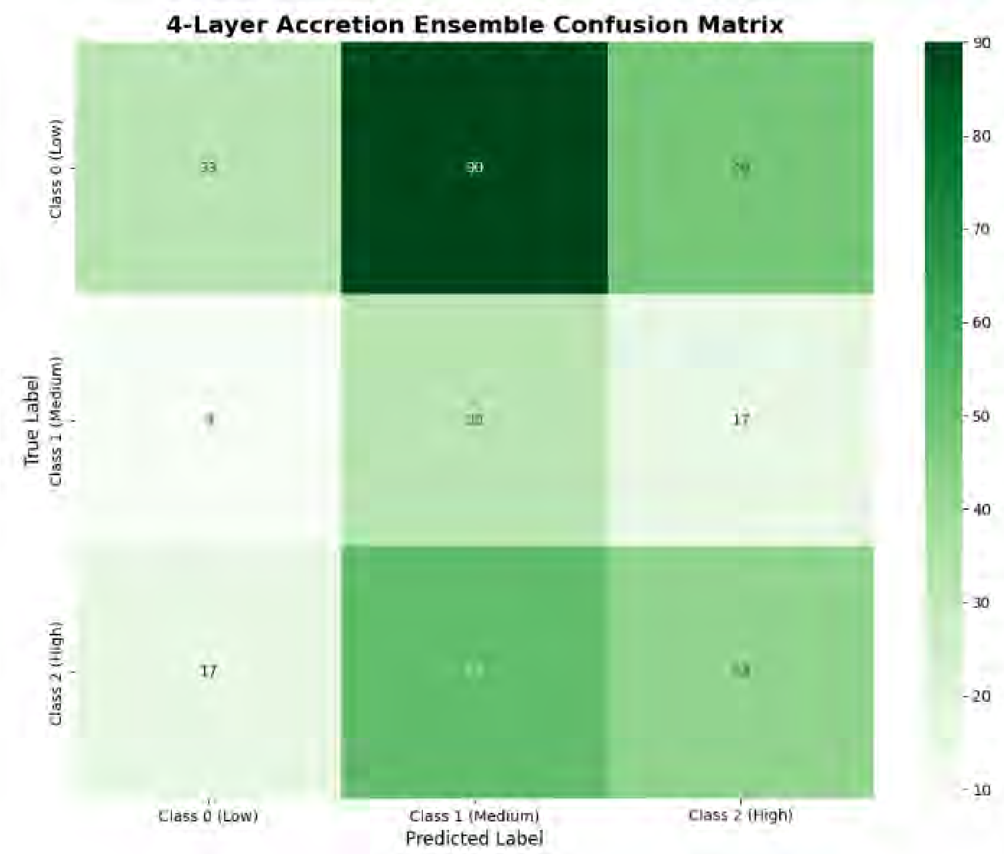


Figure 5.13: Confusion Matrix of BiLSTM-GRU for Ensemble Majority Voting for Accretion Prediction

The confusion matrix in Fig. 5.14, shows the Bidirectional LSTM-GRU model's performance in categorizing land formation intensity across three classes. In this specific case, the model shows a higher tendency to predict Class 1 (Medium) accretion, as evidenced by the high number of true negatives and false positives concentrated in the middle column. Specifically, it correctly identified 43 instances of Class 2 (High) accretion, but similar to the erosion model, it struggles with significant overlaps where high-intensity accretion is often mistaken for medium or moderate accretion events.

**Ensemble Voting System Performance Analysis of CNN-BiLSTM for Accretion**

The CNN–Bi-LSTM–Attention accretion prediction ensemble model achieved an accuracy of 37.94%, with a weighted F1-score of 37.22%, which represented a moderate positive improvement over the global model with an increase in the model accuracy of 5.81%. As with the erosion model, it has a low general reliability as represented by a Cohen Kappa of 0.0091, which indicates that there is practically no agreement other than by chance. There is a considerable bias to predicting Class 0 (No Accretion), which is different to the bias that the erosion model has. This bias can also be observed in the confusion matrix structure, in which the first column (predictions of Class 0) has the largest values of the true values of all the true labels. This implies that there are a lot of real Class 1 (Moderate Accretion) and Class 2 (High Accretion) examples that are wrongly considered to be stable, non-accreting. Thus, although the model demonstrates a modest overall increase in aggregate measures, the actual accretion events are not reliably identified in it, which results in poor per-class performance and low macro F1-score of 32.89%. This propensity of the architecture to degenerate into the no event class is an indication that the architecture is training to error reduce by choosing the most common or baseline state instead of trying to identify the fine-tuning spectral-temporal indicators of sediment deposition.

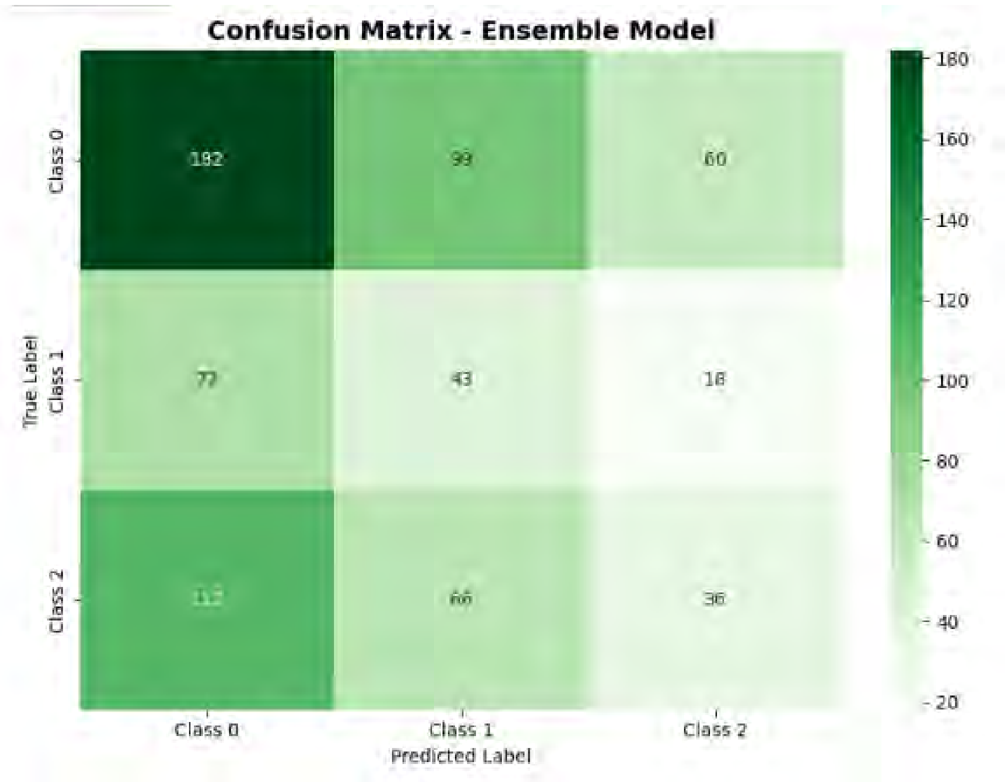


Figure 5.14: Confusion Matrix of CNN-BiLSTM for Ensemble Majority Voting for Accretion Prediction

From the confusion matrix for ensemble model in Fig. 5.14, it is seen that while the model effectively identifies the majority of Class 0 cases with 182 correct predictions, it struggles with Class 2, where 112 high-intensity instances were misclassified as low-intensity.

**Ensemble Majority Voting Results of All Models for Accretion Prediction**

Table 5.10: Ensemble Majority Voting Results for Accretion Prediction (All Models)

| Model | Accuracy | Weighted F1 | Macro F1 | Cohen's Kappa |
|---|---|---|---|---|
| Multi-level LSTM | 0.3895 | 0.3969 | 0.3754 | 0.0825 |
| CNN-LSTM with Attention | 0.3794 | 0.3722 | 0.3289 | 0.0091 |
| Multi-level Random Forest | 0.3547 | 0.2727 | 0.3265 | -0.0854 |
| Multi-level XGBoost | 0.4360 | 0.3591 | 0.2993 | 0.0304 |
| Multi-level LightGBM | 0.3233 | 0.4477 | 0.3012 | -0.0276 |
| **Bi-LSTM-GRU Hybrid** | **0.3169** | **0.3183** | **0.3180** | **0.0544** |

The table 5.10 shows the performance of various ensemble majority voting models used to predict accretion, considering performance parameters such as Accuracy, Weighted F1, Macro F1, and Cohen's Kappa.From this table 5.10, it is seen that although the Multi-level XGBoost model achieved the highest raw accuracy of 0.4360, the Bi-LSTM-GRU Hybrid (with Attention) is prioritized as a more reliable model due to its balanced performance across classes. Specifically, while its accuracy is lower at 0.3169, the hybrid model maintains a competitive Macro F1-score of 0.3180 and a positive Cohen's Kappa value of 0.0544, outperforming models like Multi-level LightGBM which shows a negative Kappa of -0.0276. Furthermore, the Multi-level Random Forest actually has a Cohen's Kappa of -0.0854, proving that high accuracy alone does not guarantee a model's ability to handle the complex accretion dynamics of these river systems.

## 5.4 Summary of All Results

**Erosion Result Summary:**

LSTM hierarchical model achieved test accuracy of 30.00% for Baleshwar, 42.31% for Bishkhali, 52.94% for Karnaphuli, 44.44% for Pashur, 42.86% for Payra and 46.67% for Sibsa, with a notable maximum accuracy of 81.25% and a weighted F1-score of 72.84% for Shurma River. At the zonal level, the model demonstrated targeted efficacy for erosion, specifically achieving a 50.00% accuracy with a 33.33% F1-score for Bishkhali Zone-5, and a 50.00% accuracy with a higher F1-score of 66.67% for Pasur Zone-14.

The Bi-LSTM model with convolutional and attention mechanisms, using kernel size k = 2 (baseline), demonstrated strong performance for erosion prediction across multiple rivers. It achieved test accuracies of 33.75% for Baleshwar, 47.12% for Bishkhali, 35.29% for Karnaphuli, 38.89% for Pasur, 44.64% for Payra, 44.17% for Shibsa, and a notable peak of 75.00% for Surma, with a weighted F1-score of 67.89%, highlighting its ability to capture local temporal patterns effectively. Increasing the convolution kernel to k = 3, which allows the model to observe all three timesteps simultaneously, resulted in lower global accuracy (32.12%), weighted F1 = 31.11%, and macro F1 = 31.27%, indicating weaker generalization. River-level performance was uneven: Baleshwar (47.50%) and Pasur (47.22%) were the best-performing rivers, while Bishkhali (29.81%), Karnaphuli (33.82%), Payra (33.93%), Shibsa (30.83%), and Surma (37.50%) showed comparatively lower accuracies, with several rivers having near-zero or negative Cohen's Kappa scores, suggesting limited agreement beyond chance. Kernel sizes k = 1 and k ¿ 3 were not used because k = 1 only processes each timestep independently, failing to capture temporal dynamics, while $k > 3$ exceeds the sequence length of three timesteps, causing most of the convolution window to include artificial padding rather than real data. Overall, k = 2 strikes the best balance between temporal sensitivity and feature stability for this short sequence, effectively capturing step-to-step changes, whereas k = 3 does not consistently improve performance and often reduces both accuracy and agreement across rivers.

Baseline models like the Random Forest model demonstrated varying degrees of performance in prediction riverbank erosion for seven rivers, providing test accuracy of 45.00% for Baleshwar, 38.46% for Bishkhali, 52.94% for Karnaphuli, 50.00% for Pashur, 23.33% for Sibsa and 43.75% for Surma, with the highest performance of 60.71% observed in the Payra River. River specific accuracies of XGBoost for predicting erosion pattern are 40.00% for Baleshwar, 30.77% for Bishkhali, 32.35% for Karnaphuli, 38.89% for Pasur, 50.00% for Payra, and 23.33% for Shibsa, with its highest performance observed in the Surma river at 62.50%. On the other hand the LightGBM model recorded accuracies of 20.00% for Baleshwar, 50.00% for Bishkhali, 52.94% for Karnaphuli, 38.89% for Pasur, 57.14% for Payra, and 40.00% for Shibsa, while achieving an exceptional peak accuracy of 100.00% for the Surma river.

**Accretion Result Summary:**

LSTM based deep learning model in terms of accretion prediction, LSTM recorded test accuracy of 40.00% for Baleshwar, 23.08% for Bishkhali, 47.06% for Karnaphuli, 50.00% for Pashur (with an F1-score of 42.96%), 32.14% for Payra and 25.00% for Surma, while the Sibsa River recorded a lower accuracy of 3.33%. For the zone level, the model maintained 50.00% accuracy and 33.33% F1-score for Baleshwar Zone-1, while reaching a balanced performance of 50.00% for both accuracy and F1-score in Karnaphuli Zone-11.
Regarding accretion, attention-based CNN-LSTM model with a kernel size of k = 2 (baseline) showed stronger results. It had test accuracies of 41.25% on Baleshwar (weighted F1 = 42.94%), 30.77% on Bishkhali, 46.32% on Karnaphuli, 41.67% on Pasur, 42.86% on Payra (weighted F1 = 43.16%), 36.67% on Shibsa, and 29.69% on Surma indicating that it was effective at capturing short-term time when the convolution kernel was increased to k = 3, (so that the model could simultaneously observe all three timesteps) the global accuracy was 32.12% with a weighted F1 = 31.11% and macro F1 = 31.27%, (weaker generalization). The best accuracies were found to be with Baleshwar (47.50%), Pasur (47.22%), whereas Bishkhali (29.81%), Karnaphuli (33.82%), Payra (33.93%), Shibsa (30.83%), and Surma (37.50) performed poorer with Cohen Kappa taking values close to zero or negative in some instances, indicating no more than chance agreement. The sizes of kernels were excluded as k = 1 assumes each timestep as an independent hypothesis that fails to capture temporal trends, whereas k larger than three surpasses the sequence length of three, where padding dominates the convolution window and generates less meaningful features. Comprehensively, k = 2 offers the most ideal balance of the short sequence such that it accurately reflects changes in steps but k = 3 does not always enhance performance and in most cases, decreases accuracy and reliability across rivers.

Baseline Models in terms of predicting accretion, Random Forest achieved accuracy of 45.00% for Baleshwar, 34.62% for Bishkhali, 32.35% for Karnaphuli, 44.44% for Pashur, 35.71% for Payra and 46.67% for Sibsa, while the highest predictive accuracy was achieved for the Surma River of 62.50%. The XGBoost model achieved test accuracies of 40.00% for Baleshwar, 30.77% for Bishkhali, 32.35% for Karnaphuli, 38.89% for Pasur, 50.00% for Payra, and 23.33% for Shibsa, again reaching its maximum predictive accuracy of 62.50% for the Surma river prediction. On the other hand, the LightGBM model yielded accuracies of 20.00% for Baleshwar, 34.62% for Bishkhali, 35.29% for Karnaphuli, 33.33% for Pasur, 26.67% for Shibsa, and 37.50% for Surma, with the most effective results observed in the Payra river at 57.14%.

### 5.4.1 Result Discussion of Erosion Prediction

The comprehensive study has led to several significant and insightful findings about the patterns of riverbank erosion and accretion in some important rivers in Bangladesh. A careful analysis of the data collected has revealed an important understanding regarding the geological changes that are taking place, as well as the possibility of land formation in multiple areas of Bangladesh.

**Identification of Critical Erosion-Prone Locations**
The ensemble system was able to come up with ten most risky locations with the highest risk value of 2.000. This score is calculated using a weighted equation with high erosion predictions (Class 2) getting a weight of 2 and moderate erosion predictions (Class 1) getting a weight of 1. This high score was reached by all ten locations because they were 100 percent high on erosion prediction rates in the two sampled years (2024 and 2025). The data is very consistent: each place consisted of two yearly samples, and both samples were all considered to be high erosion. These hotspots are geographically only located in two systems of rivers: Baleshwar (5 locations: Zones 1, 2, 3, 6, and 9) and Bishkhali (5 locations: Zones 1, 2, 3, 6, and 9). Another pattern that is quite remarkable is that the right banks are the absolute leaders, as they are 9 out of the top 10. The only exception is that of Baleshwar Zone 3 left bank. This massive right-bank exposure (90% of best locations) indicates strongly both the effects of Coriolis effect-induced circulation or regularized pattern of meander migrations in the Northern Hemisphere, where rivers tend to cut their right banks. The fact that the current year has been quite the same as the previous years suggests that these are not temporary but structural weak points that should be prioritized into stabilization.

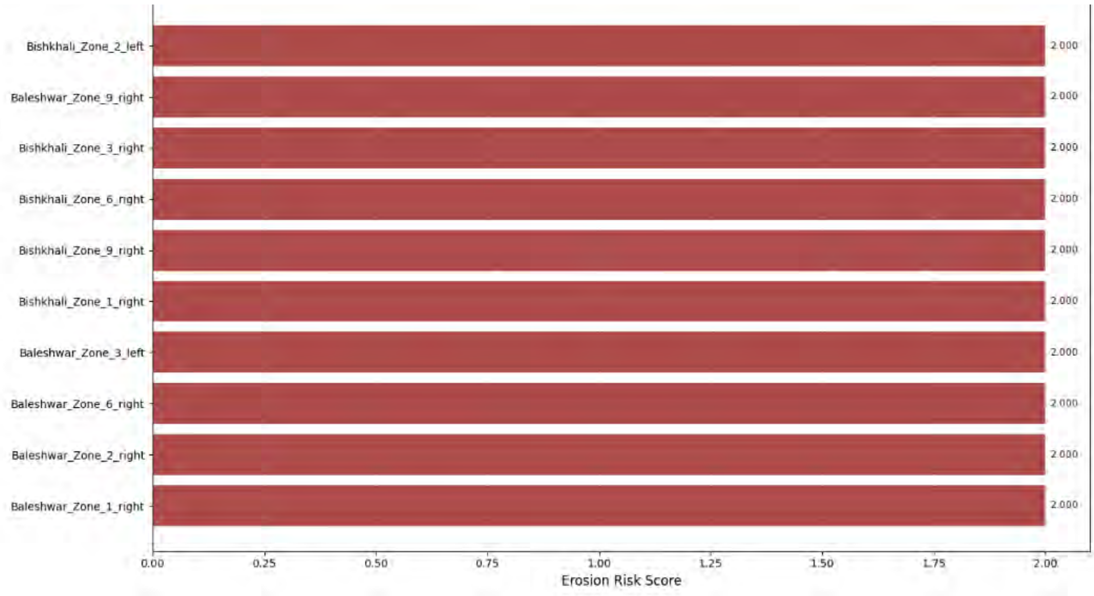


Figure 5.15: Most Erosion Prone River Zones

The plot in Fig. 5.15 highlights the most vulnerable erosion-prone locations such as Bishkhali_ zone_ 2_ left_ bank and Baleshwar_ zone_ 6_ right_ bank.

**River-Scale Erosion Risk Prioritization**

At the river basin level, Surma River emerges as the system with the most severe and widespread erosion threat. It achieved a risk score of 0.844, the highest among all rivers, driven by an extreme 84.4% high erosion rate. This means that across all 16 monitored locations within Surma, over 84 out of every 100 predictions indicated severe erosion. Crucially, all 16 of its monitored locations (100%) were classified as "High Risk," showing no spatial heterogeneity in vulnerability within its basin. Baleshwar River ranks second with a risk score of 0.440. While its high erosion rate is lower at 55.0%, its risk is concentrated, with 16 out of 20 locations (80%) deemed high-risk. Bishkhali River follows with a score of 0.370 and a 48.1% high erosion rate, but it shows the most widespread monitoring with 26 total locations, of which 20 (77%) are high-risk. The visualization graph uses a dual-axis: bars (risk score) and a line (high erosion percentage). It reveals that while Surma leads in both measures, Baleshwar's risk score (0.440) is significantly higher than Bishkhali's (0.370) despite Bishkhali having more locations and a moderately lower erosion rate (48.1% vs 55.0%). This indicates that Baleshwar's erosion, though less frequent, is perceived as more severe or concentrated, whereas Surma's problem is both highly frequent and severe. Intervention strategy therefore differs: Surma needs comprehensive, basin-wide management, while Baleshwar may benefit from targeted, high-intensity engineering at specific critical points.

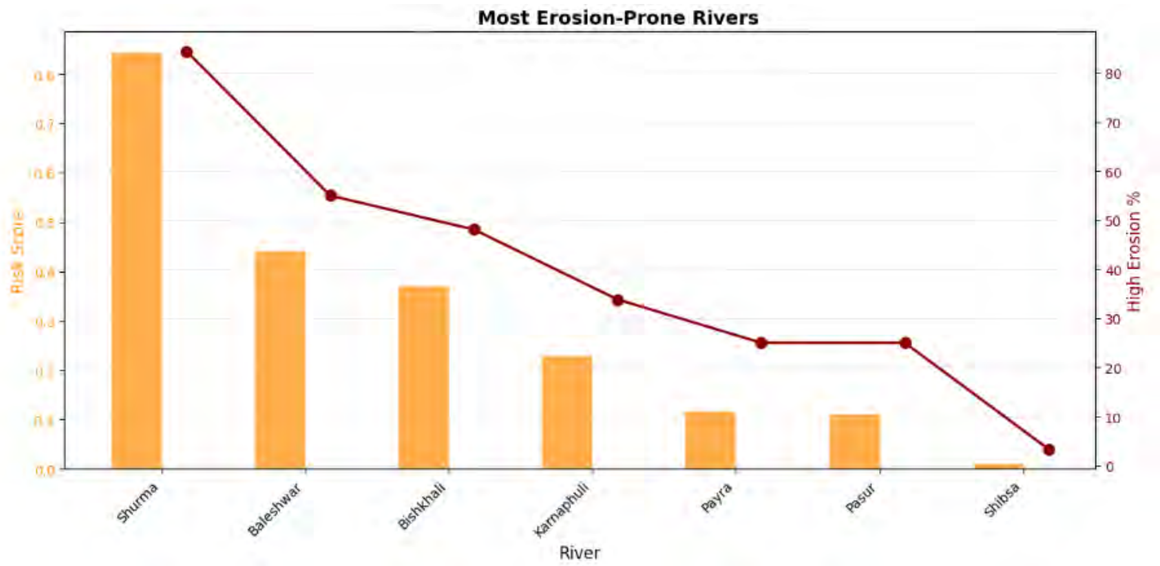


Figure 5.16: Most Erosion-Prone Rivers

The plot in Fig. 5.16 provides a broader river-level comparison where the Surma River has been listed as having overall the highest amount of risk and percentage of high-intensity events being the most erosion-prone, and the Shibsa River is the most stable among all these rivers.

**Zone-Level Vulnerability Hotspots**

Zone-level analysis provides the most detailed understanding of the geomorphic controls. Surma_Zone_3, SurmaZone7, and KarnaphuliZone16 were the top three zones with a risk score of 1.000. This score indicates that 100% of their banks were classified as high-risk and 100% of the predictions corresponded to high erosion. The heatmap visualization demonstrates that high-risk areas (marked in deep red/orange) are not randomly dispersed; instead, they are concentrated in specific rivers, particularly the Surma and Karnaphuli rivers. Among the top ten zones, seven exhibit high erosion rates ranging from 75–100%.

An important observation is the bank-level consistency within these zones. Specifically, Surma_Zone_3, KarnaphuliZone16, and Surma_Zone_7 each exhibit both indicators of a high-risk bank. A similar pattern is observed in zones such as Baleshwar_Zone_2 and Bishkhali_Zone_9 (risk score: 0.750, 2/2 high-risk banks, 75% erosion). This near-perfect bilateral vulnerability suggests that the dominant controlling factors operate at the zone-scale (or reach-scale), such as channel slope, radius of curvature, sediment characteristics, or hydraulic geometry, which simultaneously influence both banks. This contrasts with bank-specific factors, such as vegetation cover or toe protection, which would be expected to affect individual banks independently. Overall, the results indicate that zone identity is a stronger predictor of extreme erosion risk than bank side or even river identity in these cases. This finding has important management implications: erosion mitigation strategies should be designed at the reach or zone level for example, targeting entire meander bends or uniform slope reaches rather than focusing on individual banks in isolation.

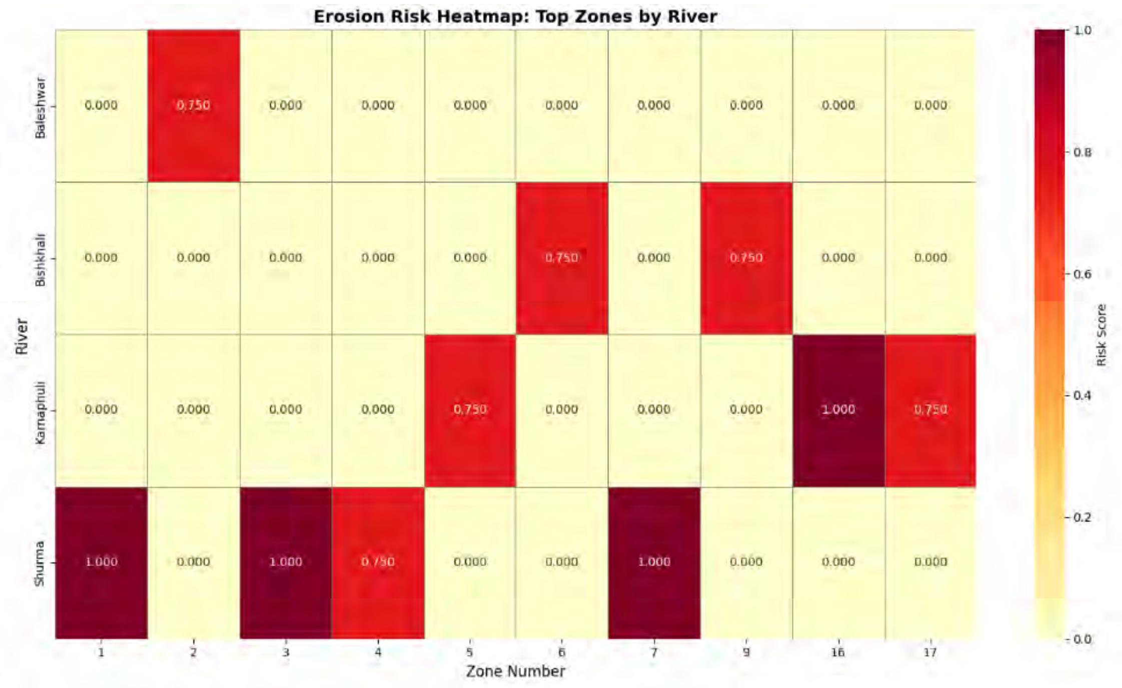


Figure 5.17: Erosion Risk Heatmap

From the erosion risk heatmap in Fig. 5.17 We can see that the concentration of extreme risks is highest in the Surma River, where Zones 1, 3 and 7 have the highest risk scores of 1,000. In comparison, the Karnaphuli River faces very localized but serious threats in Zone 16, while the Bishkhali and Baleshwar rivers exhibit moderate risk levels, primarily concentrated in specific parts such as Zone 2 in Baleshwar with scores of 0.750.

### 5.4.2 Result Discussion of Accretion Prediction

**Identification of Critical Accretion-Prone Locations**
The ensemble analysis established 10 locations that had 2.000 accretion risk score, and all of which had high accretion prediction rate of 100 percent in the two sampled years (2024- 2025). The accretion-prone sites are spread in four rivers (Surma 4 locations, Pasur 3 locations, Karnaphuli 2 locations and Baleshwar 1 location) unlike the erosion hotspots that were clustered in two river systems. The distribution of the zones is also more diverse with the Zones 1, 3, 4, 6, 7, 8, and 9. One interesting trend becomes apparent, in the bank-wise distribution: 6 out of the top ten locations are located on the right side, 4 on the left side. This is much more equal distribution than the extreme right-bank dominance in erosion but a little right-bank bias (60%) remains. The sites that have high risk scores: These are the sites that have two annual samples of high-accretion projections unanimously and at the same time and therefore with high levels of sediment deposition at the site. These ten locations with the same length of maximum bars would be represented in the visualization bar chart in a spatial order. Multiple river systems imply that drivers of accretion could be more locally regulated for example, focus on hydraulic structures, confluence zones, or source of sediments than global geomorphic tendencies as observed in erosion.

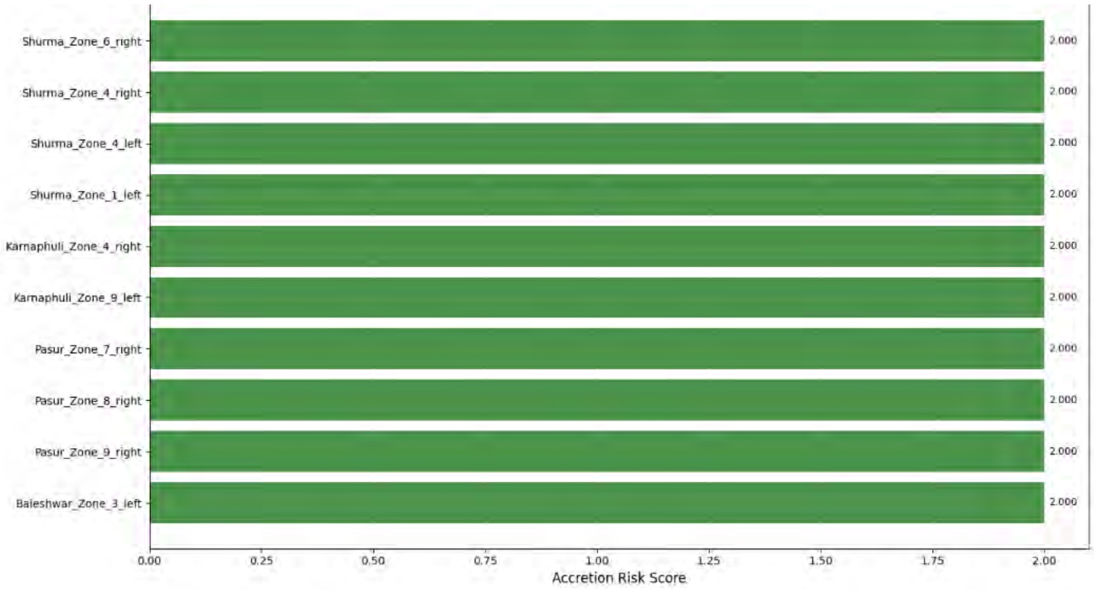


Figure 5.18: Most Accretion Prone River Zones

In the Fig. 5.18, the Surma river maintains its position as the most dynamic system, dominating the top accretion-prone locations with multiple zones reaching a maximum risk score of 2.000.

**River-Scale Accretion Risk Assessment**

Surma River illustrates itself as the most prone system by river level aggregation with a risk score of 0.703 and a high accretion rate of 75.0 percent in all the locations monitored by the river. This implies that in the 16 locations where Shurma had been in operation, every three predictions were of high accretion. Pasur and Shibsa rivers rank second with the same risk score of 0.498, but their statistics vary: Pasur has a high accretion rate of 52.8% in 18 locations ( 17 of which are high-risk), whereas Shibsa has a rate of 53.3% in 30 locations ( 28 of which are high-risk). The visualization graph on a dual axis would reveal that Surma would have the tallest bar (risk score) and the highest position on the line (accretion percentage). One of the most important results is the negative correlation between the dominance of erosion and accretion at the river scale: rivers the most likely to exhibit intensified erosion (Surma, Baleshwar) exhibit significantly different accretion patterns. Surma is the leader in both hazards and Baleshwar the second in erosion risk-last in accretion risk (0.035 score, 5.0 percentage). This counterclockwise trend implies the potential source-sink associations of sediment in the basin, high erosion regions in one river may be contributing to the supply of sediment that is deposited in other high accretion areas of other rivers, especially in Surma and Pasur.

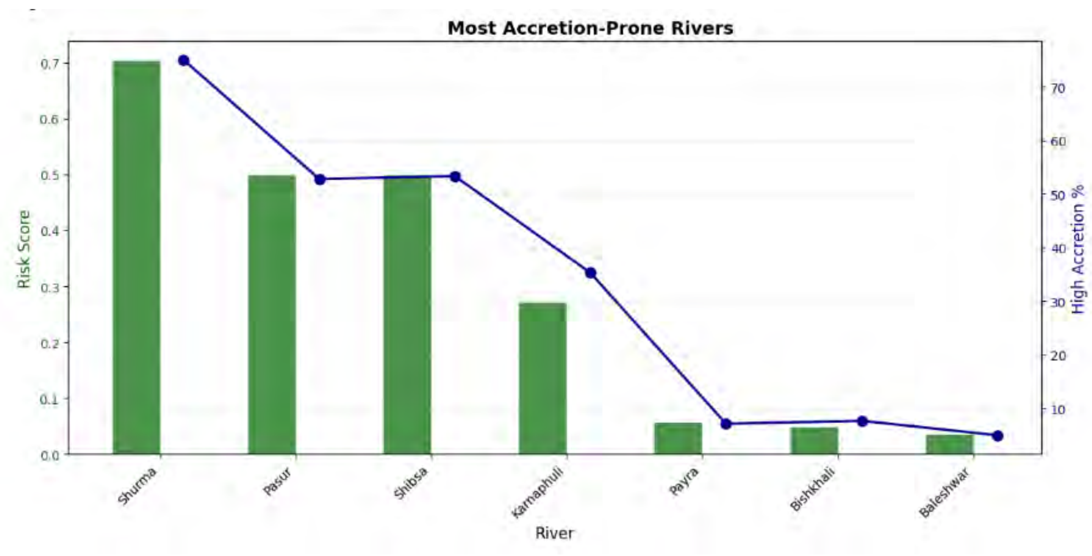


Figure 5.19: Most Accretion Prone Rivers

The findings from the research work in Fig. 5.19 it shows that, the Surma river exhibits the highest risk score and percentage of high-intensity accretion events, while rivers like the Baleshwar and Bishkhali show significantly lower potential for massive land formation.

**Zone-Level Accretion Vulnerability Hotspot Analysis**

Zone-level analysis identified seven zones with a perfect accretion risk score of 1.000, indicating that 100% of their banks were high-risk and 100% of predictions were for high accretion. These maximum-risk zones are concentrated in Shurma (Zones 3, 4, 6, 8), Karnaphuli (Zones 4, 5), and Shibsa (Zone 7). The heatmap visualization would show strong spatial clustering within these river systems, particularly in Surma where four contiguous zones (3, 4, 5, 6, 8) appear in the top ten. One of the most obvious observations is the ideal consistency of bank levels: in the upper zones, both of the two banks are high-risk. This two-way vulnerability reflects the consequences of erosion and attests to the fact that erosion, as well as erosion, is dominated by zone-scale or reach-scale geomorphological features that affect entire channel cross-sections. The existence of Karnaphuli Zones 4 and 5 and Sivasa Zone 7 as the highest risk factors which were not observed among the high erosion zones indicates that some parts of the river are areas of regular sediment deposition, regardless of the overall erosion/assemblage trend of the river. The management implications are clear: areas with perfect risk score structures are engineered sediment retention basins or natural sediment habitats that should be monitored not to stabilize banks but to control sediment deposition that could change the geometry or capacity of the channel.

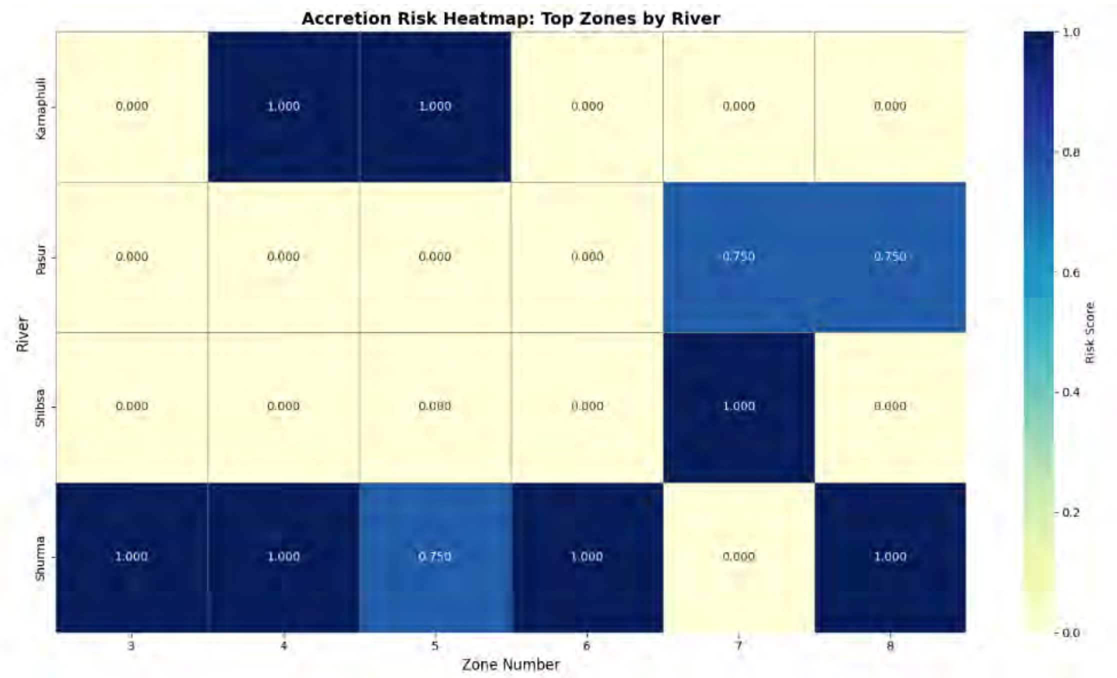


Figure 5.20: Accretion Risk Heatmap

The Accretion Risk Heatmap in Fig. 5.20 further clarifies this spatial distribution, showing that Zones 3, 4, 6, and 8 of the Shurma river, along with Zones 3 and 4 of the Karnaphuli river, carry the highest possible accretion risk score of 1.000.

## 5.5 Reasons for moderate predictive accuracy

The predictive power of the various architectures based on rich set of satellite-derived predictors and numerous advanced machine-learning and deep-learning architectures provided moderate predictive accuracy in erosion and accretion (typically 30-50% for three classes, with the best multi level hierarchical BiLSTM-GRU-Attention model reaching about 51%). A number of interacting process physics, data structure and target definition factors can explain this result and not a single modeling error.

**The absence of physical data on bank erosion and accretion**
Erosion and accretion feature sets are fully computed from annual satellite composites and static layers, land-cover indices such as Percent Veg, Percent Builtup, Per- cent Bare, spectral indices like Mean NDVI, Mean NDBI, Mean SAVI, Mean MSI, Mean NBR, Mean BAI, topography and soil properties such as Mean Elevation, Mean Slope, Soil Code, Soil Class, channel statistics such as Char Count, Char Area, Has Char, Dist to Char, and historical geomorphological changes such as Erosion vs 1988, Erosion vs Prev, Erosion vs 3yr Prev, Ero Intensity, Ero Intensity 2yr, Ero Intensity 3yr, and associated growth measures. These variables provide a broad summary of bank and floodplain morphological conditions and land-cover conditions but exclude hydrodynamic forcings such as river discharge, water level, peak flood magnitude and duration, flow velocity, or sediment load—that physically cause

erosion and accretion. Because the large events that control riverbank dynamics occur on subannual timescales and are not fully represented in the annual mean spectrum or land-cover summary, models must infer event-driven geomorphological responses from mostly static or slowly changing predictors, which inherently limits the achievable predictive accuracy

**Aggregation and loss of intra-annual variability annually**

All predictor variables are calculated using annual cloud-free composites and spatial aggregation on each char polygon or bank. This is needed to have a consistent multi-decadal dataset but narrows down the entire intra-annual variance into a single annual summary statistic. Specifically, the composites fail to separate the years of double moderate floods and years of several extreme floods, although these variations are important in bank erosion. Similarly, there are changes in vegetation cover (e.g. seasonal cropping, damage and recovery by flood) which are averaged in the annual mean indices. Therefore, a lot of the data regarding short term hydrological extremes that cause erosion and accretion are not available in the input feature space and this limits the capacity of sequence models to learn strong temporal patterns.

**Uncaptured episodic natural extremes**

River dynamics across different regions of Bangladesh, such as the southeastern hilly lands, the Sundarbans estuarine system,northeastern, and coastal region, are deeply dependent on natural disasters such as floods, cyclones, storm surges, and landslides, which contribute to sudden high-level erosion and sedimentation, even beyond annual long-term sensitivity. These processes include seasonal floods and tropical depressions, events that flow over embankments that create sudden geomorphological shocks that cannot be reduced over time, as annual geomorphological changes such as NDVI, NDWI, or DEM differences do not change over a decade. Without clear timing of events, wave detectors, or high-frequency hydrological surrogates, the models do not distinguish between disaster-driven extremes and gradual trends, which hinders the low withdrawal rate in Class 2 and adds to the overall modest accuracy scale.

**Class imbalance and rarity of high-intensity events**

There are classes of erosion and accretion that are imbalanced. The majority of rivers have no or minimal erosion/accretion along the bank of the rivers, and the actual high-intensity events (belonging to Class 2) are quite infrequent. This is characteristic of extremities in the environment, and is famous in making it difficult to classify. Despite the use of class weighting and other methods used to handle the imbalance, the models nonetheless have much fewer instances of high-erosion or high-accretion years relative to the few low-intensity years. Consequently, they are inclined to prefer the majority classes and recall on Class 2 is low even with the best models.

This impact is worse as one ascends to the zone and bank levels as compared to the global or river level. The sample size per class at such finer scales is extremely small, and even individual banks may only be having a few high-intensity events in the whole record between 1988 and 2025. In this case, even more complex architectures will not be able to learn class-specific patterns with any level of reliability, and the performance indicators reduce to the level of chance at the zone and bank level.

**Limited effective sequence length per bank**
The overall time domain of the data is large (1988-2025), but a combination of strict temporal splitting (training 1988-2016, validation 2017-2021, testing 2022-2025) and sequence lengths (2-3 years) implies that each bank provides a few sequences to be trained. As an illustration, when the sequence length equals 3 years and the test horizon starts in 2022, only a relatively small number of non-overlapping training samples can be obtained by a single bank. Moreover, their sequences are very autocorrelated, as a lot of annual predictors like soil, long-term land cover, are slowly changing over the time. This lowers the effective amount of independent information available to the LSTM and GRU layers and may cause overfitting to local instances of subtle patterns which are not particularly generalizable.

**Heterogeneity between rivers and a lack of conditioning**
These single worldwide and streamlined models are educated on information about seven rivers (Bishkhali, Baleshwar, Payra, Pasur, Surma, Shibsa and Karnaphuli), which vary in basin area, hydrology, sediment regime, tidal impacts and human alterations. In spite of the fact that some of the categorical features (River_Name, Zone_Number, Bank_Side) are present, the existing feature set might not completely capture the physical distinctions between these rivers. This heterogeneity complicates the ability of one model to gain universal patterns to be used on all basins, particularly in cases where important hydrological variables are not present. Consequently, the model is able to work reasonably well on a global scale but still has difficulties to capture the river-specific behavior with high accuracy.

**Summary of reasons for moderate accuracy**
When combined, the low to moderate accuracies that are found in this research do not imply that the modeling method is just as impossible, but it is just more challenging to predict erosion and accretion by use of only annual remote-sensing-generated geomorphic and spectral characteristics. The models have shortcomings of the lack of hydrological forcing, annual time resolution, label noise in the case of automatic geometric differentiation, large class imbalance, small effective sample in the fine spatial scales, and heterogeneity in inter-river.

# Chapter 6

# Limitations and Recommendations for Future Work

The chapter conveys a synthesis of the research findings, critical analysis of the limitations including missing physical bank measurements, class imbalance, limited sequence length per bank, uncaptured extreme events, and river heterogeneity and the visionary future work directions to transform the riverbank management in Bangladesh by using intra-annual data, expanded training sequences, and real-time satellite integration for operational riverbank monitoring systems, advanced AI-driven monitoring etc.

## 6.1 Limitations

**Using only Remote sensing as a predictor:**
models used are solely based on satellite derived geomorphic, spectral and land cover features, without considering discharge, water level or sediment transport data which is known to be the major contributors of bank erosion.

**Annual temporal resolution:**
All the features are calculated based on annual composites and spatial averages across the banks and chars. This leaves out intra-annual variability and extreme events which tend to dominate erosion and accretion, and important temporal information is lost.

**Labelling uncertainty in erosion-accretion:**
Classes of erosion and accretion are calculated automatically as geometric differencing of water extents, which is prone to classification errors, positional noise, and threshold selection, particularly in small patches and narrow channels.

**Disproportionation on the classes and the extreme rarities**
The occurrence of high-intensity erosion and accretion is also uncommon when compared to years of low intensity or stable erosion and accretion. With this imbalance, even with class weighting, this decreases the capacity of the models to correctly identify extreme classes.

**Inadequate zone-scale and bank-scale training samples**
The total amount of the dataset is large but the number of independent sequences in

each zone and each bank is small, especially in the case of temporal splitting. This limits the useful training information it can have in finescale models and variance in performance.

**Inter-river heterogeneity:**
The seven rivers under study have different hydrological and geomorphological conditions. The models can lack explicit hydrological descriptors, which diminish global generalization, even though this might not be able to capture the specific dynamics of rivers.

**Model interpretability:**
Even though there is certain interpretability of attention mechanisms, the deep architecture of the attention mechanisms is somewhat complicated and it is difficult to explicitly trace model errors to particular processes or features in the physical world.

## 6.2 Future work

**Combination of hydrology, climatic and hydraulic forcings:**
Future research ought to combine over time series of river discharge, water level, duration of floods, and in situations where possible, results of hydrodynamic models for example, 1D/2D flow models. Moreover, the predictors should be basin-scale rainfall, storm intensity, and data on large-scale human activities such as embankments, dredging, and training works. Integrating these physical and anthropogenic drivers with the geomorphic features obtained on satellites could be of great benefit in predicting erosion and accretion.

**Increased predictors and targets temporal resolution:**
Future work might require satellite products on an annual basis, but compute intra-annual indices of erosion/accretion by using seasonal or monthly products. This would enable the models to understand the occurrence of high-flow events, rainfall pulses, dredging activity and vegetation response that are significant to bank instability but would be mostly lost when aggregated on an annual basis.

**Target variables refinement and uncertainty modeling:**
Erosion and accretion might be represented as continuous normalized indices for example, gain in area relative to bank length or area, instead of three categories. The continuous and uncertain nature of geomorphic change based on remote sensing would be better modeled by regression-based predictions which may or may not include prediction intervals or probabilistic outputs and give more flexibility in defining the definition of high-risk thresholds.

**Complex management of the imbalance of classes and exceptional cases:**
The use of techniques like focal loss, event-focused sampling, synthetic minority oversampling or cost-sensitive learning may be used to enhance the detection of the high-intensity erosion and accretion events. The approach is especially applicable to the unusual years with extreme floods, heavy rainfall, or significant engineering

actions, which are not frequent but have a significant impact. Physics-guided and hybrid model methods.

It can be beneficial that hybrid models that incorporate simplified physical constraints for example, mass balance, known relationships between flow energy, rainfall-runoff response and erosion, be embedded within deep networks so that the models themselves are more generalizable and stop depending on purely data-driven correlations. In these architectures, a process-based component offers a physically consistent level, and the neural network corrects residuals and local corrections.

**Cross-river transfer learning and cross-river multi-task learning:**
Pretraining deep sequence models on a large sample of rivers and specifically training to individual basins, or multi-task learning, in which a shared backbone is used to predict erosion in many rivers, zones, and banks can mitigate data sparsity in local scales. This would enable the models to take advantage of the general patterns and yet allow river specific responses to hydrology, rainfall and human actions.

**Better interpretability and attribute assignment:**
Future applications may utilize explainable AI methodologies like SHAP values, integrated gradients, attention visualization to determine which characteristics for examples, discharge peaks, rainfall extremes, dredging indicators, vegetation loss, or char metrics and which time steps have the greatest impact on the prediction of erosion and accretion. It would enhance physical interpretability of deep models and determine which additional features and sources of data should come first.

## 6.3 Summary of Findings

This study presents an innovative framework for predicting riverbank erosion and accretion prediction as well as features for char (river island) detection ( char features were not used in the study for the time being) in seven river systems (Baleshwar, Bishkhali, Karnaphuli, Pashur, Payra, Sibsa and Surma) in different regions of Bangladesh. The study was conducted using 38 years of annual multispectral data between 1988 and 2025. The study used high-resolution imagery acquired using Landsat 5, Landsat 7 and Sentinel-2 to map the spatio-temporal dynamics by synthesizing various spectral indices (NDWI, NDVI and NDBI) using important environmental variables (soil texture, slope and elevation). Based on the analysis, there was a specific geomorphological pattern where the Karnaphuli River was dominated by uniform sediment deposition (Class 0) and the Sibsa and Payra Rivers showed a high incidence of high-level growth (Class 2), implying a high potential for new land development. The focus of this research is to develop a bidirectional LSTM-GRU hybrid with attention mechanism, which was chosen due to its special properties of dealing with imbalances between classes and predicting all intensity levels. Bi-level Bi-LSTM with Bi-GRU models with residual connections are effective because the model is able to capture the temporal dependence of local spatial variations over the long term and between different riverbanks. Bahdanou Attention is another contribution that improves performance by ranking important time-steps in some specific cases, such as Zone 8 of Pasur and Zone 1 of Payra. The system uses a combinatorial mix of layer normalization, dropout, and learning rate scheduling to provide strong generalization and effectively avoid overfitting even in complex coastal data. Though the model has good potential, due to the complexity of the fluvial dynamics there is moderate predictive success because the current feature set is based on annual satellite composites that do not capture the high-frequency hydrodynamic forcings such as river discharge, flow velocity and peak period of a flood. Moreover, the large diversity of the seven river basins that are controlled by varying tidal and sediment influences makes it difficult to generalize a universal trend by the model unless hydrological conditions are conditioned on a basin scale. In the future, this framework can be improved by incorporating river drainage, water level, and hydrodynamic flow models into physics-guided hybrid networks, reducing the use of purely data-driven correlations. Intra-annual or monthly satellite products should also be included in the work in the future to capture high-flow events and rainfall pulses that are important to learn about bank instability but which are usually lost when annual aggregations are used. In addition, it will include large-scale human processes such as dredging to provide a more detailed image of anthropogenic impacts. This system will eventually become an essential automated decision-support tool by making explainable AI approaches, such as the SHAP values or attention visualization to conceptualize critical drivers such as the loss of vegetation or the peak of discharge, to guarantee the sustainability and resilience of the vulnerable communities.

# Bibliography


[1] I. Hasan et al., "Morphological changes of river bank erosion and channel shifting assessment on arial khan river of bangladesh using landsat satellite time series images," *Progress in Disaster Science*, vol. 24, p. 100 381, 2024.

[2] R. Titlee, M. S. Islam, and N. Ahmed, "Analysis of the morphological changes of the river padma along naria upazila through supervised classification of satellite images," in *2020 2nd International Conference on Advanced Information and Communication Technology (ICAICT)*, IEEE, 2020, pp. 302–307.

[3] F. Nihal et al., "Monitoring of planform changes and computation of erosion/accretion of bishkhali estuary using satellite image,"

[4] T. Langhorst and T. Pavelsky, "Global observations of riverbank erosion and accretion from landsat imagery," *Journal of Geophysical Research: Earth Surface*, vol. 128, no. 2, e2022JF006774, 2023. DOI: 10.1029/2022JF006774

[5] M. M. Rahman, M. S. Hasan, M. K. Eusufzai, and M. M. Rahman, "Impacts of dredging on fluvial geomorphology in the jamuna river, bangladesh," *Journal of Geoscience and Environment Protection*, vol. 9, no. 6, pp. 1–20, 2021.

[6] E. Mbalibulha, I. A. Ismail, A. Khaldi, J. Wasswa, and D. Obura, "Coupling geographic information systems and remote sensing to evaluate riverbank erosion and accretion in an arid environment: A blueprint for sustainable transformation," *Sustainable Water Resources Management*, vol. 11, no. 1, p. 8, 2025.

[7] Chatrabhuj, K. Meshram, U. Mishra, and P. J. Omar, "Integration of remote sensing data and gis technologies in river management system," *Discover Geoscience*, vol. 2, no. 1, p. 67, 2024.

[8] S. Das and S. K. Gayen, "Assessment of bank erosion, accretion and lateral migration using remote sensing and gis: A study on the sankosh river of himalayan foothills," *Journal of the Indian Society of Remote Sensing*, vol. 52, no. 2, pp. 271–290, 2024.

[9] M. N. Rahman, M. M. Saleheen, H. E. Fadili, and M. N. I. Sarker, "Assessment of riverbank erosion and its prediction using geospatial and machine learning techniques," in *Modern Cartography Series*, vol. 12, Elsevier, 2024, pp. 493–509.

[10] Wikipedia contributors. "Normalized Difference Water Index — Wikipedia, The Free Encyclopedia." [Online; accessed 1-February-2025]. [Online]. Available: https://en.wikipedia.org/wiki/Normalized_difference_water_index

[11] Space4Water Portal. "Hydrology." Accessed: 2025-02-01. [Online]. Available: https://www.space4water.org/taxonomy/term/1246

[12] Wikipedia contributors, *Soil salinity*, Accessed: 2025-02-01, Wikipedia, The Free Encyclopedia, 2025. [Online]. Available: https://en.wikipedia.org/wiki/Soil_salinity

[13] Wikipedia contributors, *Soil-adjusted vegetation index*, Accessed: 2025-02-01, Wikipedia, The Free Encyclopedia, 2025. [Online]. Available: https://en.wikipedia.org/wiki/Soil-adjusted_vegetation_index

[14] Wikipedia contributors. "Long Short-Term Memory — Wikipedia, The Free Encyclopedia." [Online; accessed 1-February-2025]. [Online]. Available: https://en.wikipedia.org/wiki/Long_short-term_memory

[15] Google. "Google Earth Engine." [Online; accessed 1-February-2025]. [Online]. Available: https://earthengine.google.com/

[16] Wikipedia contributors. "QGIS — Wikipedia, The Free Encyclopedia." [Online; accessed 1-February-2025]. [Online]. Available: https://en.wikipedia.org/wiki/QGIS

[17] Wikipedia contributors. "ArcGIS — Wikipedia, The Free Encyclopedia." [Online; accessed 1-February-2025]. [Online]. Available: https://en.wikipedia.org/wiki/ArcGIS

[18] Wikipedia contributors, *Geographic information system*, Accessed: 2025-02-01, Wikipedia, The Free Encyclopedia, 2025. [Online]. Available: https://en.wikipedia.org/wiki/Geographic_information_system

[19] S. S. Kumar, M. Pandey, and A. K. Shukla, "Spatio-temporal analysis of riverbank changes using remote sensing and geographic information system," *Physics and Chemistry of the Earth, Parts A/B/C*, vol. 136, p. 103 692, 2024.

[20] A. K. Dehkordi, R. F. Nafchi, H. Samadi-Boroujeni, M. K. Boroujeni, and K. Ostad–Ali–Askari, "Assessment of morphological changes of river bank erosion using landsat satellite time-series images," *Ain Shams Engineering Journal*, vol. 15, no. 3, p. 102 455, 2024.

[21] M. Mehwish, M. J. Nasir, A. Raziq, A. M. F. Al-Quraishi, and F. A. Ghaib, "Soil erosion vulnerability and soil loss estimation for siran river watershed, pakistan: An integrated gis and remote sensing approach," *Environmental Monitoring and Assessment*, vol. 196, no. 1, p. 104, 2024.

[22] M. Laboni, S. Rahman, S. Khan, and M. Rafiq, "Quantifying riverbank erosion and associated land cover changes across the coastal upazila of hizla, bangladesh: An integrated approach using gis and machine learning," *Earth Science Malaysia*, vol. 7, pp. 164–173, Oct. 2023. DOI: 10.26480/esmy.02.2023.164.173

[23] "Riverbank migration and island dynamics of the braided jamuna river of the ganges–brahmaputra basin using multi-temporal landsat images," *Quaternary International*, vol. 263, pp. 148–161, 2012, Late Quaternary morphodynamics in East Asia, ISSN: 1040-6182. DOI: https://doi.org/10.1016/j.quaint.2012.03.016

[24] M. S. Islam and M. A. Matin, "Prediction of fluvial erosion rate in jamuna river, bangladesh," *International Journal of River Basin Management*, vol. 21, no. 4, pp. 625–637, 2023. DOI: 10.1080/15715124.2022.2068561 eprint: https://doi.org/10.1080/15715124.2022.2068561. [Online]. Available: https://doi.org/10.1080/15715124.2022.2068561

[25] S. Rahman, S. Rahman, M. T. Jawad, M. Foysal, and M. S. Hossain, "Riverbank change detection in the jamuna river basin, bangladesh: A remote sensing and machine learning approach," in *2025 International Conference on Artificial Intelligence, Computer, Data Sciences and Applications (ACDSA)*, 2025, pp. 1–6. DOI: 10.1109/ACDSA65407.2025.11166394

[26] M. F. N. Sarkar et al., "Monitoring of planform changes and computation of erosion/accretion of bishkhali estuary using satellite image," Jan. 2016.

[27] M. Rahman, M. S. Hasan, M. Eusufzai, and M. Rahman, "Impacts of dredging on fluvial geomorphology in the jamuna river, bangladesh," *Journal of Geoscience and Environment Protection*, vol. 09, pp. 1–20, Jan. 2021. DOI: 10.4236/gep.2021.96001

[28] I. Hasan et al., "Morphological changes of river bank erosion and channel shifting assessment on arial khan river of bangladesh using landsat satellite time series images," *Progress in Disaster Science*, vol. 24, p. 100 381, Oct. 2024. DOI: 10.1016/j.pdisas.2024.100381

[29] A. Haque and M. Matin, "A study on prediction of bed level changes and bank line shifting of the selected reach of jamuna river," Jun. 2023.

[30] J. Freihardt and O. Frey, "Assessing riverbank erosion in bangladesh using time series of sentinel-1 radar imagery in the google earth engine," *Natural Hazards and Earth System Sciences*, vol. 23, no. 2, pp. 751–770, 2023. DOI: 10.5194/nhess-23-751-2023 [Online]. Available: https://nhess.copernicus.org/articles/23/751/2023/

[31] P.-C. Huang, "Estimation of riverbank erosion by combining channel morphological models with ai techniques," *Geomatics, Natural Hazards and Risk*, vol. 15, no. 1, p. 2 359 983, 2024.

[32] A. Rahman et al., "Analysis on river bank erosion-accretion and bar dynamics using multi-temporal satellite images," *ResearchGate*, 2017. [Online]. Available: https://www.researchgate.net/profile/Afeefa-Rahman/publication/321156460_Analysis_on_River_Bank_Erosion-Accretion_and_Bar_Dynamics_Using_Multi-Temporal_Satellite_Images/links/5a119ce8458515cc5aa98bc0/Analysis-on-River-Bank-Erosion-Accretion-and-Bar-Dynamics-Using-Multi-Temporal-Satellite-Images.pdf

[33] L. Nguyen et al., "Long short-term memory (lstm) neural networks for short-term water level prediction in mekong river estuaries," *ResearchGate*, 2022. [Online]. Available: https://www.researchgate.net/profile/Liem-Nguyen-18/publication/360513858_Long_Short-Term_Memory_LSTM_neural_networks_for_short-term_water_level_prediction_in_Mekong_river_estuaries/links/634023d8ff870c55ce0ac7b0/Long-Short-Term-Memory-LSTM-neural-networks-for-short-term-water-level-prediction-in-Mekong-river-estuaries.pdf

[34] N. Author, "Application of machine learning in riverbank erosion prediction," Ph.D. dissertation, University of North Dakota, 2025. [Online]. Available: https://commons.und.edu/cgi/viewcontent.cgi?article=8027&context=theses